DISSERTATION

SIMULATING THE FATE AND TRANSPORT OF SALINITY SPECIES IN A SEMI-ARID AGRICULTURAL GROUNDWATER SYSTEM: MODEL DEVELOPMENT AND APPLICATION

Submitted by

Saman Tavakoli Kivi

Department of Civil and Environmental Engineering

In partial fulfillment of the requirements

For the Degree of Doctor of Philosophy

Colorado State University

Fort Collins, Colorado

Summer 2018

Doctoral Committee:

Advisor: Ryan T. Bailey
Co-Advisor: Timothy K. Gates

Michael J. Ronayne
Aditi Bhaskar

ABSTRACT

SIMULATING THE FATE AND TRANSPORT OF SALINITY SPECIES IN A SEMI-ARID AGRICULTURAL GROUNDWATER SYSTEM: MODEL DEVELOPMENT AND APPLICATION

Many irrigated agricultural areas worldwide suffer from salinization of soil, groundwater, and nearby river systems. Increased salinity concentrations, which can lead to decreased crop yield, are due principally to the presence of salt minerals and high rates of evapotranspiration. High groundwater salt loading to nearby river systems also affects downstream areas when saline river water is diverted for additional uses.

Irrigation-induced salinity is the principal water quality problem in the semi-arid region of the western United States due to the extensive background quantities of salt in rocks and soils. Due to the importance of the problem and the complex hydro-chemical processes involved in salinity fate and transport, a physically-based spatially-distributed numerical model is needed to assess soil and groundwater salinity at the regional scale. Although several salinity transport models have been developed in recent decades, these models focus on salt species at the small scale (i.e. soil profile or field), and no attempts thus far have been made at simulating the fate, storage, and transport of individual interacting salt ions at the regional scale within a river basin. The required model must be able to handle variably-saturated groundwater systems; sources and sinks of groundwater within an agricultural system such as canal seepage, infiltrated water from flood and sprinkler irrigation, groundwater pumping, and evapotranspiration from both the unsaturated and shallow saturated zones; root zone processes such as salt ions cycling, crop uptake, and

leaching to the water table; addition of salt mass via fertilizer and irrigation water; chemical kinetics affecting salt ions such as the influence of dissolved oxygen and nitrate on the chemical processes of anions such as sulfate (SO_4); and equilibrium chemistry processes such as precipitation-dissolution, complexation, and cation exchange.

This dissertation develops a physically-based, spatially-distributed groundwater reactive transport model that simulates the fate and transport of major salt ions in an agricultural groundwater system and can be applied to regional scale areas to address salinity problems. The model is developed by 1) constructing an equilibrium chemistry model that includes all the fate and transport processes that affect salt ions in an agricultural soil-groundwater system, including precipitation-dissolution of salt minerals, ions complexation, and cation exchange; and 2) coupling the module with UZF-RT3D (Bailey et al., 2013) a MODFLOW-based numerical modeling code that simulates the transport of multiple interacting reactive solutes in a variably-saturated soil-groundwater system. The model accounts for dissolved oxygen, nitrogen cycling in the soil-plant system (crop uptake, organic matter decomposition, mineralization/immobilization), oxidation-reduction reactions, including chemical reduction of dissolved oxygen and nitrate in the presence of marine shale, and sorption. UZF-RT3D has been amended to also include processes that directly affect SO_4, one of the major salt ions, such as sulfur cycling in the plant-soil system and the release of SO_4 from pyrite (FeS_2)-laden marine shale in the presence of dissolved oxygen and nitrate. The developed model is applied to a salinity-affected irrigated alluvial stream-aquifer region to demonstrate its applicability and to assess remediation strategies on soil and groundwater salinity, salt mass loading to streams, and crop yield. The study area is a 500 km^2 region of the Lower Arkansas River Valley (LARV) in southeastern Colorado, with the model tested against an extensive set of field data (soil salinity,

groundwater salinity, salt loading from the aquifer to the Arkansas River) for the years 2006-2009. Parameter estimation is accomplished via a mixed manual-automated method, with estimation of both equilibrium and kinetic chemical parameters. Research results are presented through published and submitted articles. Results of preliminary best management practice (BMP) scenario testing indicates that reducing the volume of applied irrigation water and sealing earthen irrigation canals can have a significant effect on the root zone salinity, groundwater salinity, groundwater salt loading from the aquifer to the river network, and crop yield.

ACKNOWLEDGEMENTS

It is a great pleasure to thank the people who made this dissertation possible. First and foremost, I would like to express my most sincere gratitude to my advisor Dr. Ryan T. Bailey and my co-adviser, Dr. Timothy K. Gates. They have been mentors for me both academically and non-academically. Without their persistent help, support, and motivation this dissertation would not have been possible. I would also like to thank my exceptional committee members, Dr. Michael J. Ronayne, and Dr. Aditi Bhaskar, for their encouragement and insightful comments. Finally, I express appreciation to my friends and colleagues at our research lab whose company, assistance, and friendship were always heartwarming. And last but not least, I have to thank my lovely wife for her patience and encouragement. Without her unconditional support, this dissertation would not have been accomplished.

DEDICATION

For my wife, parents, and family for their unconditional love, tremendous support, and encouragement

TABLE OF CONTENTS

LIST OF TABLES

LIST OF FIGURES

CHAPTER 1

LITERATURE REVIEW AND RESEARCH OVERVIEW

1.1. Objective and Expected Significance

The overall aim of this dissertation is to develop a numerical modeling framework capable of simulating the fate and transport of major salt ions within a regional-scale variably-saturated agricultural groundwater system. This model then can be used to assess current conditions of salinity in a semi-arid irrigated agricultural system; investigate the potential impact of remediation strategies on soil salinity, groundwater salinity, and salt loading to streams; and determine required implementation levels of these strategies to provide sustainable crop yield in the coming decades. This overall aim will be accomplished by through the following specific objectives:

- Develop a Salinity Equilibrium Chemistry (SEC) module for groundwater salt ion chemistry that simulates the concentration of sulfate, calcium, magnesium, sodium, potassium, chloride, carbonate, and bicarbonate due to precipitation-dissolution of salt minerals, complexation, and cation exchange; this module also simulates sulfur (S) cycling, which includes soil-plant-water cycling and the release of SO_4 from marine shale in the presence of dissolved oxygen and nitrate;
- Couple the SEC module with the finite difference groundwater multi-species reactive transport model UZF-RT3D, to create a single modeling code that simulates the fate and transport of salt ions due to advection, dispersion, equilibrium chemical reactions, first-order kinetics, and sorption within an agricultural groundwater system; UZF-RT3D also accounts for

mass cycling of carbon and nitrogen due to mineralization/immobilization, crop uptake, leaching, and first-order redox reactions. The coupled model is referred to as UZF-RT3D/SEC throughout the dissertation;

- Apply the model to a salinized regional-scale study area and estimate the parameters of the model using a hybrid method for distributing the salt solids within the soil profiles manually and using an automated parameter estimation method (PEST) to achieve a satisfactory match between observed and simulated target variables. Target variables include spatially-averaged C_{SO_4-S}, C_{Ca}, C_{Mg}, C_{Na}, C_{Cl}, C_{HCO_3}, and C_{TDS} in the saturated zone; spatially-averaged C_{TDS} of soil water in the root zone; the relative frequency distribution of all major salt ions in the saturated zone; the relative frequency distribution of C_{TDS} in soil water in the root zone; and groundwater mass loading of SO_4 and TDS to the Arkansas River. The site is a 500 km^2 region of the Lower Arkansas River Valley in southeastern Colorado, selected due to its extremely high soil salinity and groundwater salinity concentrations, an abundance of hydrologic and salinity data collected by Colorado State University researchers during the past two decades, and the existence of a tested groundwater flow model for the region (Morway et al., 2013). The potential for altering soil salinity, groundwater salinity, groundwater salt loading to surface water, and crop yield is explored by simulating several Best Management Practices (BMPs) in a preliminary manner.

1.2. Background

Salinization of soil and shallow groundwater is an inevitable problem in irrigated agricultural fields and poses a major challenge to sustaining crop yield (Sparks, 2003, Gates et al.; 2002, Morway et al., 2012; Lin et al., 2008; Wichelns et al., 2015; Vaze et al., 2003, Hutmacher et al., 1996, Ebrahimi et al., 2016, Jamshidzadeh et al., 2011). Reduction in crop yield is an important

economic consequence of salt build-up in the root zone in many regions of the world including Iran (Jalali, 2007; Jamshidzadeh et al., 2011; Ebrahimi et al, 2016), India (Singh, 2005; Jeevanandam et al., 2007; Misra et al., 2007; Lorenzen et al., 2012), the western United States (e.g. San Joaquin Valley in California, Schoups et al., 2006), Pakistan (Mahmood et al., 2001; Qureshi et al., 2008; Latif et al., 2009), China (Pereira et al. 2007; Chen et al, 2010; Wang et al. 2018), and Australia (Herczeg et al., 2001; Tweed et al., 2007; Skrzypek et al., 2013). Approximately one-fourth of all irrigated lands in the world are impaired by high salinity (Rhoades, 1993, Ghassemi et al., 1995) with the salt-affected areas increasing by approximately 1 to 1.5 million ha each year (Barghouti and Le Moigne, 1991). High salinity can be brought about by waterlogging from shallow groundwater with associated evaporative upflux and concentration (Morway and Gates, 2012; Harrington et al., 2014); dissolution of salt minerals such as gypsum ($CaSO_4$), calcite ($CaCO_3$), and halite (NaCl) (Harrington et al., 2014; Farid et al., 2015,); and seawater intrusion in coastal areas (Shammas et al., 2007; Sherif et al., 2011; Blanco et al., 2013).

Irrigation-induced salinity is the principal water quality problem in the semi-arid region of the western United States due to the extensive background quantities of salt in rocks and soils (El-Ashry, 1985) and high potential evapotranspiration. Specific areas with acute salinity problems include the Colorado River Basin with the downstream areas of the Imperial Valley and the Coachella Valley experiencing the greatest salinity problems; the Rio Grande Basin of New Mexico and Texas; the Central Valley of California, particularly within the agriculturally-important San Joaquin Valley; the Yakima River Basin in Washington; the Snake River Basin in Idaho; and the Arkansas and South Platte River Basins in Colorado, Nebraska, Kansas, and

Oklahoma. Studies show that about 300,000 acres in Montana are no longer productive as salinity increases in the region (USDA, 2002).

The impact of possible remediation practices on high groundwater and soil salinity often is assessed using models that attempt to capture the major hydrologic processes and chemical reactions that govern the transport and distribution of salt species in coupled soil-aquifer systems. These models also are used to provide insights into processes that govern salt species transport within these systems. Models are employed at a variety of spatial scales, ranging from one-dimensional (1D) soil profiles to river basins, and include varying degrees of complexity, from simple advective transport to multi-species reactive transport coupling equilibrium and kinetic chemistry.

Numerous geochemical models such as PHREEQE (Parkhurst et al., 1980; Parkhurst & Appelo, 1999), MINTEQ (Felmy et al., 1984), WATEQ (Truesdell & Jones, 1974), The Geochemist's Workbench (Bethke, 1994, 1996), MINTEQA2 (Allison et al., 1991), GEOCHEM (Sposito & Mattigod, 1980), UNSATCHEM-2D (Simunek and Suarez, 1994), SAHYSMOD (Oosternbaan, 2005; Singh and Panda, 2012), CATSALT (Tuteja and Vaze, 2003), and WATSUIT (Oster and Rhoades, 1975) have been introduced since 1970's. The main difference between these models is the approach which each model uses to determine the species distribution at equilibrium. Table 1.1 presents a summary comparison of the capabilities of each model.

Table 1.1. Chemical reaction processes included in existing geochemical models

Program	Complexation	Precipitation-dissolution	Ion Exchange	Adsorption Isotherms	Davis Activity	Debye-Huckel Activity
PHREEQC	×	×	×		××	××
MINTEQA2	×	×	×	×	××	××
WATEQ	×				××	××
Geochemist's Workbench	×	×			××	××
GEOCHEM		×		×		
UNSATCHEM	×	×	×		××	××
TRANQL	×			×		

Several models include many of the governing physical and chemical processes for salt fate and transport. UNSATCHEM-2D (Simunek and Suarez, 1994) includes chemical reactions such as precipitation-dissolution of salt minerals, cation exchange, and complexation to simulate spatio-temporal concentration of major salt ions in soil-water systems. HYDRUS-1D (Simunek et al., 2005), a finite element model for simulating the movement of water and multiple solutes in variably-saturated porous media, was amended to include the UNSATCHEM module for major salt ion chemistry (Simunek et al., 2012). The HP1 model couples HYDRUS-1D with PHREEQC to address a broader range of ions but is restricted to 1D transport (Jacques et al., 2003, Jacques et al., 2005). LEACHM (Wagenet and Hutson, 1987) simulates salt and pesticide movement in the soil zone. These models, however, have been applied only at small spatial scales, typically soil profiles at experimental field plots (Goncalves et al., 2006; Tafteh et al., 2012; Rasouli et al., 2013), due to high computational costs and data requirements.

A second subset of salinity models are applied at a large spatial scale (catchment to river basin), but do not include chemical processes (e.g. precipitation-dissolution) that often govern salt ion concentration in variably-saturated groundwater systems. Table 1.2 shows a list of salt transport modeling studies applied at the regional scale and selected features of the respective model used for each study. The area of the study region and the modeled physical and chemical processes also are included.

Table 1.2. Salinity transport modeling studies applied at the regional scale.

Study Area	Area of the study region	Model Used	Simulated Salt species	Reference
San Joaquin Valley, California, USA	1400 km^2	Coupled MODHMS and UNSATCHEM	Gypsum and Calcite	Shoups et al., 2005
Lower Arkansas River Valley, Colorado, USA	244 km^2	Modified WATSUIT	Gypsum, Calcite, and Magnesite	Lin and Garcia (2008)
Haryana State, India	920 km^2	SAHYSMOD	N/A	Singh et al., 2012
Mandagery Creek Catchment, Australia	1668 km^2	CATSALT	N/A	Tuteja et al., 2003
Lower Arkansas River Valley, Colorado, USA	500 km^2	MT3DMS + Water and Salt balance model for unsaturated zone	N/A	Burkhalter and Gates (2005)

A hydro-salinity model that couples MODHMS with UNSATCHEM was used by Schoups et al. (2005) to simulate subsurface salt transport and storage in a 1,400 km^2 region of the San Joaquin Valley. The coupling of the two models for three-dimensional salinity reactive transport, however, is not explained in the paper, and the modeling system does not account for element (carbon, nitrogen, sulfur) mass cycling in the plant-soil system. SAHYSMOD (Oosterbaan, 2005) is an integrated agro-hydro-salinity model that can be applied to large scale agricultural fields but handles processes based exclusively on water and salt balances and does not account for chemical reactions. SAHYSMOD has been applied to simulate the water and salt behavior in

the semi-arid irrigated area of Haryana State in India where waterlogging and salinization has impacted the region for more than 40 years (Singh et al., 2012). Tuteja et al., (2003) assessed the effect of land use changes on salt and water balance in the Mandagery Creek catchment of New South Wales, Australia using CATSALT, a distributed water balance model linked with a salt transport module. Lin and Garcia (2008) applied WATSUIT, a steady-state model that calculates soil-water interaction in the root zone, in Colorado's LARV to determine the salinity of deep percolation water. They modified WATSUIT to simulate dynamic conditions with a monthly time step and applied the model to simulate unsaturated flow for a 12-month period in the root zone of fields. Burkhalter and Gates (2005) applied a modified version of MT3DMS incorporating a water and salt balance module for unsaturated zone to Colorado's LARV from 1999 to 2001. Results indicated that average crop yield reduction due to the salinity varies from 0% to 89% in fields across the region.

Other models link geochemistry and multi-species reactive transport in saturated or variably-saturated porous media [e.g. VAM2D, (Huyakorn et al., 1991); HYDROGEOCHEM (Yeh et al., 2004); DYNAMIX (Narasimhan et al., 1986); PHAST (Parkhust et al., 2004)], but have not been applied to salinity fate and transport and do not always include the necessary chemical reactions, e.g. cation exchange, or are limited to the saturated zone (e.g. PHAST). Table 1.3 summarized the coupled most common geochemical model. Overall, the chemical processes that often govern salt species' fate and transport, such as precipitation-dissolution, complexation, cation exchange, first-order degradation, and redox reactions have not been represented in modeling efforts at a large spatial scale. Nevertheless, the degradation of aquifers and streams by the accumulation of salts, as well as their remediation, is brought about by practices and processes that interact from field to field over vast spatial extents. Models are needed that can adequately simulate these

practices and processes to allow salinization over regional landscapes to be better understood and alternatives for its mitigation to be explored.

The foremost motivation of this research is the salinity problem in the alluvial stream-aquifer system of the LARV in southeastern Colorado. Due to the high salt concentration in the root zone and groundwater, availability of an extensive data set collected by Colorado State University over a 15-year period, and existence of a groundwater flow model for the region. It is important to note that although the model is applied to LARV, it could be applied to other regions, regardless of size and scale, with high salinity and hence could be used to investigate management practices to remediate salt concentration and mass loading. This fulfills the main objective of this dissertation in providing a tool that simulates the fate and transport of salinity in stream-aquifer system.

Table 1.3. Overview of coupled reactive transport models.

Program	1D-2D-3D	Small(S) or Large(L) scale	Complexation	Precipitation-dissolution	Ion Exchange	Adsorption Isotherms	Davis Activity	Debye-Huckel Activity	Root Zone	Saturated Zone
HYDRUS	123	S	×	×	×	×	×	×	×	×
HYDROGEOCHEM	123	S	×	×	×		×		×	×
MPATH	1	S	×	×						
AquaChem	1		×	×			×	×		
DYNAMIX	12	S	×	×			×	×		
PHAST	123		×	×	×		×	×	×	
VAM2D	12	S				×				

1.3. Significance of Research

This dissertation presents a numerical model that simulates the fate and transport of major salt ions in a regional-scale variably-saturated agricultural groundwater system while accounting for major salt inputs, equilibrium chemical reactions, oxidation-reduction reactions, and the cycling of carbon (C), nitrogen (N), and sulfur (S) in the plant-soil system. The model uniquely combines these capabilities with a number of other features important to the transformation and distribution of salts over large agricultural regions. It is based on UZF-RT3D (Bailey et al., 2013a), a finite difference FORTRAN code that simulates reactive transport of multiple interacting chemical species in variably-saturated groundwater flow systems and that uses flow and source/sink output from a MODFLOW groundwater flow model. UZF-RT3D has been used previously for simulating the cycling and transport of N, S, and selenium (Se) species in a regional-scale aquifer system (Bailey et al., 2014; Tavakoli Kivi and Bailey, 2017), and includes organic matter decomposition and mineralization, plant uptake, sorption, oxidation-reduction, and fertilizer loading.

This model is unique because of the capability of modeling in three dimensions, ability to simulate the saturated and un-saturated zone both at the same time, capability of application to both large-scale watershed studies and small-scale field studies, fitness for handling external sources such as fertilizer or irrigation more easily, capability of considering more salt species based on local conditions, and its linkage with MODFLOW. As MODFLOW is used worldwide, the UZF-RT3D/SEC model developed in this research has the potential to be applied in many regions worldwide dealing with salinity issues.

1.4. Organization of the dissertation

The remainder of the dissertation is organized in four chapters. The second chapter presents a recently published paper dealing with sulfur cycle modeling; the third chapter is a paper currently under review by a journal, presenting the coupled reactive transport and equilibrium chemistry model for assessment of salinity in a regional-scale agricultural area; the fourth chapter demonstrates a framework for assessment of BMPs for salt remediation; and the fifth chapter provides conclusions and recommendations for future research.

REFERENCES

Allison, J., Kevin, J., 1991, MINTEQA2: A geochemical assessment model for environmental systems: Version 3.0 User's manual, Technical Report, 600/3-91/021.

Barghouti, S., and G. Le Moigne (1991), Irrigation and the environmental challenge. Finance Dev. 28 (2), 32 – 33.

Bethke, C.M., 1996, Geochemical reaction modeling-Concepts and applications. Oxford Univ. Press, New York, NY.

Bethke, C.M., 1994, The Geochemist's Workbench. Version 2.0, A Users Guide to Rxn, Act2, Tact, React, and Gtplot, Hydrogeology Program, University of Illinois.

Blanco, R.I., Naja, G.M., Rivero, R.G. and Price, R.M., 2013. Spatial and temporal changes in groundwater salinity in South Florida. Applied geochemistry, 38, pp.48-58.Brassard, P., Bodurtha, P., 2000, A feasible set for chemical speciation problems, Computers & Geosciences, 26 (3), pp. 277–291.

Burkhalter, J. P., and Gates, T. K. 2005. "Agroecological impacts from salinization and waterlogging in an Irrigated river valley". Journal of Irrigation and Drainage Engineering, 131(2): 197 - 209.

Chen, W., Hou, Z., Wu, L., Liang, Y., and Wei, C. 2010. "Evaluating salinity distribution in soil irrigated with saline water in arid regions of northwest China. Agric. Water Mgmt., 97(12), 2001 – 2008.

Ebrahimi, M., Kazemi, H., Ehtashemi, M., Rockaway, T., 2016, Assessment of groundwater quantity and quality and saltwater intrusion in the Damghan basin, Iran, Chemie der Erde – Geochemistry, vol: 76 (2) pp: 227-241.

El-Ashry, M.T., van Schilfgaarde, J., and S. Schiffman, 1985, Salinity pollution from irrigated agriculture. J. Soil and Water Conservation 40(1), 48-52.

Felmy, A.R., 1995. GMIN, A computerized chemical equilibrium program using a constrained minimization of the Gibbs free energy: summary report. In: Loeppert, R.H. (Ed.), Chemical Equilibrium and Reaction Models. American Statistical Association and SSSA, Madison, WI, pp. 377±407.

Ghassemi, F., Jakeman, A., and Nix, H., 1995, Salinization of land and water resources: Human causes, extent, management, and case studies in salinity-affected regions, University pf New South Wales Press, Sydney, Australia.

Harrington, N., Cook, P., 2014, Groundwater in Australia, National Centre for Groundwater Research and Training, Australia.

Herczeg, A.L., Dogramaci, S.S., Leanet, F.W.J., 2001, Origin of dissolved salts in a large, semi-arid groundwater system: Murray Basin, Australia, Marine Freshwater Research, 52, 41-52.

Huyakorn, P.S., J.B. Kool, and Y.S. Wu. 1991. VAM2D-Variably saturated analysis model in two dimensions.Version 5.2 with hysteresis and chained decay transport. Documentation and user's guide. NUREG/CR-5352, Rev. 1. U.S. Nuclear Regulatory Commission, Washington, DC.

Hutmacher, R.B., Ayars, J.E., Vail, S.S., Bravo, A.D., Dettinger, D, Schoneman, R.A., 1996, Uptake of shallow groundwater by cotton: growth stage, groundwater salinity effects in column lysimeters, 31, pp. 205-223

Jacques, D. and J. Simhek, 2005. Multicomponent - Variable Sat- urated Transport Model, Description, Manual, Verification and Examples, Waste and Disposal. SCKoCEN, BLG-998, Mol, Belgium.

Jacques, D., J. Simhek, D. Mallants, and M. Th. van Genuchten, 2003. The HYDRUS-PHREEQC Multicomponent Transport Model for Variably-Saturated Porous Media: Code Verification and Application. In: MODFLOW and More 2003: Understanding Through Modeling, E. Poeter, Ch. Zheng, M. Hill, and J. Doherty (Editors). Int. Ground Water Modeling Center, Colorado School of Mines, FOG Collins, Colorado, pp, 23-27.

Jalali, M., 2007. Salinization of groundwater in arid and semi-arid zones: an example from Tajarak, western Iran. Environmental Geology, 52(6), pp.1133-1149.

Jamshidzadeh, Z., Mirbagheri, S.A., 2011, Evaluation of groundwater quantity and quality in the Kashan Basin, Central Iran, Desalination, 270 (1–3), pp. 23–30.

Jeevanandam, M., Kannan, R., Srinivasalu, S., Rammohan, V., 2007, Hydrogeochemistry and Groundwater Quality Assessment of Lower Part of the Ponnaiyar River Basin, Cuddalore District, South India, Environmental Monitoring and Assessment, Volume 132, Issue 1, pp 263–274.

Latif, M., Ahmad, M.Z., 2009, Groundwater and soil salinity variation in a canal command area in Pakistan, Irrigation and Drainage, 58: 456-468.

Lin, Y.W., Garcia, L., 2008, Development of a Hydro-Salinity Simulation Model for Colorado's Arkansas Valley, Journal of Irrigation and Drainage Engineering, Vol. 134, 757-767.

Lorenzen, G., Sprenger, C., Baudron, P., Gupta, D. and Pekdeger, A., 2012. Origin and dynamics of groundwater salinity in the alluvial plains of western Delhi and adjacent territories of Haryana State, India. Hydrological Processes, 26(15), pp.2333-2345.

Mahmood, K., Morris, J., Collopy, J. and Slavich, P., 2001. Groundwater uptake and sustainability of farm plantations on saline sites in Punjab province, Pakistan. Agricultural Water Management, 48(1), pp.1-20.

Misra, A.K. and Mishra, A., 2007. Study of quaternary aquifers in Ganga Plain, India: focus on groundwater salinity, fluoride and fluorosis. Journal of Hazardous Materials, 144(1), pp.438-448.

Morway, E.D., Gates, T.K., 2012, Regional assessment of soil water salinity across an intensively irrigated river valley, Journal of Irrigation and Drainage Engineering, Vol. 138, No. 5, 393-405.

Morway, E.D., Gates, T.K. and Niswonger, R.G., 2013. Appraising options to reduce shallow groundwater tables and enhance flow conditions over regional scales in an irrigated alluvial aquifer system. Journal of hydrology, 495, pp.216-237.

Narasimhan, T. N., A. F. White, and T. Tokunaga, 1986, Groundwater contamination from an inactive uranium mill tailings pile, 2, Application of a dynamic mixing model, Water Resour. Res., 22(13), 1820-1834.

Oosterbaan, R. J., 2005, SAHYSMOD (version 1.7a), Description of principles, user manual and case studies, International Institute for Land Reclamation and Improvement, Wageningen, Netherlands, 140.

Oster, J.D., Rhoades, J.D., 1975, Calculated drainage water composition and salt burdens resulting from irrigation with river waters in the western United States, Journal of Environmental Quality, 73-79.

Parkhust, D.L., Appelo, C.A.J., 2013, Description of Input and Examples for PHREEQC Version 3- A Computer Program for Speciation, Batch-Reaction, One-Dimensional Transport, and Inverse Geocehmical Calculations, Chapter 43 of Section A, Groundwater, Book 6, Modeling Techniques.

Parkhurst, D.L., Kipp, K.L., Engesgaard, Peter, and Charlton, S.R., 2004, PHAST—A program for simulating ground-water flow, solute transport, and multicomponent geochemical reactions: U.S. Geological Survey Techniques and Methods 6–A8, 154 p.

Parkhust D., Appelo, 1999, User's guide to PHREEQC (Version-2)-a computer program for speciation, batch-reaction, one-dimensional transport, and inverse geochemical calculations, USGS, Report 99(4259), 326.

Paz-García J., Johannesson, B., Ottosen, L., Ribeiro, A., Rodríguez-Maroto, J., 2013, Computing multi-species chemical equilibrium with an algorithm based on the reaction extents, Computers & Chemical Engineering, Vol: 58 pp: 135-143.

Pereira, L. S., Goncalves, J. M., Dong, B., Mao, Z. and Fang, S. X. 2007. "Assessing basin irrigation and scheduling strategies for saving irrigation water and controlling salinity in the upper Yellow River Basin, China." Agric. Water Mgmt., 93(3), 109 – 122.

Qureshi, A.S., McCornick, P.G., Qadir, M. and Aslam, Z., 2008. Managing salinity and waterlogging in the Indus Basin of Pakistan. Agricultural Water Management, 95(1), pp.1-10.

Rasouli, F., Pouya, A.K. and Šimůnek, J., 2013. Modeling the effects of saline water use in wheat-cultivated lands using the UNSATCHEM model. Irrigation science, 31(5), pp.1009-1024.

Rhoades, J.D., 1993, Electrical conductivity methods for measuring and mapping soil salinity, Adv. Agron. 49, 201-251.

Schoups, G., Hopmans, J.W., Young, C.A., Vrugt, J.A., Wallender, W.W., Tanji, K.K., and S. Panday (2005), Sustainability of irrigated agriculture in the San Joaquin Valley, California.

Proceedings of the National Academy of Sciences of the United States of America, 102(43), 15352-15356.

Shammas, M.I., Jacks, G., 2007, Seawater intrusion in the Salalah plain aquifer, Oman, Journal of Environmental Hydrology, Volume 15 Paper 19.

Sherif, M., Mohamed, M., Kacimov, A., Shetty, A., 2011, Assessment of groundwater quality in the northeastern coastal area of UAE as precursor for desalination, Desalination Volume 273, Issues 2–3, Pages 436–446.

Singh, A., Panda, S.N., 2012, Integrated salt and water balance modeling for the management of waterlogging and salinization; I: Validation of SAHYSMOD, Journal of Irrigation and Drainage Engineering, Vol. 138, 955-963.

Singh, N. T. 2005. Irrigation and soil salinity in the Indian subcontinent: Past and present. Lehigh Univ. Press, Bethlehem, PA.

Šimůnek, J., M. Šejna, and M. Th. van Genuchten, 2012, The UNSATCHEM Module for HYDRUS (2D/3D) Simulating Two-Dimensional Movement of and Reactions Between Major Ions in Soils, Version 1.0, PC Progress, Prague, Czech Republic, 54 pp.

Šimunek, J., Šejna, M ., Van Genuchten, MT, 2005, HYDRUS-1D, version 4.14, code for simulating the one-dimensional movement of water, heat, and multiple solutes in variably saturated porous media, Tech. rep., University of California Riverside.

Šimůnek, J., and D. L. Suarez, 1994, Two-dimensional transport model for variably saturated porous media with major ion chemistry, Water Resources Research, 30(4), 1115-1133.

Sparks, D.L., 2003, Environmental soil chemistry, Academic press, Second Edition.

Tafteh, A. and Sepaskhah, A.R., 2012. Application of HYDRUS-1D model for simulating water and nitrate leaching from continuous and alternate furrow irrigated rapeseed and maize fields. Agricultural Water Management, 113, pp.19-29.

Tweed, S.O., Leblanc, M., Webb, J.A. and Lubczynski, M.W., 2007. Remote sensing and GIS for mapping groundwater recharge and discharge areas in salinity prone catchments, southeastern Australia. Hydrogeology Journal, 15(1), pp.75-96.

Tavakoli Kivi, S., and Bailey, R. T. 2017. Modeling sulfur cycling and sulfate reactive transport in an agricultural groundwater system. Agric. Water Mgmt., 185(1), 78 – 92.

Truesdell, A.H., Jones, B.F., 1974, WATEQ-a computer program for calculating chemical equilibrium for natural waters, US Geological Survey.

Tuteja, N.K., Beale, G., Dawes, W., Vaze, J., Murphy, B., Barnett, P., Rancic, A., Evans, R., Geeves, G., Rassam, D., Miller, M., 2003, Predicting the effects of landuse change on water and salt balance—a case study of a catchment affected by dryland salinity in NSW, Australia, Journal of Hydrology, 283, 67-90.

Vaze, J., Beale, G.T.H., Barnett, P. and Tuteja, N.K., 2003, Predicting the spatial and temporal effects of landuse change using the CATSALT modelling framework. MODSIM 2003

Wagenet, R.J., and J.L. Hutson. 1987, LEACHM-Leaching estimation and chemistry model. Center Environ. Res., Cornell Univ., Ithaca, NY.

Wang, Y., Deng, C., Liu, Y., Niu, Z., and Li, Y. 2018. "Identifying change in spatial accumulation of soil salinity in an inland river watershed." Sci. Total Environ., 621, 177 – 185.

Wichelns, D., Qadir, M., Achieving sustainable irrigation requires effective management of salts, soil salinity, and shallow groundwater, 2015, Agricultural Water Management, 157, 31-38.

Yeh, G.T., Tripathi, V.S., Gwo, J.P., Cheng, H.P., Cheng, J.C., Salvage, K.M., Li, M.H., Fang, Y., Li, Y., Sun, J.T., Zhang, F., Siegel, M.D., 2004, HYDROGEOCHEM 5.0: A Three-Dimensional Model of Fluid Flow, Thermal Transport, and HYDROGEOCHEMical Transport through Variably Saturated Conditions, Oak Ridge National Laboratory

CHAPTER 2

MODELING SULFUR CYCLING AND SULFATE REACTIVE TRANSPORT IN AN AGRICULTURAL GROUNDWATER SYSTEM[1]

Highlights

Many irrigated agricultural areas worldwide suffer from salinization of soil, groundwater, and nearby river systems. Increasing salinity concentrations are due principally to a high water table that results from excessive irrigation, canal seepage, and a lack of efficient drainage systems, and lead to decreased crop yield. High groundwater salinity loading to nearby river systems also impacts downstream areas, where saline river water is diverted for application on irrigated fields. This study presents a physically-based, spatially-distributed groundwater reactive transport model that simulates the fate and transport of sulfate, the principal salt ion in many salt-affected watersheds, in an agricultural groundwater system. The model, developed from the UZF-RT3D model that simulates chemical species transport in variably-saturated subsurface systems, accounts for sulfur cycling (crop uptake, organic matter decomposition, mineralization/ immobilization) in the soil-plant system, oxidation-reduction reactions, including the oxidation of residual Sulfur in marine shale, and also the effect of dissolved oxygen and nitrate on sulfate chemical reduction. The model is tested at the small scale (i.e. soil profile) and at the regional scale (500 km^2) in the Lower Arkansas River Valley (LARV) in southeastern Colorado, an area acutely affected by salinization in the past few decades. Results demonstrate that although the major sulfate reactive transport processes are accounted for, the model consistently

[1] As published in *Agricultural Water Management*, Saman Tavakoli Kivi, Ryan T. Bailey, Used with permission, from *Agricultural Water Management* 185, 78-92

under-predicts measured soil and groundwater sulfate concentrations, pointing to the need for a comprehensive salinity module that accounts not only for advection, dispersion, sulfur cycling, and oxidation-reduction, but also salt ion equilibrium chemistry that includes the dissolution and precipitation of salt minerals in the soil-aquifer system. However, the model can be a useful tool to assess sulfate fate and transport in areas that are not dominated by salt mineral precipitation and dissolution.

2.1. Introduction

Salinization of soil and shallow groundwater is an almost inevitable problem in irrigated agricultural fields and a major challenge to sustain crop yield (Sparks, 2003, Gates et al.; 2002, Morway et al., 2012; Lin et al., 2008; Wichelns et al., 2015; Vaze et al., 2003, Hutmacher et al., 1996). Approximately one-fourth of all irrigated lands in the world are impaired by high salinity (Rhoades, 1993, Ghassemi et al., 1995), with the salt-affected area increasing by approximately 1 to 1.5 million ha each year (Barghouti and Le Moigne, 1991). Within the United States, approximately one third of irrigated land is impaired (Tanji, 1990). Salt accumulates in top soil due to the presence of salt minerals in the soil and evaporative-concentration, with the latter occurring particularly in areas of shallow groundwater (Gowing et al., 2009). Shallow water tables result from poor natural soil drainage, poorly designed artificial drainage systems, and excessive water application. Furthermore, irrigation water often has high concentrations of salts. Salinization occurs particularly in arid and semiarid regions, due to high potential evapotranspiration, low rainfall rates, and hence the need for irrigation.

Irrigation-induced salinity is the principal water quality problem in the semi-arid region of the western United States, due to the extensive background quantities of salt in rocks and soils (El-Ashry, 1985). Specific areas with acute salinity problems include the Colorado River Basin, with

the downstream areas of the Imperial Valley and the Coachella Valley experiencing the greatest salinity problems; the Rio Grande Basin of New Mexico and Texas; the Central Valley of California, particularly within the agriculturally-important San Joaquin Valley; the Yakima River Basin in Washington; the Snake River Basin in Idaho; and the Arkansas and South Platte River Basins in Colorado, Nebraska, Kansas, and Oklahoma.

High ions concentration not only has a significant effect in soil and aquifer systems, but also can cause serious damage to surface water areas such as wetlands. For example, elevated sulfate contamination impaired the Florida Everglades by stimulating production of methyl mercury (Corrales et al., 2011). The tail water runoff from the agricultural area of the Everglades discharge to the wetlands and causes the high sulfate concentration.

To assess the implementation of practices to remediate soil and groundwater salinization, application of different tools or methodologies needs to be considered. Numerous field strategies have been attempted, including improving on-farm water management (van der Leedenet al., 1975), lining irrigation canals to reduce seepage to the aquifer (van der Leeden et al., 1975; Singh and Panda, 2012), dry-drainage practices (Tuteja et al., 2003; Konukcu et al., 2006), controlled multi-level subsurface drainage systems (Ayars et al., 2006; Hornbuckle et al., 2007), and increasing groundwater pumping volume (Singh and Panda, 2012). Generally these practices focus on the scale of a single field or multiple fields.

Investigators also have used an assortment of process-based salinity mass balance models, such as UNSATCHEM-2D (Simunek and Suarez, 1994) which predicts the major ion chemistry (precipitation-dissolution, cation exchange, complexation) for small-scale soil-water systems; and SAHYSMOD (Oosternbaan, 2005; Singh and Panda, 2012), an integrated agro-hydro-salinity model which can be applied to large-scale agricultural fields and is based on seasonal

input data. SAHYSMOD has been applied to simulate the water and salt behavior in the semiarid irrigation area of Haryana State of India which has been impaired by - waterlogging and salinization for the last forty years (Singh et al., 2012). CATSALT (Tuteja and Vaze, 2003) is a distributed water balance model which is linked with the salt transport module. Tuteja et al., (2003) assessed the effect of landuse change on salt and water balance in Mandagery Creek catchment which is located in New South Wales of Australia using CATSALT. WATSUIT, a steady-state model which developed by Oster and Rhoades (1975), can calculate soil-water interaction with depth in the root zone. Gates et al. (2002), Burkhalter and Gates (2005), and Burkhalter et al. (2006) used a MODFLOW-MT3DMS (Zheng and Wang, 1999) model for groundwater flow and salinity transport in the Lower Arkansas River Valley in southeastern Colorado to estimate the effects of management practices such as reducing the recharge rate from irrigation, reducing seepage from irrigation canals, and installing sub-surface drainage systems. They used total dissolved solids (TDS) as a surrogate for salinity.

In regards to assessing salinity problems at the regional and basin scale, we present in this study a model that simulates the cycling of sulfur (S) and the related fate and transport of sulfate (SO_4) at multiple scales within an agricultural groundwater system. We focus on SO_4 since often it is the dominant ion in salt-affected groundwater. Reactive transport of S species is simulated using a reaction module imbedded in the UZF-RT3D model (Bailey et al., 2013a), a finite difference modeling code that simulates the transport of multiple interacting reactive chemical species in a variably-saturated groundwater environment. UZF-RT3D was developed by modifying RT3D (Reactive Transport in 3 Dimensions: Clement, 1997; Clement et al., 1998), a model that simulates reactive transport of multiple interacting chemical species in saturated groundwater systems, to include transport in the unsaturated zone. UZF-RT3D reads output

from MODFLOW-NWT (Niswonger et al., 2011) simulations that employ the UZF1 (Unsaturated Zone Flow) package (Niswonger et al, 2006). The model has been used successfully to simulate reactive transport of nitrate (NO_3) and selenium (Se) in irrigated groundwater systems (Bailey et al., 2014). Specific processes represented in the S module include organic matter decomposition and mineralization, oxidation-reduction reactions, and mass inputs/outputs such as infiltrated irrigation fertilizer, canal seepage, groundwater pumping, and plant mass cycling. The model also accounts for the effect of dissolved oxygen (O_2) and nitrate (NO_3), and includes the fate and transport of selenium (Se) species as a constraint on the S cycling and transport parameter values.

The use of the model is demonstrated through application to a small-scale site (soil profile) and a regional-scale area (500 km^2) within the Lower Arkansas River Valley (LARV) in southeastern Colorado, where significant salinization has occurred in recent decades. To our knowledge, this is the first attempt at simulating S cycling in a reactive transport model, and at simulating SO_4 reactive transport at the regional scale. This study serves as a first step in representing salt chemistry in a regional-scale agricultural groundwater system. Following a presentation of S cycling and transport in soil and groundwater systems and its inclusion in UZF-RT3D, the application of the model to the study area will be presented.

2.2. Sulfur Cycling and Reaction Module for UZF-RT3D

2.2.1. Sulfur Cycling in Agricultural Subsurface Systems

The principal processes governing S cycling in the soil and groundwater zone of an agricultural area are presented in Figure 1.1. Cycling of S mass occurs as organic S is incorporated into soil organic matter, composed of litter (fast-decomposing) and humus (slow-decomposing), via plowing; mineralized to SO_4; and then taken up by crop roots during the growing season. S and SO_4 mass also are added to the subsurface via fertilizer, irrigation water,

and canal seepage. SO_4 can be chemically reduced via a microbially-mediated reaction (Frind et al., 1990):

$$SO_4^{2-} + 2C_{org} + 2H_2O \rightarrow 2HCO_3^- + H_2S \quad (1)$$

This reaction, however, is inhibited by the presence of O_2 and NO_3 due to the succession of terminal electron (e^-)-acceptor processes. Furthermore, SO_4 can released from pyrite (FeS_2) via autotrophic reduction of O_2 and NO_3 (Frind et al., 1990; Postma et al., 1991; Pauwels et al., 1998):

$$2FeS_2 + 7O_2 + 2H_2O \rightarrow 2Fe^{2+} + 4SO_4^{2-} + 4H^+ \quad (2a)$$

$$5FeS_2 + 14NO_3^- + 4H^+ \rightarrow 5Fe^{2+} + 10SO_4^{2-} + 7N_2 + 2H_2O \quad (2b)$$

This process is represented in Figure 2.1. Pyrite often can be found in Cretaceous marine shale.

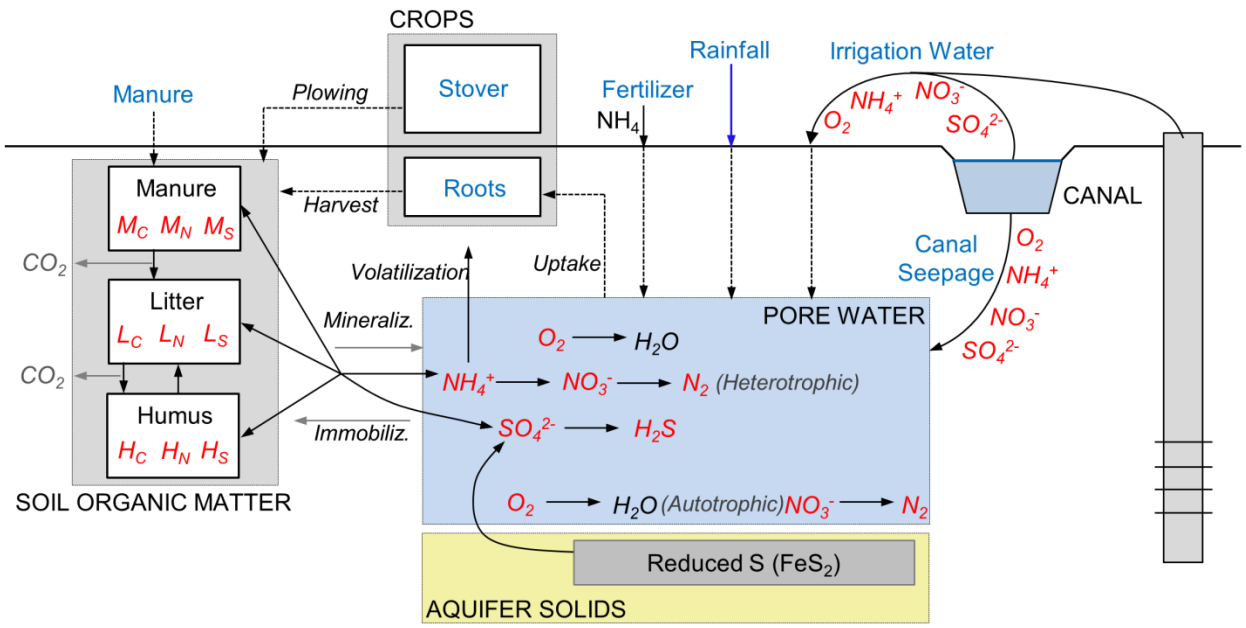

Figure 2.1. Sulfur cycling in soil and groundwater system in an agricultural area, including plant mass inputs/output, organic matter decomposition, mineralization/immobilization, and oxidation-reduction reactions.

2.2.2. Sulfur Reaction Module for UZF-RT3D

2.2.2.1. Mass Balance Equations

The S reaction module for UZF-RT3D consists of mass balance equations, chemical reaction rate laws, and sources and sinks of S mass (fertilizer loading, crop uptake, and loading in irrigation water and canal seepage) that are typical of agricultural systems. A glossary of model parameter terms is included at the end of the chapter for reference. UZF-RT3D solves a system of advection-dispersion-reaction (ADR) equations for both dissolved-phase and solid-phase species in variably-saturated groundwater systems using a finite difference approach (Bailey et al., 2013a):

$$\frac{\partial(C_k\theta)}{\partial t}R_k = -\frac{\partial}{\partial x_i}(\theta v_i C_k) + \frac{\partial}{\partial x_i}\left(\theta D_{ij}\frac{\partial C_k}{\partial x_j}\right) + q_f C_{f_k} + \theta r_f \qquad k = 1,2,...,m \tag{3a}$$

$$\frac{\partial(C_l\varepsilon)}{\partial t} = \alpha_l P_s + \varepsilon r_s \qquad l = 1,2,...,n \tag{3b}$$

where C is solute concentration [$M_f L_f^{-3}$], with f denoting fluid phase; D_{ij} is the hydrodynamic dispersion coefficient [L^2T^{-1}]; v is the pore velocity [L_bT^{-1}] with b denoting the bulk phase; θ is the volumetric water content [$L_f^3 L_b^{-3}$]; q_f is the volumetric flux of water representing sources and sinks [$L_f^3T^{-1}L_b^{-3}$] such as irrigation water, canal and seepage, groundwater discharge to the river, or pumped groundwater; C_f is the concentration of solute in the source or sink water [$M_f L_f^{-3}$]; r_f represents the rate of all reactions that occur in the dissolved phase [$M_f L_f^3 T^{-1}$]; ε is the volumetric solid content [$L_s^3 L_b^{-3}$] with s denoting the solid phase, and is equal to $1-\phi$, with ϕ representing porosity; and R_j is the retardation factor for species j and is equal to $1+(\rho_b K_{dj})/\theta$,

where ρ_b is the bulk density of the porous media [$M_b L_b^{-3}$] and K_{dj} is the partitioning coefficient [$L_f^{-3} M_b$]. UZF-RT3D uses output from a MODFLOW-NWT (Niswonger et al., 2011) that uses the Unsaturated Zone Flow (UZF1) package (Niwsonger et al., 2006) for *v* and q_f.

Using the form of the ADR equation in Equation 3a, the following equations are written for SO_4-S (dissolved-phase), S in the litter pool (L_S), S in the humus pool (H_S), and S in the manure pool (M_S), with the latter three solid-phase species:

$$\frac{\partial\left(C_{SO_4-S}\theta\right)}{\partial t}R_{SO_4-S} = -\frac{\partial}{\partial x_i}\left(\theta v_i C_{SO_4-S}\right)+\frac{\partial}{\partial x_i}\left(\theta D_{ij}\frac{\partial C_{SO_4-S}}{\partial x_j}\right)+q_f C_{f_{SO_4-S}}+F_{SO_4-S}-U_{SO_4-S}+\varepsilon\left(r_{s,S}^{min}-r_{s,S}^{imm}\right) + \theta\left(r_{f,SO_4-S}^{auto}-r_{f,SO_4-S}^{het}\right) \tag{4a}$$

$$\frac{\partial\left(C_{L_S}\varepsilon\right)}{\partial t} = \alpha_{Rt,S}P_{Rt}+\alpha_{St,S}P_{St}+\varepsilon\left(r_{s,S(H\to L)}^{dec}+r_{s,S(M\to L)}^{dec}+r_{s,S(L\to L)}^{dec}-r_{s,S(L)}^{dec}\right) + \varepsilon\left(r_{s,S(L)}^{imm}-r_{s,S(L)}^{min}\right) \tag{4b}$$

$$\frac{\partial\left(C_{H_S}\varepsilon\right)}{\partial t} = \varepsilon\left(r_{s,S(L\to H)}^{dec}-r_{s,S(H)}^{dec}\right)+\varepsilon\left(r_{s,S(H)}^{imm}-r_{s,S(H)}^{min}\right) \tag{4c}$$

$$\frac{\partial\left(C_{M_S}\varepsilon\right)}{\partial t} = M_S-\varepsilon r_{s,S(M)}^{dec}+\left(r_{s,S(M)}^{imm}-r_{s,S(M)}^{min}\right) \tag{4d}$$

For the SO_4-S equation (Equation 4a), *F* is the inorganic fertilizer application rate of S [$M_f L_b^{-3} T^{-1}$]; *U* is the uptake rate [$M_f L_b^{-3} T^{-1}$]; *min* and *imm* signify mineralization and immobilization, respectively; and *auto* and *het* represent autotrophic and heterotrophic chemical reduction, respectively. Release of SO_4-S from FeS_2 via autotrophic reduction of O_2 and NO_3 occur according to Equation 2, and are represented in Figure 2.1 as reduced S transferred to SO_4-S in the pore water.

For Equations (4b-d), r_s represents the rate of all reactions that occur in the solid phase [$M_S L_s^{-3} T^{-1}$]; P_{Rt} and P_{St} are the mass application rates of root and after-harvest stover mass, respectively, that are plowed into the soil; $\alpha_{Rt,S}$ and $\alpha_{St,S}$ are the portions of the root and stover mass attributed to S, respectively; the super-script *dec* signifies organic matter decomposition; and *L*, *H*, and *M* in the subscript of each term represent the litter, humus, and manure pool, respectively, with the arrow representing the direction of mass flow during the decomposition process.

Due to the influence of O_2 and NO_3 on the fate and transport of SO_4-S, UZF-RT3D also solves mass balance equations for NH_4, NO_3, and O_2, and includes C and N cycling using similar equations to Equations (4b-d), after Birkinshaw and Ewen (2000). As will be shown in later sections of this chapter, the chemical parameters governing the release of SO_4-S from marine shale formations must be constrained by their associated influence on the release of selenate (SeO_4-Se). Therefore, the fate and transport of Se species, including SeO_4, also is included. The Se reaction module for UZF-RT3D is described in Bailey et al. (2013b). Besides N fertilizer loading, uptake of NH_4, NO_3, and SeO_4-Se, specific reactions included for these additional species include nitrification, NH_4 volatilization, heterotrophic denitrification, and chemical reduction of SeO_4.

2.2.2.2. Sulfur Transformation Processes

The reaction rates governing S in the solid phase, i.e. the r_s terms in Equations 4b-d, are now presented. They are analogous to the reaction rates governing Se in the solid phase (Bailey et al., 2013b). Rate expressions defining the decomposition of L_S, H_S, M_S and inter-pool mass transfers are:

$$
\begin{aligned}
r^{dec}_{s,S(H)} &= \lambda_H C_{H_S} E \\
r^{dec}_{s,S(H\to L)} &= \lambda_H \left(C_{H_S} / H_{C/S} \right) f_e E \\
r^{dec}_{s,S(M)} &= \lambda_M C_{M_S} E \\
r^{dec}_{s,S(M\to L)} &= \lambda_M \left(C_{M_S} / B_{C/S} \right) E \\
r^{dec}_{s,S(L)} &= \lambda_L C_{L_S} E \\
r^{dec}_{s,S(L\to H)} &= \lambda_L \left(C_{L_S} / B_{C/S} \right) f_e f_h E \\
r^{dec}_{s,S(L\to L)} &= \lambda_L \left(C_{L_S} / B_{C/S} \right) f_e \left(1 - f_h \right) E
\end{aligned}
\qquad (5)
$$

where λ_L, λ_H, λ_M are the first-order rate constants for litter, humus, and manure decomposition [T^{-1}], respectively, and the remaining terms are defined in the Appendix. E (environmental reduction factor) scales the reaction rates due to current θ and soil temperature T.

2.2.2.3. Rate Law Expressions

The microbial-mediated chemical reduction of SO_4 (Equation 1) is represented by the term r^{het}_{f,SO_4} in Equation (4a) and is simulated by the following rate law expression:

$$
r^{het}_{f,SO_4-S} = \lambda^{het}_{SO_4-S} C_{SO_4-S} \left(\frac{CO_{2,prod}}{K_{CO_2} + CO_{2,prod}} \right) \left(\frac{I_{O_2}}{I_{O_2} + C_{O_2}} \right) \left(\frac{I_{NO_3}}{I_{NO_3} + C_{NO_3}} \right) \left(\frac{I_{SeO_4}}{I_{SeO_4} + C_{SeO_4}} \right) E \qquad (6)
$$

where K_j is the Monod half-saturation constant for species j [$M_f L_f^{-3}$]; I_{O_2}, I_{NO_3}, and I_{SeO_4} are the O_2, NO_3, and SeO_4 inhibition constants [$M_f L_f^{-3}$] signifying the species concentration at which lower-redox species can undergo appreciable rates of reduction; and $CO_{2,prod}$ is the total amount of CO_2 produced during decomposition of L_C, H_C, M_C and is used as an indicator of available OC for microbial consumption (Birkinshaw and Ewen, 2000). Similar expressions are written for the chemical reduction of O_2, NO_3, and SeO_4, with denitrification inhibited by the presence of O_2, and SeO_4 reduction inhibited by the presence of both O_2 and NO_3.

The oxidation of reduced S in FeS_2 to SO_4 is represented by the term r_{f,SO_4}^{auto} in Equation (4a), and is simulated by calculating the rate of autotrophic reduction of O_2 and NO_3 (Equation 7) and then using these results and the stoichiometry of Equation (1):

$$r_{f,O_2}^{auto} = \lambda_{O_2}^{auto} C_{O_2} \left(\frac{C_{O_2}}{K_{O_2} + C_{O_2}} \right) \tag{7}$$

$$r_{f,NO_3}^{auto} = \lambda_{NO_3}^{auto} C_{NO_3} \left(\frac{C_{NO_3}}{K_{NO_3} + C_{NO_3}} \right) \left(\frac{I_{O_2}}{I_{O_2} + C_{O_2}} \right) \tag{8}$$

$$r_{f,SO_4-S}^{auto} = r_{f,O_2}^{auto} \left(\frac{\xi - 1}{\xi} \right) Y_{S:O_2} + r_{f,NO_3}^{auto} \left(\frac{\xi - 1}{\xi} \right) Y_{S:NO_3} \tag{9}$$

where $Y_{S:O_2}$ is the mass of S produced for O_2 consumed in Equation (2a), $Y_{S:NO_3}$ is the mass of S produced for NO_3 consumed in Equation (2b), and ξ is the ratio of S to Se in the shale material, recognizing that a small portion of both O_2 and NO_3 releases SeO_4 in addition to than SO_4. Referring to Equation (2), $Y_{S:O_2}$ is equal to 0.57 (128.2 g / 224.0 g) and $Y_{S:NO_3}$ is equal to 1.64 (320.7 g / 196.0 g). These equations assume that FeS_2 is in limitless supply in any shale material.

2.3. Model Application: Arkansas River Valley, Southeastern Colorado

The functionality of the S module for UZF-RT3D is demonstrated for two study sites in the Arkansas River Valley in southeastern Colorado. The first application is at a test field at the Arkansas Valley Research Center (AVRC) near Rocky Ford, CO, and the second application is for a 500 km^2 regional groundwater system in the same area. For each application, N and Se species fate and transport are included in the model simulations.

2.3.1. Field Scale Application

2.3.1.1. Study Site and Data Collection

The fate and transport of S species using UZF-RT3D is first demonstrated for two corn test fields at the AVRC (see Figure 2.2). A similar model application for the Se module of UZF-RT3D has been performed previously (Bailey et al., 2013b). For the 2009 growing season, the test fields received fertilizer (280.8 kg/ha of N, 20 kg/ha of S) seven days before planting (April 27, 2009), with irrigation water from a nearby canal applied 9 times between June 17 and August 10, with an average applied depth of 9.5 cm. The runoff (i.e. tail water) fraction is approximately 5%. The irrigation water was analyzed for C_{NH_4} and C_{NO_3} using a continuous flow analyzer QuickChem (Lachat Quickchem FIA+8000 Series, Lachat Instruments), and $C_{SO_4\text{-}S}$, $C_{SeO_4\text{-}Se}$, and C_{O_2} were measured in the canal from which the irrigation water was taken. Canal samples were collected using a peristaltic pump, filtered through disposable in-line 0.45 μm capsule filters, placed in 0.12 L bottles, acidified, stored on ice and sent to the Olson Biochemistry Laboratories (South Dakota State University, Brookings, SD, USEPA certified) for Se analysis and to Ward Laboratories, Inc. in Kearney, NE for SO_4. For Se, the laboratory used the Official Methods of Analysis of AOAC International, 17th edition, test number 996.16 Selenium in Feeds and Premixes, Fluorometric Method. For SO4, the laboratory used Method 375.4 (USEPA, 1983). $C_{SO_4\text{-}S}$ was 104.0 mg/L for the first four irrigation events (6/17/2009 to 7/4/2009) and 107.0 mg/L for the last five irrigation events (7/10/2009 to 8/10/2009). C_{O_2} was measured during sample collection using a calibrated YSI 600QS Multiparameter Sampling System. Values of $C_{SeO_4\text{-}Se}$, C_{NH_4}, C_{NO_3}, and C_{O_2} in the irrigation water for each irrigation event are presented in Bailey et al. (2013b).

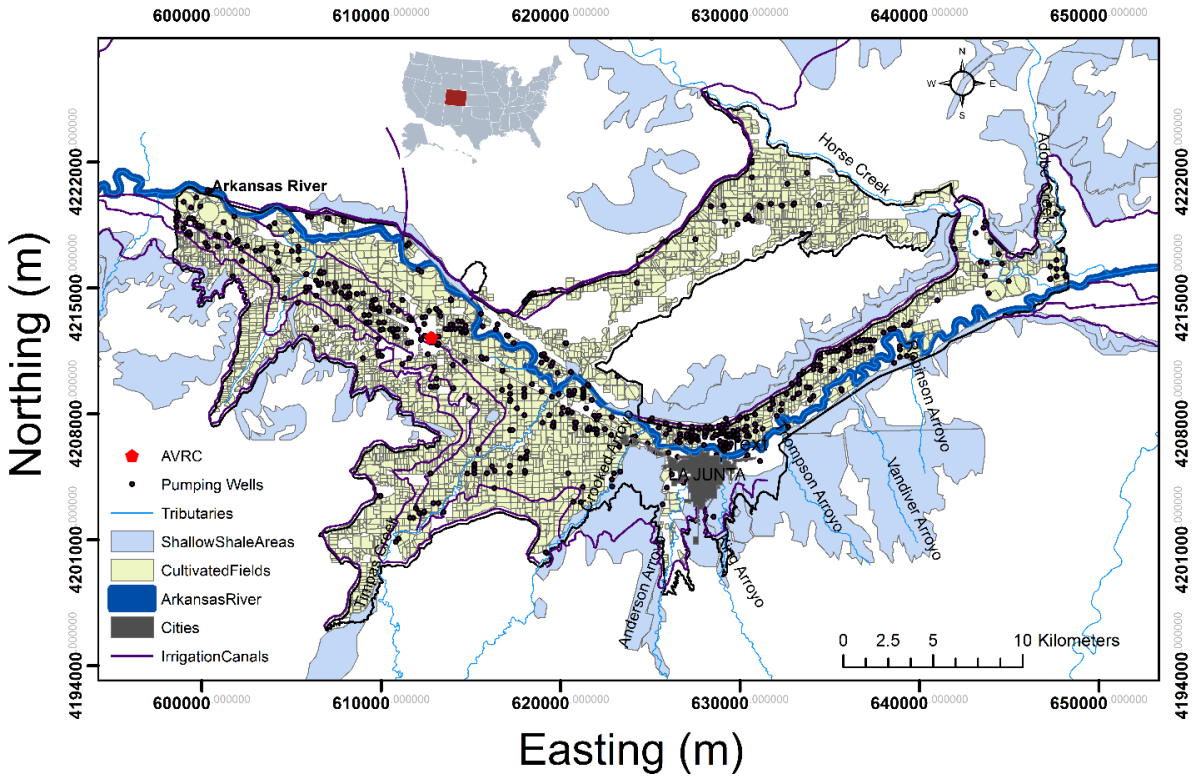

Figure 2.2. Location of the study region, showing the Arkansas River and its tributaries, irrigation canals, and cultivated fields.

Soil samples were collected from the field in October 2009, just after the corn had been harvested, to test for $C_{SO_4\text{-}S}$ of the soil water. These concentration values were used to test the output from UZF-RT3D (see Section 3.1.2). Soil was sampled at 7 depths (0.15 m, 0.30 m, 0.61 m, 0.91 m, 1.22 m, 1.52 m, and 1.83 m) using a hand auger, placed on ice, and then transported to the USDA Natural Resources Research Center in Fort Collins, CO for analysis using saturated paste extracts. Samples were air-dried, ground, passed through a 2-mm sieve, and then mixed with water to create a saturated paste. A 80 kPa vacuum was applied to extract the soil water, which was sent to Olson Laboratories for analysis. Measured $C_{SO_4\text{-}S}$ in the soil water, along with C_{NH_4}, C_{NO_4}, and C_{SeO_4} as measured according to the methods described in Bailey et al. (2013b), is presented in Section 3.1.3 along with model results.

2.3.1.2. UZF-RT3D Model Setup

The UZF-RT3D model using the S module was applied to the two test fields at the AVRC. The finite difference grid had one column and seven layers, with each layer corresponding to a depth at which the soil was sampled for easy comparison between observed and simulated results. For unsaturated zone flow, a MODFLOW-UZF model was constructed with forcing terms consisting of daily precipitation, irrigation water from the nine irrigation events, and daily ET. Porosity was set to 0.45, saturated hydraulic conductivity to 0.15 m/d, residual water content to 0.20, the Brooks-Corey exponent to 5.0, and the ET extinction depth to 1.2 m, based on the estimated rooting depth of the corn. Daily ET depths were calculated using the Penman-Monteith reference ET equation (Allen et al., 2005), with climate data measured at the AVRC weather station.

Using the 1D vertical flow field generated by MODFLOW-UZF, an ensemble of 200 UZF-RT3D simulations were run in a Monte Carlo simulation approach to determine the influence of model parameters and forcing terms on the resulting SO_4 concentration in the soil profile. Since no apparent difference exists between the cultivation and irrigation practices at the two test fields, the results of the ensemble are applied to both fields. The model parameters used in the simulations are shown in Table 2.1, with the corresponding values of coefficient of variation (CV) provided for factors that were perturbed in the ensemble of model runs. The CV was selected according to the resulting range of parameter values, with these ranges verified either through literature review or by Dr. Michael Bartolo at the AVRC (personal communication, June 2010). For example, rooting depth $d_{rt,max}$ ranges between 1.10 m and 1.39 m, seasonal S uptake S_{up} ranges from 5.9 kg/ha to 13.9 kg/ha, and SO_4 reduction rate $\lambda_{SO_4}^{het}$ ranges from 0.001 d^{-1} to 0.074 d^{-1}. Parameters governing cycling and transport of C, N, and Se species that are also used

in the UZF-RT3D simulations are presented as Table S1 in Supplementary Data in Appendix A. Each model simulation was run for 10 years, with the input data for 2009 repeated 10 times to eliminate bias from initial conditions. Results shown in the next section are only for the final year of the simulation.

Table 2.1. Agricultural management, crop, and chemical reaction parameter symbols, units, and values for the field-scale model application at the AVRC near Rocky Ford, CO. For parameters that are perturbed during the Monte Carlo simulations, the coefficient of variation (CV) value also is shown. Parameter for other species (O_2, NO_3, NH_4, Se) are presented as Table S1 in Supplementary Data.

Parameter	Units	Mean Value	CV*
Agricultural Management & Parameters			
Planting Day	-	27-Apr	-
Harvest Day	-	10-Oct	-
Plowing Day	-	7-Nov	-
d_{pw}	m	1.0	0.05
F_{NH_4}	kg ha^{-1}	280.8	-
F_S	kg ha^{-1}	20.0	-
P_{Rt}	kg ha^{-1}	500	0.05
$\alpha_{Rt,S}$	-	0.0035	-
P_{St}	kg ha^{-1}	5616	0.05
$\alpha_{St,S}$	-	0.0023	-
Crop Parameters			
$d_{rt,max}$	m	1.20	0.05
S_{up}	kg ha^{-1}	10.0	0.15
Irrigation Water			
$C_{SO_4-S,\text{Canal}}$	mg/L	104.0 / 107.0	15
Chemical Reaction Parameters			
Q_{10}	-	2.5	-
T_B	^{0}C	20.0	-
Organic Matter Decomposition			
λ_H	d^{-1}	0.003	0.5
λ_L	d^{-1}	0.25	0.5
f_e	-	0.5	-
f_h	-	0.2	-
$H_{C/S}$	-	120	-
$B_{C/S}$	-	80	-
Oxidation-Reduction			
$\lambda_{SO_4}^{het}$	d^{-1}	0.01	0.2
ξ	-	3000	-
I_{NO_3}	mg/L	0.5	-
I_{O_2}	mg/L	1.0	-
K_{CO_2}	mg/L	0.75	-

* For Monte Carlo simulation

2.3.1.3. Results and Discussion

Basic results from one of the model simulations of the ensemble are shown in Figure 2.3. Figure 2.3A shows the daily simulated water content θ by the MODFLOW-UZF model throughout 2009; Figure 2.3B shows daily simulated mass (g) of SO_4-S reduced (see Equation 1), the mass of organic S mineralized to SO_4-S, and the S uptake by crops (in the form of SO_4); and Figure 2.3C shows the daily mass (g) of CO_2 produced due to organic matter decomposition. The temporal patterns of each system response are dependent on the cultivation practices, with the sharp increases in θ during June and July due to the 9 irrigation events and the daily SO_4-S uptake increasing during June and the slowly decreasing in magnitude during the remainder of the growing season. Mineralization of organic S to SO_4-S decreases during the growing season, but increases sharply after the Harvest (October 10) and Plowing (November 7) days, when stover and dead root mass are plowed back into the soil, providing new inputs of organic S to be mineralized during the late fall and winter seasons.

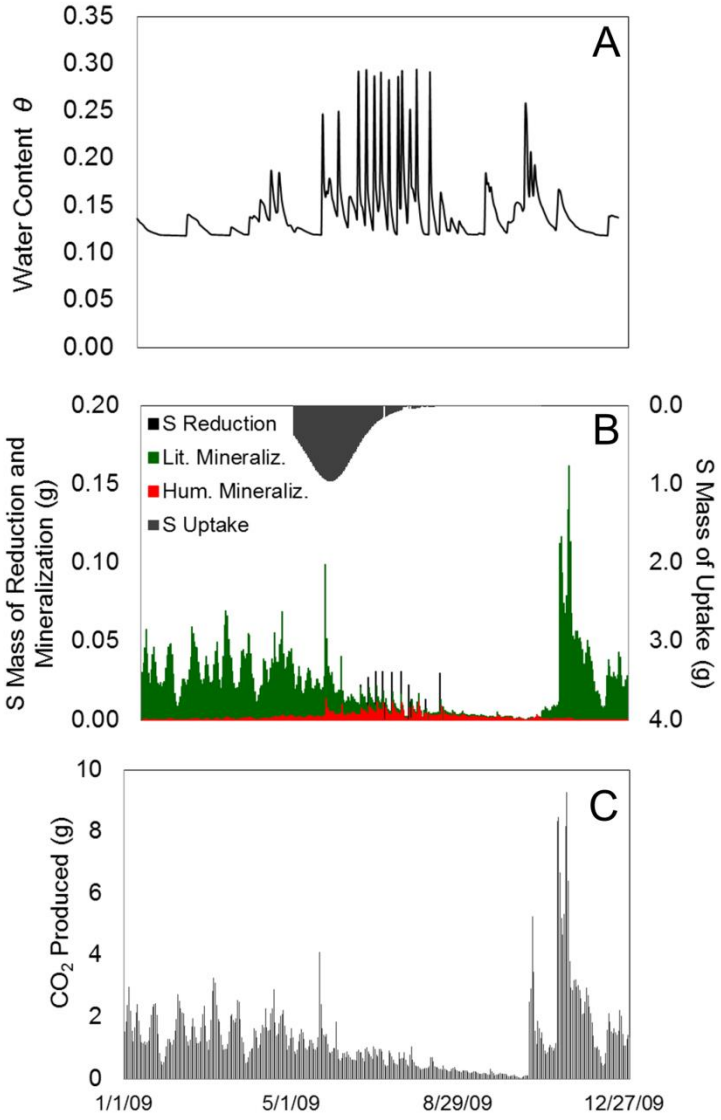

Figure 2.3. Daily time series of (A) soil water content, (B) mass of SO_4 reduction, mineralization, and crop uptake, and (C) and CO_2 produced during organic matter decomposition during 2009, as simulated by the UZF-RT3D S module for the test fields at the Arkansas Valley Research Center.

The simulated time series of $C_{NH_4\text{-}N}$, $C_{NO_3\text{-}N}$, and $C_{SeO_4\text{-}Se}$ in Layer 1 throughout the year are shown in Figure 2.4 (A, B, C) for each of the 200 simulations of the ensemble. These are provided for context of the SO_4 model results analysis. The average of the ensemble is shown with a solid red line. Particularly for $C_{NH_4\text{-}N}$ and $C_{NO_3\text{-}N}$, there is a high degree of scatter across the simulations due to changes in rates of nitrification, denitrification, and N crop uptake. The sharp increase in concentration is due to N fertilizer loading just before and after the planting day

(April 27). The dynamic fluctuations in concentration during June and July are due to irrigation events, with additional N mass brought into the soil profile with the irrigation water and leaching to the lower layers also occurring. There is far less scatter in the $C_{SeO_4\text{-}Se}$ ensemble, with all simulations dominated by the SeO_4 mass brought into the soil profile with the irrigation events.

The time series of $C_{SO_4\text{-}S}$ in Layer 1 (Figure 2.4D) closely resembles the plot for $C_{SeO_4\text{-}Se}$, except that $C_{SO_4\text{-}S}$ increased sharply near the planting day due to the application of S in the fertilizer. There is only slight scatter in $C_{SO_4\text{-}S}$ between the simulations of the ensemble, with slightly more scatter in Layer 3 (Figure 2.4E) and Layer 5 (Figure 2.4F). From these results, it appears that $C_{SO_4\text{-}S}$ in the soil water is not sensitive to changes in the general crop parameters that were varied in the ensemble (see Table 2.1): plowing depth d_{pw}; root and stover mass plowed into the soil, P_{Rt} and P_{St}; rooting depth $d_{rt,max}$; rate of litter pool and humus pool decomposition, λ_L and λ_H; and the parameters governing N and Se species (see Table S1 in Supplementary Data in Appendix A), such as N_{up} and $\lambda_{NO_3}^{het}$.

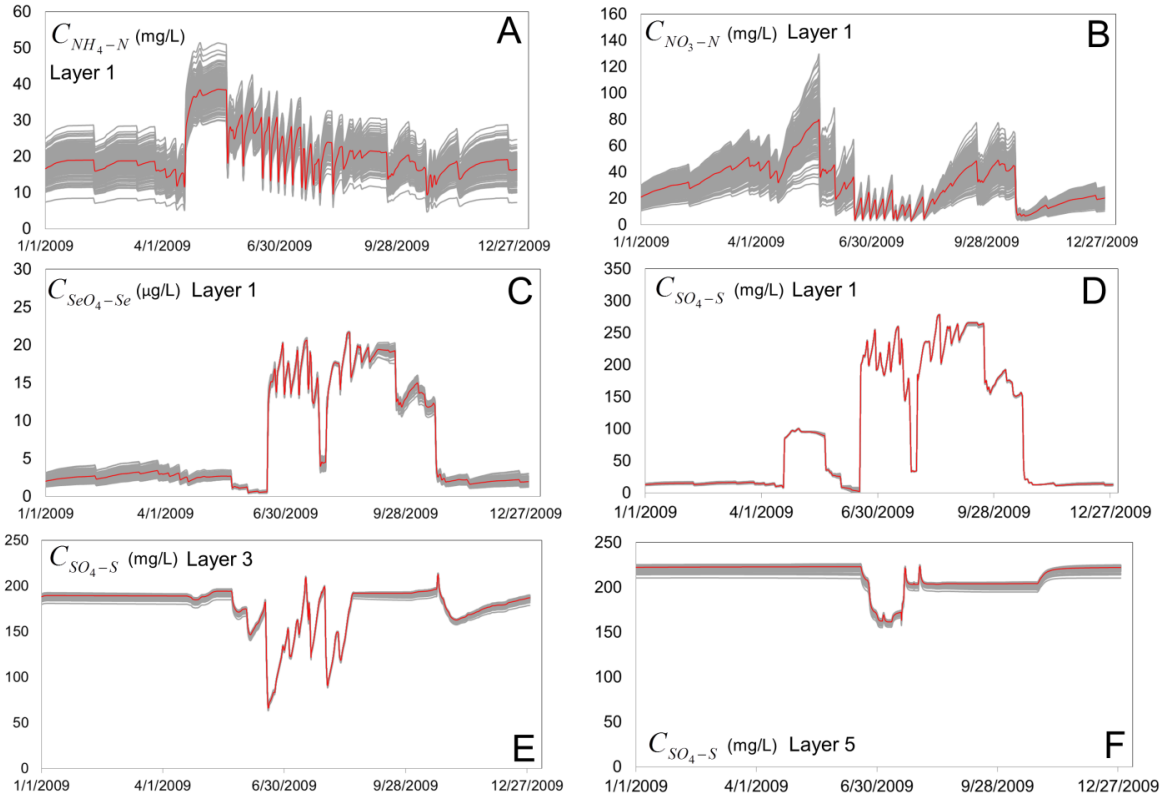

Figure 2.4. Time series of daily concentrations simulated by UZF-RT3D for the AVRC field study site: (A) NH_4-N in layer 1 of the model (0.15 m depth in the soil profile), (B) NO_3-N in layer 1, (C) SeO_4 in layer 1, and SO_4 in (D) Layer 1, (E) Layer 3 (0.6 m depth), and (F) Layer 5 (1.2 m) of the model. For (A) and (B), the large fluctuations in concentration during the summer months are due to N input due to fertilizer and N-laden irrigation water followed by leaching events. During the fall months (September through November), NO_3-N increases due to nitrification of NH_4 and mineralization of organic N, with the latter plowed into the soil after harvest. For (C) and (D), SeO_4 and SO_4 enter the soil profile due to irrigation events, with irrigation water containing both SeO_4 and SO_4. The same occurs for layers (E) 3 and (F) 5, as the layer receives leached SO_4 from the above layers.

The relationship between several of these parameters and the resulting $C_{SO_4\text{-}S}$ is explored visually in Figure 2.5 (D, E, F), showing the parameter value and concentration value for each of the 200 simulations. Factors initially thought to govern $C_{SO_4\text{-}S}$, specifically seasonal uptake of S (S_{up}) and the SO_4 concentration of the irrigation water ($C_{SO_4,Canal}$), also are shown (Figure 2.5G, H), with no significant trend. The only parameter that has a strong trend is the rate of SO_4 chemical reduction λ_{SO_4}, with results shown in Figure 2.5A, B, and C for Layer 1, 4, and 7, respectively. The R^2 value for these three layers is 0.94, 0.93, and 0.89.

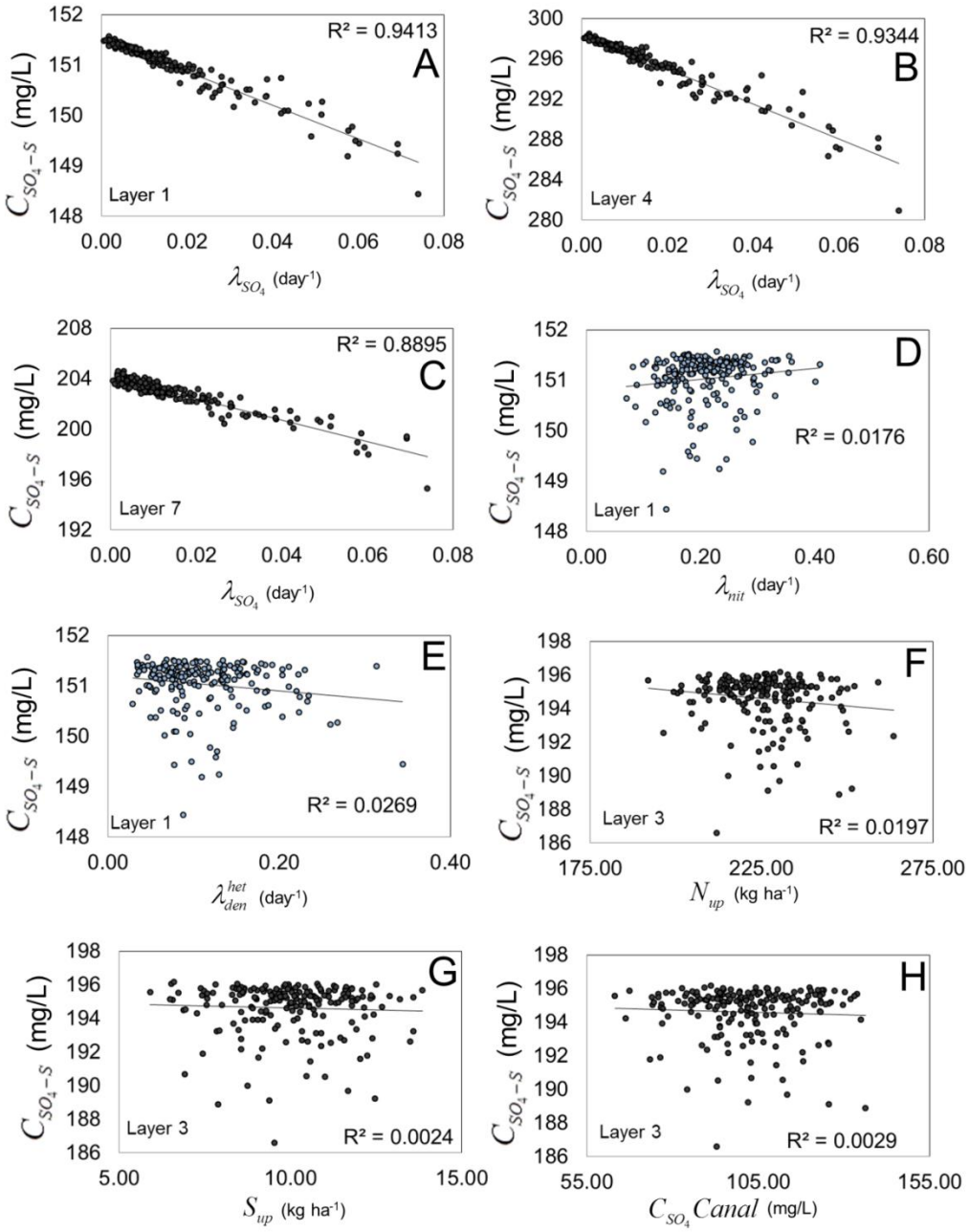

Figure 2.5. Selected scatter-plot relationships between λ_{SO_4} (first-order reduction rate of SO_4) and C_{SO4} in (A) Layer 1, (B) Layer 4, and (C) Layer 7; and between C_{SO4} and (D) λ_{nit} (first-order nitrification rate), (E) λ_{den}^{het} λ_{den}^{het} (first-order rate of heterotrophic denitrification), (F) N_{up} (seasonal application rate of N fertilizer), (G) S_{up} (seasonal application rate of SO_4) and (H) $C_{SO4,Canal}$ (concentration of SO_4 in the canal water, which is the source of the irrigation water).

The lack of substantial influence of model parameters on $C_{SO_4\text{-}S}$ in the soil water is further displayed in Figure 2.6, which shows the ensemble of concentration values with depth in the soil

profile, as compared to the observed values from both test fields. The average values of the ensemble are shown with a solid red line. It should be noted that since observed values were obtained using saturated paste extracts, concentrations correspond to a saturated soil environment. Accordingly, the model results shown in Figure 2.6 were obtained by multiplying simulated $C_{SO_4\text{-}S}$ by the ratio of water content to porosity (θ/ϕ). While there is noteworthy scatter between the two test fields, e.g. 492 mg/L in Field 1 and 320 mg/L in Field 2 at a depth of 1.2 m, the model ensemble has minimal scatter and each simulation greatly under-estimates $C_{SO_4\text{-}S}$ in the soil water, particularly in the upper layers of the soil profile. For the entire profile, average $C_{SO_4\text{-}S}$ for the model ensemble, Field 1, and Field 2 are 84 mg/L, 406 mg/L, and 356 mg/L. In contrast, simulated $C_{NO_3\text{-}N}$ and $C_{SeO_4\text{-}Se}$ match much more closely with observed values (Bailey et al., 2013b).

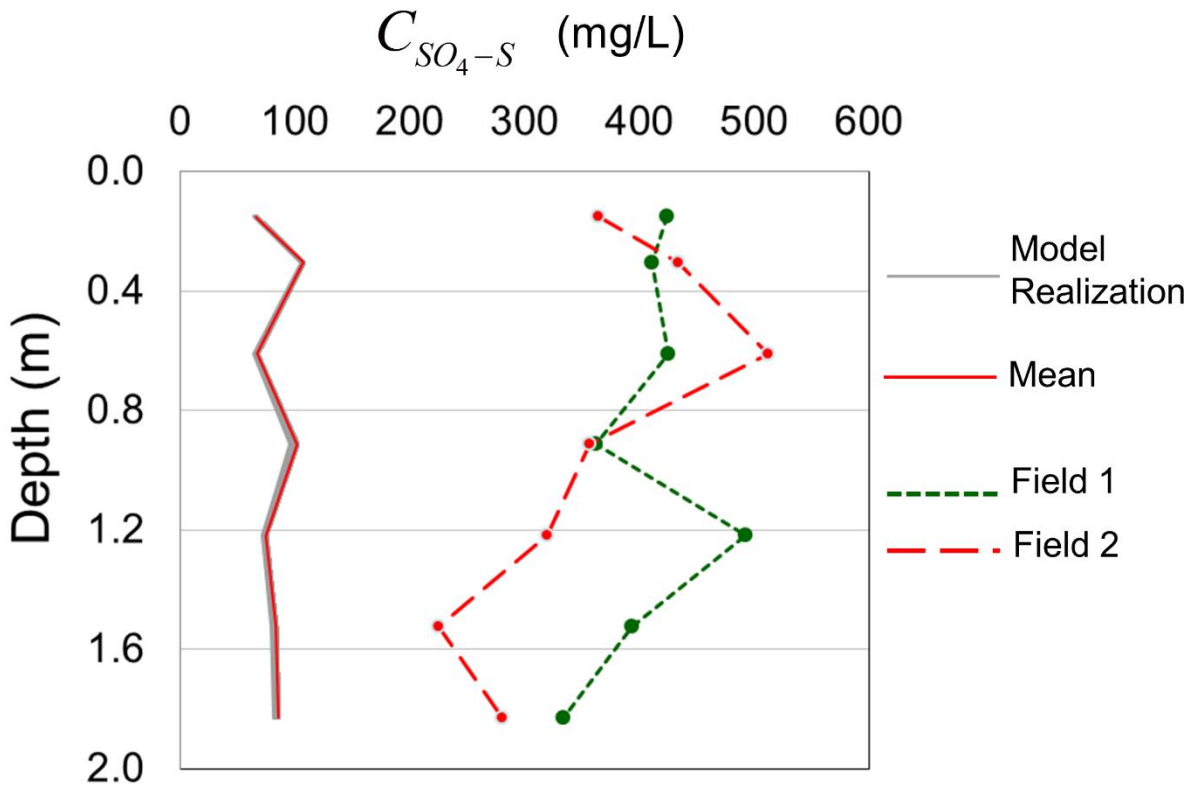

Figure 2.6. Observed and simulated concentrations of SO4-S with depth for the test field at the Arkansas Valley Research Center. The observed concentrations are shown with dashed lines, the ensemble of model simulations is shown with gray lines, and the mean of the ensemble is shown with a solid red line. While there is significant scatter between the two test fields, the model consistently under-estimates C_{SO_4} in the soil water, particularly in the upper layers of the soil profile.

With perturbing model parameters producing little effect on the individual UZF-RT3D simulations, modifying parameter values cannot lead to an improved match between observed and simulated values, pointing to a deficiency in the numerical model itself. We hypothesize that this deficiency is due to the absence of salt ion equilibrium chemistry in the model, particularly the process of mineral dissolution and precipitation, highlighting the importance of this process in the study area. A recent study (Cooper, 2006) demonstrated that gypsum is prevalent in the soil throughout the LARV. In addition, the USDA's SSURGO database indicates that both calcite and gypsum are present in the soil at varying degrees (approximately 0-10% dry weight) throughout the study region.

2.3.2. Regional Scale Application

2.3.2.1. Study Area Description

The second application of the S module of UZF-RT3D is to a 500 km^2 irrigated aquifer-stream system (Figure 2.1) located within the Lower Arkansas River Valley (LARV) in southeastern Colorado. The field-scale application site at the AVRC is located within this region. The climate is semi-arid, with average monthly temperatures and monthly precipitation depths ranging from -1.0 ^oC and 0.7 cm during the winter months, respectively, to 25 ^oC and 5.0 cm during the summer months. The study region covers about 50,600 ha, of which approximately 26,400 ha has been irrigated since the late 19^{th} century. In general, the LARV has served as one of the most productive agricultural areas for the state of Colorado. As shown in Figure 2.7A, alfalfa, melons, corn, beans, sorghum, wheat, grass, and vegetables are the most dominant crops, with fields irrigated from six main canals in the (Rocky Ford Highline, Catlin, Otero, Rocky Ford, Fort Lyon, and Holbrook) or from groundwater using shallow pumps (see Figure 2.1). The irrigation season typically occurs between March 15 and November 15 of each year, with water diverted into the canals from the Arkansas River.

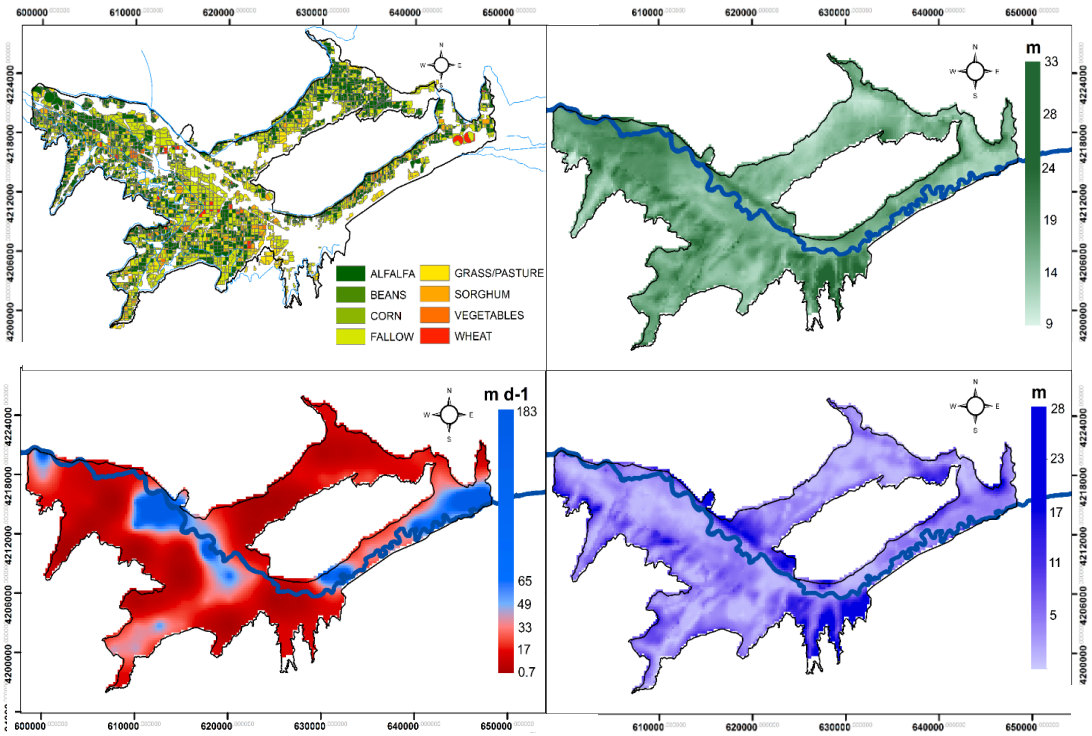

Figure 2.7. (A) Crop type of each cultivated area during the 2006 growing season, (B) thickness of the alluvium (ground surface to the shale bedrock), (C) Hydraulic conductivity (m/day) of the upper alluvium material, based on a tested groundwater flow model of the region (Morway et al., 2013), and (D) Average depth to the water table (m), as simulated by the flow model.

The alluvial aquifer of the LARV ranges from 4-34 m in thickness, dominated by calcareous and gypsiferous soils and underlain by Cretaceous shale (Figure 2.7B). There are also many outcrops of shale which along with the bedrock shale, have led to release of SO_4 and selenate (SeO_4) into the alluvial aquifer (Gates et al., 2009). A substantial set of water samples has been collected from groundwater monitoring wells from June 2006 to July 2009 (Gates et al., 2009). In total, 398 samples were collected from 84 groundwater monitoring wells and analyzed for major salt ion concentration, including sulfate, $C_{SO_4\text{-}S}$. The location of the monitoring wells and their relation to the 6 respective irrigation canal command areas (i.e. the set of fields that receive irrigation water from the same canal) is shown in Figure 2.8. The frequency distribution of measured groundwater $C_{SO_4\text{-}S}$ is shown in Figure 2.9, with an average value of 630 mg/L (which is 1889 mg/L when converted to $C_{SO_4\text{-}S}$). The high groundwater salinity can be caused by the

presence of salt minerals, return flow of irrigation waters through the aquifer, and evaporative concentration due to the capillary upflux (Konikow and Person, 1985; Hukkinen, 1993; Goff et al., 1998; Gates et al., 2002, Morway et al., 2012).The high values of $C_{SO_4\text{-}S}$ (mg/L) also have contributed to high soil salinity and associated crop yield reduction. Within the LARV, surveyed soil salinity levels under about 70% of the area exceed threshold tolerances for crops, with the regional average of crop yield reduction from salinity and waterlogging estimated to range from 11 to 19% (Gates et al., 2002; Morway and Gates, 2012). In the 1990s, 68% of producers stated that high salinity levels are a significant concern (Frasier et al., 1999).

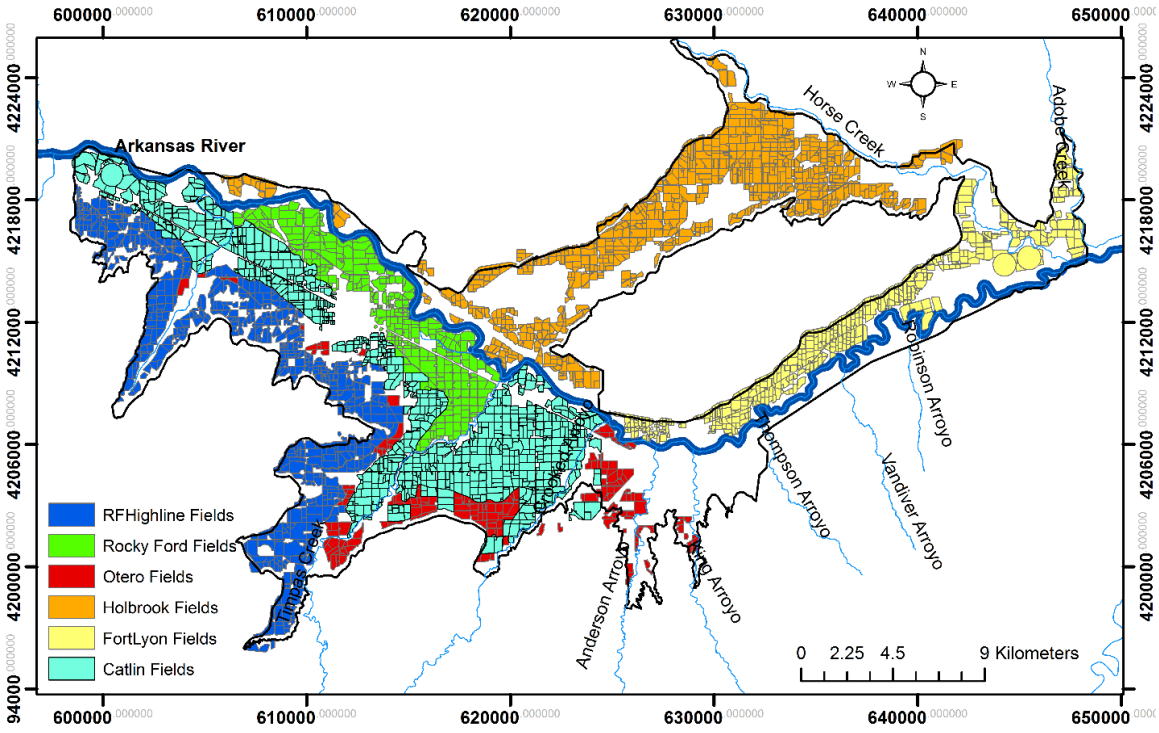

Figure 2.8. Location of groundwater wells and division of command averages with fields receiving irrigation from Highline, Rocky Ford, Otero, Holbrook, Fort Lyon, and Catlin canals.

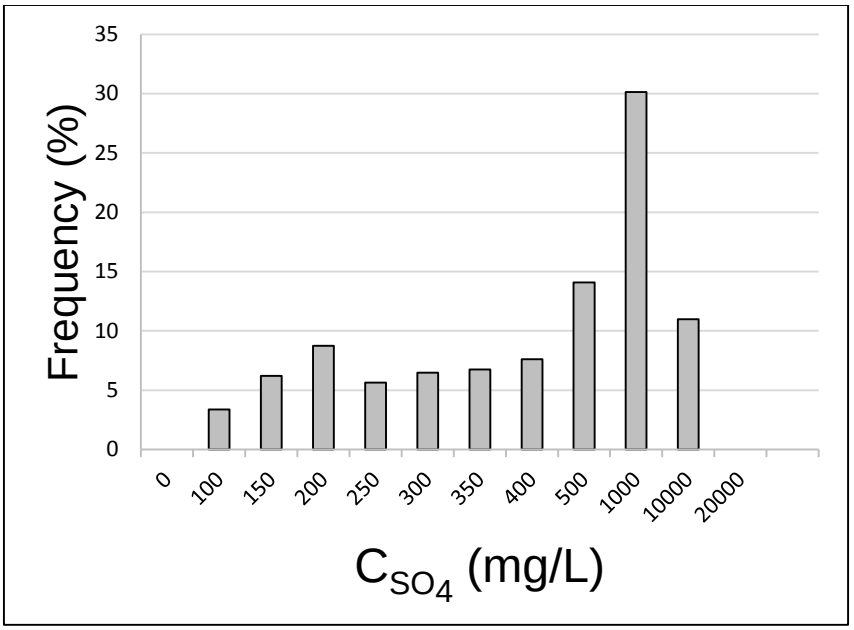

Figure 2.9. Frequency (%) distribution of $C_{SO_4\text{-}S}$ concentration (mg/L) from 84 monitoring wells located in the study region, sampled between 2006 and 2009.

The groundwater flow patterns and groundwater inputs/outputs in the region have been simulated using a tested MODFLOW groundwater flow model (Morway et al., 2013) that employs the UZF1 package (Niswonger et al., 2006) to simulate flow in the unsaturated zone. The region is discretized into lateral finite difference cells of 250 m by 250 m dimensions, comparable to dimensions of cultivated fields. The alluvial aquifer is divided into two layers, and a third layer constitutes the bedrock. Groundwater inputs include infiltrated rainwater and irrigation water, with the latter derived either from canals or from groundwater pumps, canal seepage, and seepage from the Arkansas River and its tributaries. Outputs include ET from both the unsaturated zone and from the saturated zone, the latter occurring if the water table resides within the ET extinction depth and also groundwater pumping and discharge to the Arkansas River and its tributaries. The model was run from April 1999 to October 2007. The calibrated field of hydraulic conductivity (m/d) is shown in Figure 2.7C, and the cell-by-cell average depth to water table during the simulation period is shown in Figure 2.7D.

2.3.2.2. UZF-RT3D Model Setup

The S module for UZF-RT3D is applied to the study region, using the flow patterns and sources/sinks from the MODFLOW model. The study area is discretized with 250 m by 250 m finite difference grid cells, using the same cell size as the MODFLOW grid. The alluvial aquifer is discretized into 6 vertical layers, three of which correspond approximately to the unsaturated zone ($\leq$ 2 m below the ground surface) and the other three spanning the saturated zone. A seventh layer represents the marine shale bedrock, which contains FeS_2 and hence is a source of SO_4 in the presence of oxygenated groundwater (see Equations 2a and 2b, quantified by the rate law expression in Equation 9). In several locations, shale also is present as outcrops. The material type (alluvium or shale) assigned to each grid cell in each layer is shown in Figure S-1 in Supplementary Data in Appendix A. Within the UZF-RT3D modeling code, the rate law expression of Equation 9 proceeds if the cell next to a cell designated as shale contains O_2 or NO_3 in the groundwater.

The baseline model is run from January 1, 2006 through October 31, 2009 using daily time steps. Sources and sinks of S and SO_4 mass include S fertilizer (at the beginning of the growing season), with average loadings for each crop provided by Dr. Michael Bartolo at the AVRC (personal communication, June 2010); seasonal S mass uptake by crop roots; mass removal of SO_4 via groundwater pumping and then redistribution on the land surface via irrigation; mass loading of SO_4 via applied canal irrigation water; and mass exchange of SO_4 between the aquifer and the canals, Arkansas River, and tributaries. If the aquifer discharges groundwater to the surface water bodies, UZF-RT3D calculates the mass loading to surface water using the simulated values of $C_{SO_4\text{-}S}$ in the grid cells containing the surface water body. If, on the other hand, the surface water body seeps water to the aquifer, mass loading to the aquifer is calculated

using the volumetric flow rate multiplied by $C_{SO_4\text{-}S}$ in the surface water, with these concentration values coming from field-measured values (see Table S-1 in Supplementary Data in Appendix A). These values also are used to determine $C_{SO_4\text{-}S}$ in the canal irrigation water.

S fertilizer loading, S seasonal crop uptake, depths and timing of applied irrigation water, crop root growth rate, planting day, harvest day, and plow day, and mass of S in plowed stover are determined by crop type, with values presented in Table 2.2. The timing of each event during a typical growing season is shown as Figure S-2 in Supplementary Data in Appendix A. Crop type for each field can change between growing seasons, with the spatial distribution of crop type shown in Figure 2.8A for the 2006 growing season. Parameter values involving organic matter decomposition, O_2, N species, and S species are shown in Table 2.3, with most values calibrated from the model application to Se reactive transport (Bailey et al., 2014). Values for other parameters are shown in Supplementary Data in Appendix A (Table S-2). The low value for $\lambda_{SO_4}^{het}$ (0.0009 d^{-1}) is intended to increase average $C_{SO_4\text{-}S}$ in the groundwater which, as will be seen in the results (Section 3.2.3), is low compared to field-measured data

Table 2.2. Agricultural management and crop parameter values for the model application to the study region in the Arkansas River Valley in southeastern Colorado.

Crop Type	Planting Day	Harvest Day	Plow Day	P_{St}	$d_{rt,max}$	F_S	S_{up}	$\alpha_{St,S}$	$\alpha_{Rt,S}$
Units	-	-	-	kg ha^{-1}	m	kg ha^{-1}	kg ha^{-1}	-	-
Alfalfa	30-Apr	30-Sep	20-Oct	561.6	1.83	20	24.5	0.0035	0.0023
Bean	20-May	30-Sep	20-Oct	561.6	0.91	20	20.0	0.0035	0.0023
Corn	1-May	25-Oct	14-Nov	5616	1.22	20	10.0	0.0035	0.0023
Melon	15-May	10-Aug	30-Aug	561.6	1.22	20	20.0	0.0035	0.0023
Onion	20-Mar	15-Sep	5-Oct	561.6	0.46	20	21.0	0.0035	0.0023
Pasture	30-Aug	30-Sep	20-Oct	0	0.91	20	10.0	0.0035	0.0023
Pumpkin	1-Jun	30-Sep	20-Oct	561.6	0.91	20	20.0	0.0035	0.0023
Sorghum	20-May	15-Oct	4-Nov	1684.8	0.91	20	11.5	0.0035	0.0023
Spring Grain	1-Apr	15-Jul	4-Aug	1684.8	0.91	20	11.5	0.0035	0.0023
Squash	20-May	25-Jul	14-Aug	561.6	0.91	20	20.0	0.0035	0.0023
Sunflower	1-Jun	10-Oct	30-Oct	561.6	0.91	20	20.0	0.0035	0.0023
Vegetable	25-Apr	30-Aug	19-Sep	561.6	0.91	20	20.0	0.0035	0.0023
Winter Wheat	30-Sep	5-Jul	25-Jul	1684.8	0.91	20	11.5	0.0035	0.0023

d_{pw} (depth of plowing) is 1.0 m for all crops except beans (0.8 m)
P_{Rt} (seasonal mass of root mass) is 500 kg ha^{-1} for all crop types

A spin-up simulation of 30 years is used to achieve spatially-distributed initial concentrations of each species for the 2006-2009 simulation. In addition to the baseline 2006-2009 simulation, a second simulation was run with higher rates of $\lambda_{NO_3}^{auto}$ and $\lambda_{O_2}^{auto}$ (both set to a spatially uniform value of 0.5 d^{-1}) in an attempt to increase groundwater $C_{SO_4\text{-}S}$. As a constraint on this procedure, the fate and transport of SeO_4 also is simulated, with groundwater $C_{SeO_4\text{-}Se}$ compared with field-measured values. The ratio of S mass to Se mass contained in the shale material is given an average value of 3000, representative of published S:Se ratios in marine shale material (Bailey et al., 2014).

Table 2.3. Parameters for chemical reactions involving organic matter decomposition, dissolved oxygen, nitrogen species, and selenium species.

Parameter	Value	Unit
$\lambda_{O_2}^{auto}$	0.00012 – 3.0*	mg/L
$\lambda_{NO_3}^{auto}$	0.0002 – 1.0*	mg/L
I_{O_2}	1.0	mg/L
I_{NO_3}	0.50	mg/L
K_{CO_2}	0.75	mg/L
$\lambda_{SO_4}^{het}$	0.0009	d^{-1}
ξ	3000	-

Range of command area values, based on model calibration for Se reactive transport (Bailey et al., 2014)

2.3.2.3. Results and Discussion

Results of the 30-year spin-up simulation are shown in Figure 2.10, which plots the frequency distribution of $C_{SO_4\text{-}S}$ in the alluvial aquifer. Values are taken from each cell in layer 4 of the model grid, which corresponds approximately to the shallow saturated zone of the aquifer. The frequency distribution is plotted for each successive 10-year period of the 30-year simulation, to demonstrate that concentrations have reached an approximate steady condition in preparation for the 2006-2009 simulation initial concentrations.

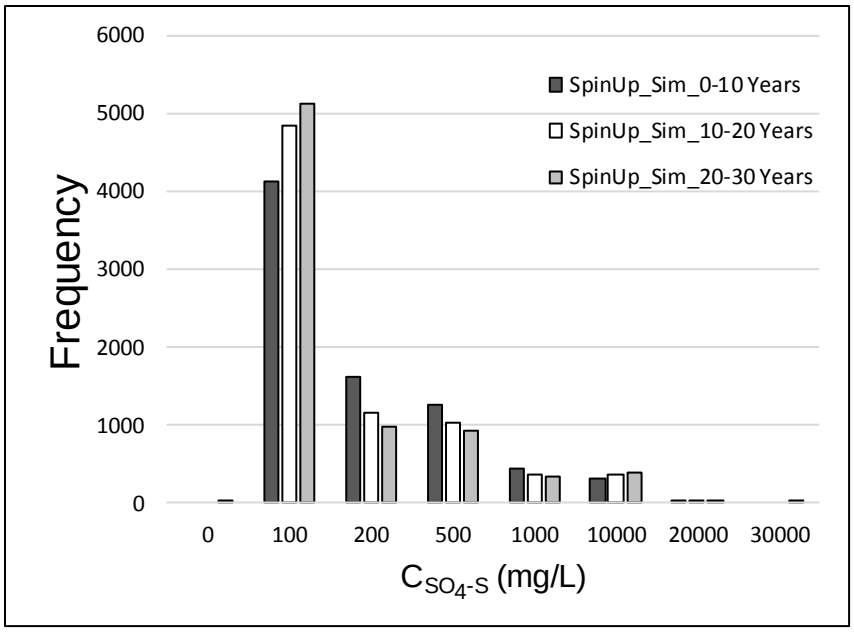

Figure 2.10. Frequency distribution of simulated cell-by-cell groundwater $C_{SO_4\text{-}S}$ concentration in layer 4 of the UZF-RT3D model during successive 10-year periods of the 30-year spin-up simulation.

General model results for the 2006-2009 simulation are shown in Figures 2.11-2.14. Figure 2.11 shows a contour plot of average $C_{SO_4\text{-}S}$ during the 2006-2009 period, and demonstrates the effect of shale material, with high values of $C_{SO_4\text{-}S}$ typically occurring near shallow shale outcrops. Figure 2.12 shows the spatial distribution of organic S in the humus pool (Figure 2.12A) and in the litter pool (Figure 2.12B) in the top layer (< 0.5 m below ground surface) of the model. Figure 2.13 shows the total crop uptake of SO_4-S on each day of the simulation within the top 0.5 m of the soil profile. Spatial distribution of daily groundwater SO_4-S loading (kg) to the Arkansas River, averaged over the simulation period, is shown in Figure 2.14. Red bars indicate mass transfer from the aquifer to the river, and green bars indicate mass transfer to the aquifer from the river. For the majority of locations, the aquifer loads SO_4-S mass to the river. However, in some locations, particularly in the eastern section of the study region, SO_4-S is leached to the aquifer due to low water table elevation and pumping wells that pull river water into the aquifer.

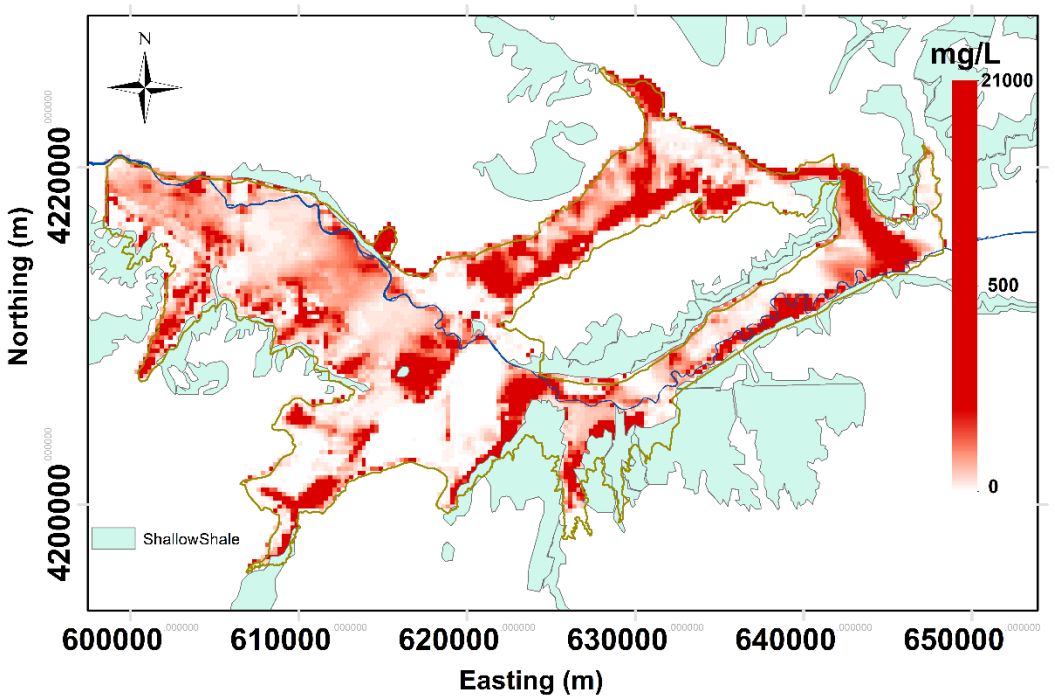

Figure 2.11. Contour plots of average $C_{SO_4\text{-}S}$ (mg/L) in the middle alluvium layer (layer 4 of the model) during the 2006-2009 simulation.

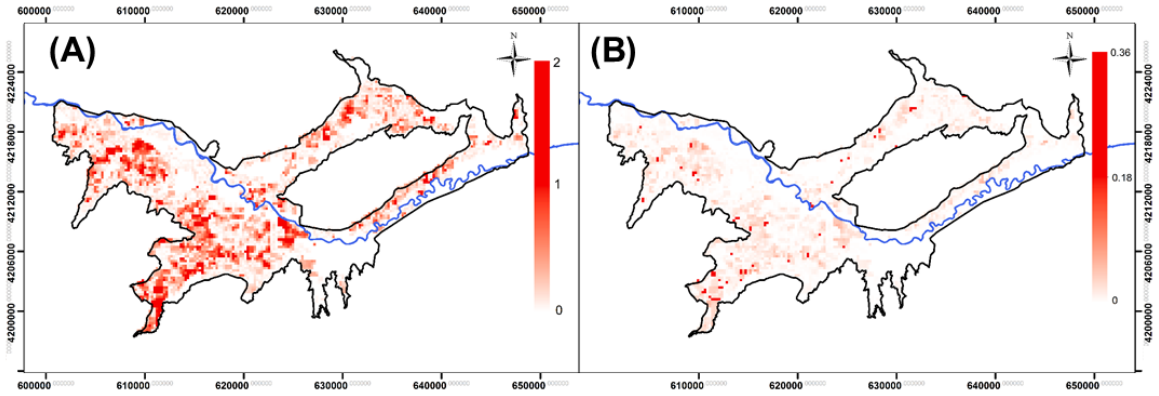

Figure 2.12. Contour plots for concentration of organic S in the (A) Humus pool H_S (mg/kg) and (B) Litter pool L_S (mg/kg) of the soil organic matter in layer 1 (< 0.5 m) of the model for 2006-2009 simulation.

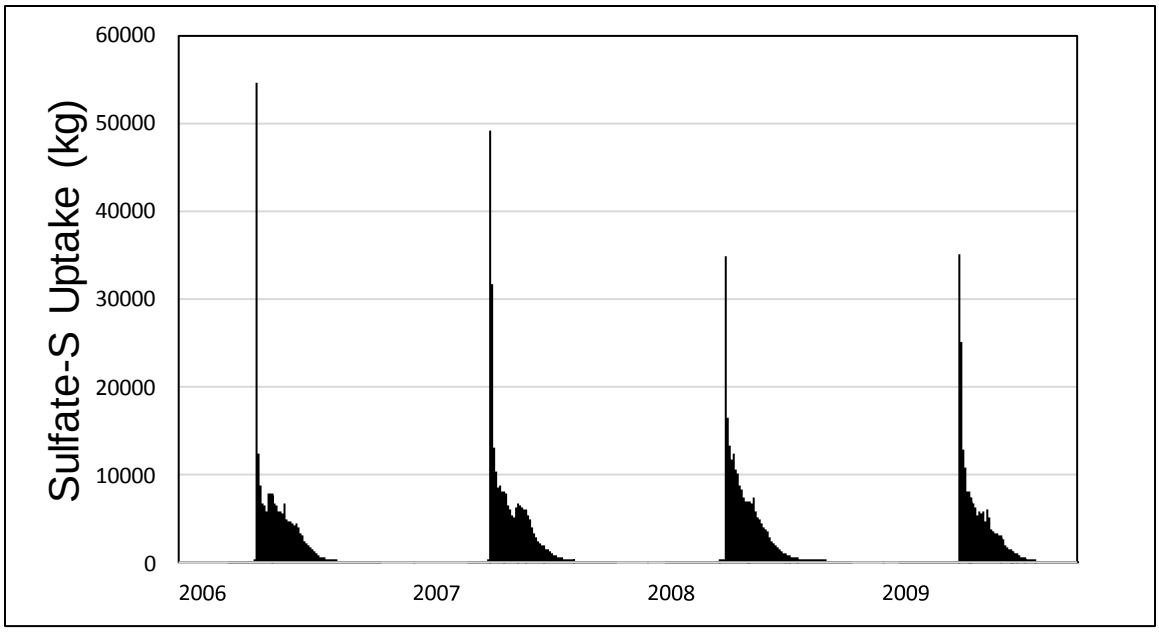

Figure 2.13. Aggregate daily uptake (kg) of SO_4-S by crop roots in layer 1 (0-0.5 m below ground surface) of the model.

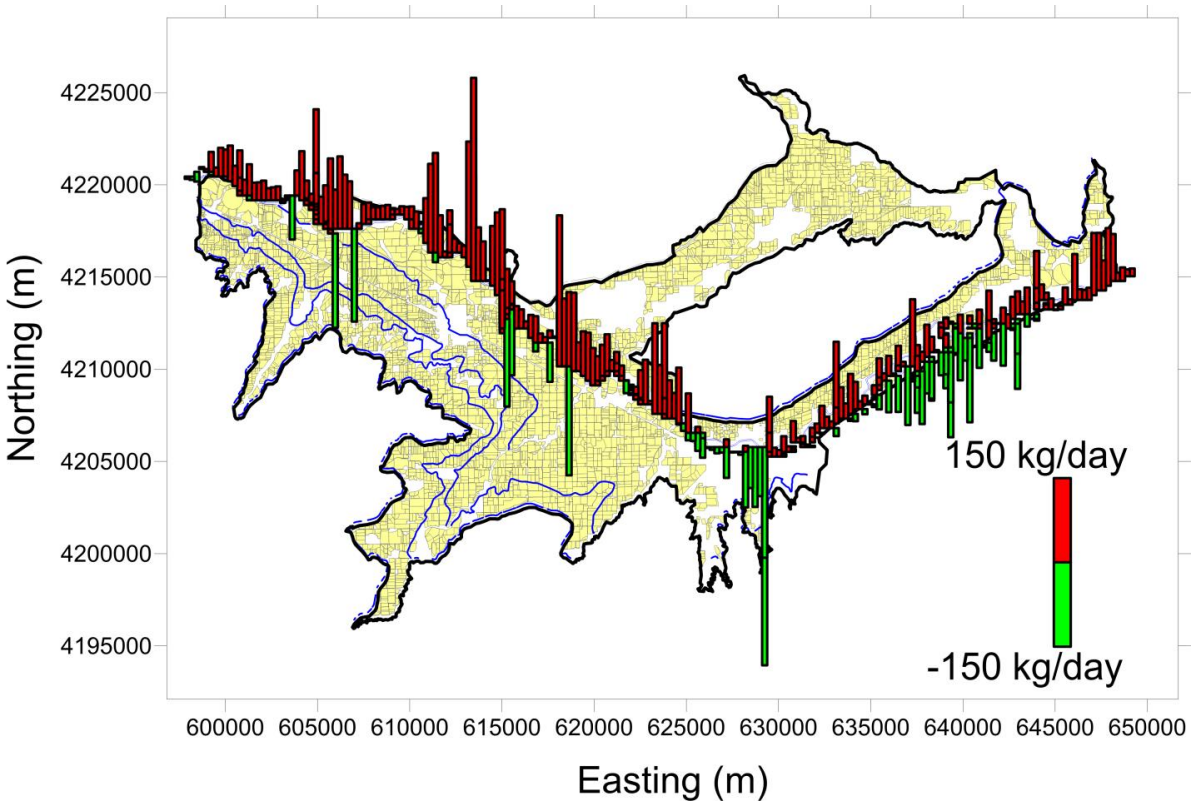

Figure 2.14. Spatial distribution of average mass loading of SO_4-S (kg/d) to the Arkansas River from the aquifer, as simulated by the 2006-2009 UZF-RT3D simulation.

Overall, the model under-predicts the magnitude of $C_{SO_4\text{-}S}$ in the aquifer. This is seen by comparing frequency distribution plots of simulated and observed data (Figure 2.15), with the simulated data corresponding to cell-by-cell $C_{SO_4\text{-}S}$ from layer 4 of the model, corresponding to the elevation of the monitoring well screens. As can be seen in the figure, the distribution of the observed data contains many more high values than the simulated data. The majority of simulated $C_{SO_4\text{-}S}$ values are between 100 and 150 mg/L, whereas the majority of observed values are higher than 400 mg/L. This under-prediction is shown further in Figure 2.16A, which shows the averaged simulated and observed data for each command area (see Figure 2.8 for the spatial area covered by each command area). For each command area, particularly the Highline Canal command area (930 mg/L vs. 191 mg/L), the Catlin Canal command area (627 mg/L vs. 187 mg/L), and the Rocky Ford Ditch command area (568 mg/L vs. 188 mg/L), the simulated concentration values are much lower than the observed data. The sum of the absolute differences between observed and simulated values for each command area is 2150 mg/L.

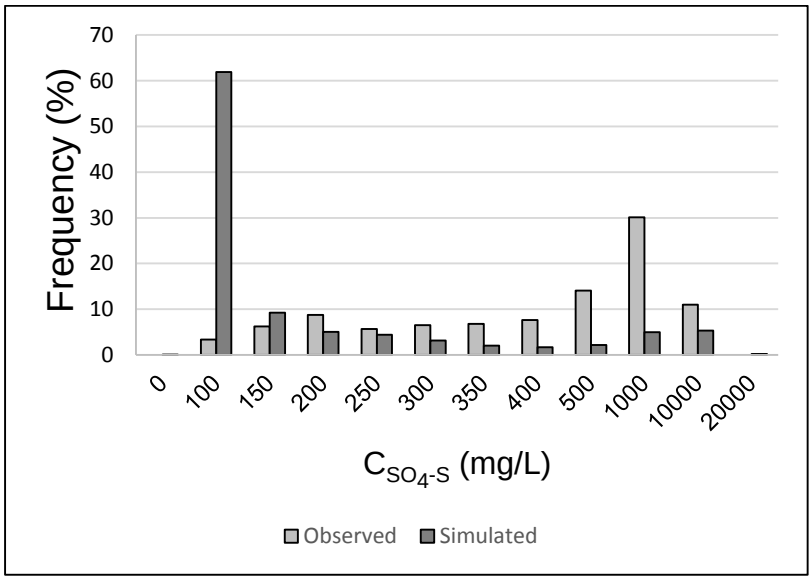

Figure 2.15. Comparison of frequency (%) distribution between observed and simulated groundwater $C_{SO_4\text{-}S}$.

This discrepancy could be a result of several compounding factors. First, the monitoring wells could be placed in areas of high $C_{SO_4\text{-}S}$ as compared to other locations throughout the study region, and hence the values do not represent an average alluvial condition as represented by the model. Second, processes simulated by the model are not represented in the correct order of magnitude. Or third, the model may not be accounting for important physical-chemical processes that increase $C_{SO_4\text{-}S}$ in the soil water and groundwater. To the first point, the wells have been placed in cultivated areas, fallow areas, naturally-vegetated areas, and riparian areas, and hence the observation data represents average aquifer conditions.

To the second point, the rate of autotrophic reduction of O_2 ($\lambda_{O_2}^{auto}$) and NO_3 ($\lambda_{NO_3}^{auto}$) was increased to 0.5 d^{-1} to determine if the mechanism of S oxidation from marine shale is a principle process for high $C_{SO_4\text{-}S}$. Results (Figure 2.16B) show a slight improvement (sum of the absolute differences = 2043 mg/L) in comparison with measured data. However, the values of $C_{SeO_4\text{-}Se}$ are much too high as compared to observation data (Figure 2.16D) (sum of the absolute differences = 450 µg/L), with the calibrated, lower values of $\lambda_{O_2}^{auto}$ and $\lambda_{NO_3}^{auto}$ providing a much better fit (sum of the absolute differences = 126 µg/L) with observation data (Figure 2.16C) (Bailey et al., 2014). Hence, although a significant process in SO_4 fate and transport in the groundwater system, S oxidation from shale is not solely responsible for elevated $C_{SO_4\text{-}S}$ in the aquifer.

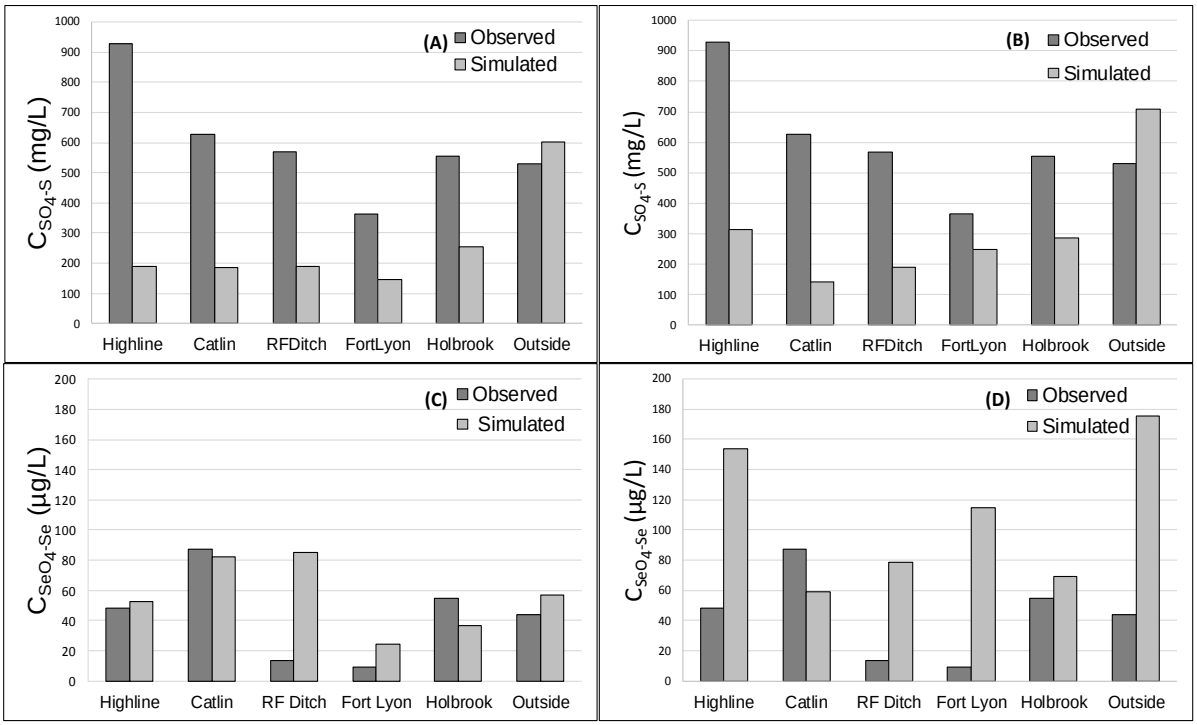

Figure 2.16. Comparison between simulated and observed average $C_{SO_4\text{-}S}$ for each command area for the 2006-2009 simulations using (A) varied calibrated values of $\lambda_{NO_3}^{auto}$ (first-order rate of nitrate autotrophic reduction) and $\lambda_{O_2}^{auto}$ (first-order rate of oxygen autotrophic reduction) and (B) a spatially-uniform higher value of 0.5 d^{-1}. Comparison between simulated and observed average $C_{SeO_4\text{-}Se}$ for each command area using (C) varied calibrated values of $\lambda_{NO_3}^{auto}$ and $\lambda_{O_2}^{auto}$ and (D) a spatially-uniform higher value of 0.5 d^{-1}.

To the third point, and as discussed in Section 3.1.3, modifying parameter values does not lead to an acceptable match between general statistics of observed and simulated values, and therefore the processes included in the current S module of the UZF-RT3D model are not sufficient to track SO_4 fate and transport in an irrigated soil-aquifer system with salinity concentrations as high as observed in the LARV. Based on field data and modeling results, Cooper (2006) demonstrated that gypsum is prevalent in the soil profile throughout the LARV. Multiple (up to 14 in some cases) extractions were performed on the same soil sample, with electrical conductivity (EC) in the extracted soil solution remaining constant, suggesting a significant salt mineral reservoir in the soil. Results were verified with the HYDRUS-1D model. Hence, salt mineral dissolution and general salt ion equilibrium chemistry are thought to be

processes that elevate concentrations of salt ions throughout the regional aquifer system, and could account for the high values of $C_{SO_4\text{-}S}$ observed in the system.

2.4. Summary and Conclusions

This study presents a groundwater reactive transport model for SO_4 fate and transport in an irrigated soil-aquifer-stream system. The model, based on the UZF-RT3D modeling code, accounts for S cycling in the crop-soil zone (S organic matter composition, mineralization/immobilization, root uptake), oxidation-reduction reactions, including release of reduced S from marine shale material containing pyrite (FeS_2), and mass inputs/outputs associated with groundwater sources and sinks (irrigation, pumping, groundwater-surface water interactions). The model is applied at two scales (soil profile, regional aquifer system: 500 km^2) in the Lower Arkansas River Valley in southeastern Arkansas, a region with extremely high salinity, to demonstrate its capabilities. In both applications, the model under-predicted SO_4 concentration despite perturbations in key model parameters such as root uptake rate, chemical reduction of SO_4, and oxidation of SO_4 from shale. Hence, results point to the importance of salt mineral dissolution and precipitation in this particular soil-aquifer system.

As constructed, the S module for UZF-RT3D can be used to assess SO_4 fate and transport in agricultural areas that are not dominated by salt mineral dissolution and precipitation. However, for areas of extremely high salt ion concentration, such as in the LARV, these processes will need to be included to provide a modeling framework that can be used to investigate salinity remediation strategies. Another key element to be included is the influence of subsurface tile drains, which are present in some districts, on the movement and export of salt mass from the groundwater system.

The model executable, and input and output files for the applications presented in this chapter are available upon request from the authors.

REFERENCES

Allen, R.G., Walter, I.A., Elliott, R., Howell, T., Itenfisu, D., Jensen, M., 2005. The ASCE Standardized Reference Evapotranspiration Equation. ASCE—Environmental andWater Resources Institute Task Committee Report, January, 2005.

Ayars, J.E., Christen, E.W., and J.W. Hornbuckle, 2006, Controlled drainage for improved water management in arid regions irrigated agriculture. Agricultural Water Management 86, 128-139.

Bailey, R.T., Gates, T.K., Halvorson, A.D., 2013a, Simulating variably-saturated reactive transport of selenium and nitrogen in agricultural groundwater systems, J. Contam. Hydrology, 149, 27-45.

Bailey, R.T., Morway, E.D., Niswonger, R., and Gates, T.K., 2013b, Modeling variably saturated multispecies reactive groundwater solute transport with MODFLOW-UZF and RT3D. Groundwater, 51(5), 752-761.

Bailey, R.T., Gates, T.K., Ahmadi, M., 2014, Simulating reactive transport of selenium coupled with nitrogen in a regional-scale irrigated groundwater system, Journal of Hydrology, 515, 29-46.

Barghouti, S., and G. Le Moigne (1991), Irrigation and the environmental challenge. Finance Dev. 28 (2), 32 – 33.

Birkinshaw, S.J., Ewen, J., 2000, Nitrogen transformation component for SHETRAN catchment nitrate transport modelling. J. Hydrol. 230, 1–17.

Burkhalter, J.P., Gates, T.K., 2005, Agroecological impacts from salinization and waterlogging in an irrigated river valley, Journal of Irrigation and Drainage Engineering, Vol. 131, No. 2, 197-209.

Burkhalter, J.P., Gates, T.K., 2006, Evaluating regional solutions to salinization and waterlogging in an irrigated river valley, Journal of Irrigation and Drainage Engineering, Vol. 132, No. 1, 21-30

Clement, T.P., 1997, RT3D-A modular computer code for simulating reactive multi-species transport in 3-dimensional groundwater aquifer. Draft report. PNNL-SA-28967. Pacific Northwest National Laboratory, Richland, Washington.

Clement, T.P., Sun, Y., Hooker, B.S., Peterson, J.N., 1998, Modeling multispecies reactive transport in groundwater. Ground Water Monitoring and Remediation 18, 79–92.

Corrales, J., Naja., G.M., Dziuba, C., Rivero, R.G., Orem, W., 2011, Sulfate threshold target to control methylmercury levels is wetland ecosystems, Science of the Total Environment, 409, 2156-2162.

Cooper, C.A., 2006, Salt chemistry effects on salinity assessment and soil solution modeling in the Arkansas River Basin, Colorado, Submitted in Department of Soil and Crop Sciences

El-Ashry, M.T., van Schilfgaarde, J., and S. Schiffman, 1985, Salinity pollution from irrigated agriculture. J. Soil and Water Conservation 40(1), 48-52.

Frasier, W.M., Waskom, R.M., Hoag, D.L., and T.A. Bauder, 1999, Irrigation Management in Colorado: Survey Data and Findings. Technical Report TR99-5 Agricultural Experiment Station, Colorado State University. Fort Collins, CO.

Frind, E.O., Duynisveld, W.H.M., Strebel, O., Boettcher, J., 1990, Modeling of multicomponent transport with microbial transformation in groundwater: The Fuhrberg case, Water Resources Research, Vol. 26, NO. 8, 1707-1719.

Gates, T.K, Cody, B.M., Donnelly, J.P., Herting, A.W., Bailey, R.T., Mueller-Price, J., 2009, Assessing selenium contamination in the irrigated stream-aquifer system of the Arkansan River, Colorado. J. Environ. Qual. 38, 2344-2356.

Gates, T.K., Burkhalter, J.P., Labadie, J.W., Valliant, J.C., Broner, I., 2002, Monitoring and modeling flow and salt transport in a salinity-threatened irrigated valley, Journal of Irrigation and Drainage Engineering, Vol. 128, No. 2, 88-99.

Ghassemi, F., Jakeman, A., and Nix, H., 1995, Salinization of land and water resources: Human causes, extent, management, and case studies in salinity-affected regions, University pf New South Wales Press, Sydney, Australia.

Goff, K., M.E. Lewis, M.A. Person, and L.F. Konikow. 1998. Simulated effects of irrigation on salinity in the Arkansas River Valley in Colorado. Ground Water 36:76-86.

Gowing, J.W., Rose, D.A., Gha,arnia, H., 2009, The effect of salinity on water productivity of wheat under deficit irrigation above shallow groundwater, Agricultural Water Management, 96, pp. 517-524

Hornbuckle, J.W., Christen, E.W., and R.D. Faulkner, 2007, Evaluating a multi-level subsurface drainage system for improved drainage water quality. Agricultural Water Management, 89, 208-216.

Hutmacher, R.B., Ayars, J.E., Vail, S.S., Bravo, A.D., Dettinger, D, Schoneman, R.A., 1996, Uptake of shallow groundwater by cotton: growth stage, groundwater salinity effects in column lysimeters, 31, pp. 205-223

Hukkinen, J. 1993. Institutional distortion of drainage modeling in Arkansas River Basin. J Irrigation and Drain Eng. 119:743-755.

Konikow, L.F., and M. Person. 1985. Assessment of long-term salinity changes in an irrigated stream aquifer system. Water Resources Research 21:1611-1624.

Konukcu, F., Gowing, J.W., and D.A. Rose, 2006, Dry drainage: a sustainable solution to waterlogging and salinity problems in irrigation areas? Agricultural Water Management 83, 1-12.

Lin, Y.W., Garcia, L., 2008, Development of a Hydro-Salinity Simulation Model for Colorado's Arkansas Valley, Journal of Irrigation and Drainage Engineering, Vol. 134, 757-767.

Morway, E.D., Gates, T.K., 2012, Regional assessment of soil water salinity across an intensively irrigated river valley, Journal of Irrigation and Drainage Engineering, Vol. 138, No. 5, 393-405.

Niswonger, R.G., Prudic, D.E., Regan, R.S., 2006. Documentation of the unsaturated zone flow (UZF1) Package for Modeling Unsaturated flow Between the Land Surface and the Water Table with MODFLOW-2005, U.S. Geological Survey Techniques and Methods 6-A19.

Niswonger, R.G., Panday, Sorab, and Ibaraki, Motomu, 2011. MODFLOW-NWT, A Newton Formulation for MODFLOW-2005: U.S. Geological Survey Techniques and Methods 6-A37, 44p.

Oosterbaan, R. J., 2005, SAHYSMOD (version 1.7a), Description of principles, user manual and case studies, International Institute for Land Reclamation and Improvement, Wageningen, Netherlands, 140.

Oster, J.D., Rhoades, J.D., 1975, Calculated drainage water composition and salt burdens resulting from irrigation with river waters in the western United States, Journal of Environmental Quality, 73-79.

Pauwels, H., W. Kloppmann, J.-C. Foucher, A. Martelat, and V. Fritsche, 1998, Field tracer test for denitrification in a pyrite-bearing schist aquifer. Applied Geochemistry. 13:767-778.

Postma, D., Boesen, C., Kristiansen, H., and F. Larsen, 1991, Nitrate reduction in an unconfined sandy aquifer: water chemistry, reduction processes, and geochemical modeling. Water Resources Research 27(8), 2027-2045.

Rhoades, J.D., 1993, Electrical conductivity methods for measuring and mapping soil salinity, Adv. Agron. 49, 201-251.

Tanji, K.K., 1990, Agricultural salinity assessment and management, ASCE manuals and Reports on Engineering Practice, No. 71, ASCE, New York.

Singh, A., Panda, S.N., 2012, Integrated salt and water balance modeling for the management of waterlogging and salinization; I: Validation of SAHYSMOD, Journal of Irrigation and Drainage Engineering, Vol. 138, 955-963.

Šimůnek, J., and D. L. Suarez, 1994, Two-dimensional transport model for variably saturated porous media with major ion chemistry, Water Resources Research, 30(4), 1115-1133.

Sparks, D.L., 2003, Environmental soil chemistry, Academic press, Second Edition .

Tuteja, N.K., Beale, G., Dawes, W., Vaze, J., Murphy, B., Barnett, P., Rancic, A., Evans, R., Geeves, G., Rassam, D., Miller, M., 2003, Predicting the effects of landuse change on water and salt balance—a case study of a catchment affected by dryland salinity in NSW, Australia, Journal of Hydrology, 283, 67-90.

USEPA. 1983. Methods for chemical analysis of water and waste. EPA/600/4‑79/020. USEPA, Washington, DC.

van der Leeden, F., Cerrillo, L.A., and D.A. Miller, 1975, Groundwater problems in the northwestern United States, U.C. Environmental Protection Agency, Office of Research and Devleopment. EPA-660/3-75-018. Washington, D.C. 361 pp.

Vaze, J., Beale, G.T.H., Barnett, P. and Tuteja, N.K., 2003, Predicting the spatial and temporal effects of landuse change using the CATSALT modelling framework. MODSIM 2003

Wichelns, D., Qadir, M., Achieving sustainable irrigation requires effective management of salts, soil salinity, and shallow groundwater, 2015, Agricultural Water Management, 157, 31-38.

Zheng, C. and Wang, P.P., 1999, MT3DMS: a modular three-dimensional multispecies transport model for simulation of advection, dispersion, and chemical reactions of contaminants in groundwater systems; documentation and user's guide. University of Alabama, Tuscaloosa, A

CHAPTER 3

A COUPLED REACTIVE TRANSPORT AND EQUILIBRIUM CHEMISTRY MODEL FOR ASSESSMENT OF SALINITY IN A REGIONAL-SCALE AGRICULTURAL GROUNDWATER SYSTEM[1]

Highlights

A three dimensional coupled groundwater reactive transport and equilibrium chemistry model has been developed to simulate the fate and transport of salt ions in regional agricultural groundwater systems. The UZF-RT3D/SEC model amends the base model UZF-RT3D with a new Salinity Equilibrium Chemistry (SEC) module to create a coupled model that simulates the movement and transformation of major salt ions (calcium, magnesium, sodium, potassium, sulfate, chloride, bicarbonate, and carbonate) due to advection, dispersion, source/sink mixing, redox reactions, precipitation-dissolution, complexation, and cation exchange. For application in agricultural areas, the model also accounts for crop uptake, soil organic matter decomposition, and mineralization/immobilization of carbon, nitrogen, and sulfur species. The SEC module uses the stoichiometric algorithm, which allows more flexibility in including additional salt minerals into the solution algorithms if necessary. Both the Debye-Huckel and Davis expressions are used to calculate ion activities. The model is applied to a salinity-impaired regional scale (500 km^2) agricultural area in the Lower Arkansas River Valley of Colorado. The model is tested against extensive data, including total dissolved solids concentration in the unsaturated zone, salt ion concentrations in the alluvial aquifer, and groundwater salt loads discharging to the stream network of the Arkansas River. Results indicate that the model can be a useful tool in

[1] To be submitted to *Environmental Modelling & Software*, Saman Tavakoli Kivi, Ryan T. Bailey, Timothy K. Gates

simulating salt ion fate and transport in highly-salinized aquifers with the potential for application to other salt-affected regions worldwide.

3.1. Introduction

High salinity in groundwater and soils afflicts many areas of the world, specifically arid and semi-arid agricultural regions that rely on irrigation for sustaining crop yield. Reduction in crop yield is an important economic consequence of salt build-up in the root zone in many regions of the world including Iran (Jalali, 2007; Jamshidzadeh et al., 2011; Ebrahimi et al, 2016), India (Singh, 2005; Jeevanandam et al., 2007; Misra et al., 2007; Lorenzen et al., 2012), the western United States (e.g. San Joaquin Valley in California, Schoups et al., 2006), Pakistan (Mahmood et al., 2001; Qureshi et al., 2008; Latif et al., 2009), China (Pereira et al. 2007; Chen et al, 2010; Wang et al. 2018), and Australia (Herczeg et al., 2001; Tweed et al., 2007; Skrzypek et al., 2013). High salinity can be brought about by waterlogging from shallow groundwater with associated evaporative upflux and concentration (Morway and Gates, 2012; Harrington et al., 2014); dissolution of salt minerals such as gypsum ($CaSO_4$), calcite ($CaCO_3$), and halite (NaCl) (Harrington et al., 2014; Farid et al., 2015,); and seawater intrusion in coastal areas (Shammas et al., 2007; Sherif et al., 2011; Blanco et al., 2013).

The impact of possible remediation practices on high groundwater and soil salinity often is assessed using models that attempt to capture the major hydrologic processes and chemical reactions that govern the transport of salt species in coupled soil-aquifer systems. These models also are used to provide insights into processes that govern salt species transport in these systems. Models are employed at a variety of spatial scales, ranging from one-dimensional (1D) soil profiles to river basins, and include varying degrees of complexity, from simple advective transport to multi-species reactive transport coupling equilibrium and kinetic chemistry.

Several models include many of the governing physical and chemical processes for salt fate and transport. UNSATCHEM-2D (Simunek and Suarez, 1994) includes chemical reactions such as precipitation-dissolution of salt minerals, cation exchange, and complexation to simulate spatio-temporal concentration of major salt ions in soil-water systems. HYDRUS-1D (Simunek et al., 2005), a finite element model for simulating the movement of water and multiple solutes in variably-saturated porous media, was amended to include the UNSATCHEM module for major salt ion chemistry (Simunek et al., 2012). The HP1 model couples HYDRUS-1D with PHREEQC to address a broader range of ions but is restricted to 1D transport (Jacques et al., 2003, Jacques et al., 2005). LEACHM (Wagenet and Hutson, 1987) simulates salt and pesticide movement in the soil zone. These models, however, have been applied only at small spatial scales, typically soil profiles at experimental field plots (Goncalves et al., 2006; Tafteh et al., 2012; Rasouli et al., 2013), due to high computational costs and data requirements.

A second subset of salinity models are applied at a large spatial scale (catchment to river basin), but do not include chemical processes (e.g. precipitation-dissolution) that often govern salt ion concentration in variably-saturated groundwater systems. Table 3.1 shows a list of salt transport modeling studies applied at the regional scale and selected features of the respective model used for each study. The area of the study region and the modeled physical and chemical processes are included.

Table 3.1. Salinity transport modeling studies applied at the regional scale.

Study Area	Area of the study region	Model Used	Simulated Salt species	Reference
San Joaquin Valley, California, USA	1400 km^2	Coupled MODHMS and UNSATCHEM	Gypsum and Calcite	Shoups et al., 2005
Lower Arkansas River Valley, Colorado, USA	244 km^2	Modified WATSUIT	Gypsum, Calcite, and Magnesite	Lin and Garcia (2008)
Haryana State, India	920 km^2	SAHYSMOD	N/A	Singh et al., 2012
Mandagery Creek Catchment, Australia	1668 km^2	CATSALT	N/A	Tuteja et al., 2003
Lower Arkansas River Valley, Colorado, USA	500 km^2	MT3DMS + Water and Salt balance model for unsaturated zone	N/A	Burkhalter and Gates (2005)

A hydro-salinity model that couples MODHMS with UNSATCHEM was used by Schoups et al. (2005) to simulate subsurface salt transport and storage in a 1,400 km^2 region of the San Joaquin Valley. The coupling of the two models for three-dimensional salinity reactive transport, however, is not explained in the paper, and the modeling system does not account for element (carbon, nitrogen, sulfur) mass cycling in the plant-soil system. SAHYSMOD (Oosterbaan, 2005) is an integrated agro-hydro-salinity model that can be applied to large scale agricultural fields but handles processes based exclusively on water and salt balances and does not account for chemical reactions. SAHYSMOD has been applied to simulate the water and salt behavior in the semi-arid irrigated area of Haryana State in India where waterlogging and salinization has impacted the region for more than 40 years (Singh et al., 2012). Tuteja et al., (2003) assessed the effect of land use changes on salt and water balance in the Mandagery Creek catchment of New South Wales, Australia using CATSALT, a distributed water balance model linked with a salt transport module. Lin and Garcia (2008) applied WATSUIT, a steady-state model that calculates soil-water interaction in the root zone, in Colorado's Lower Arkansas River Valley to determine the salinity of deep percolation water. They modified WATSUIT to simulate dynamic conditions

with a monthly time step and applied the model to simulate unsaturated flow for a 12-month period in the root zone of fields.

Other models link geochemistry and multi-species reactive transport in saturated or variably-saturated porous media [e.g. VAM2D, (Huyakorn et al., 1991); HYDROGEOCHEM (Yeh et al., 2004); DYNAMIX (Narasimhan et al., 1986); PHAST (Parkhust et al., 2004)], but have not been applied to salinity fate and transport and do not always include the necessary chemical reactions, e.g. cation exchange, or are limited to the saturated zone (e.g. PHAST). Overall, the chemical processes that often govern salt species' fate and transport, such as precipitation-dissolution, complexation, cation exchange, first-order degradation, and redox reactions have not been represented in modeling efforts at a large spatial scale. Nevertheless, the degradation of aquifers and streams by the accumulation of salts, as well as their remediation, is brought about by practices and processes that interact from field to field over vast spatial extents. Models are needed that can adequately simulate these practices and processes to allow salinization over regional landscapes to be better understood and alternatives for its mitigation to be explored.

This study presents a numerical model that simulates the fate and transport of major salt ions in a regional-scale variably-saturated agricultural groundwater system while accounting for major salt inputs, equilibrium chemical reactions, oxidation-reduction reactions, and the cycling of carbon (C), nitrogen (N), and sulfur (S) in the plant-soil system. The model uniquely combines these capabilities with a number of other features important to the transformation and distribution of salts over large agricultural regions. It is based on UZF-RT3D (Bailey et al., 2013a), a finite difference FORTRAN code that simulates reactive transport of multiple interacting chemical species in variably-saturated groundwater flow systems and that uses flow and source/sink output from a MODFLOW groundwater flow model. UZF-RT3D has been used

previously for simulating the cycling and transport of N, S, and selenium (Sespecies in a regional-scale aquifer system (Bailey et al., 2014; Tavakoli Kivi and Bailey, 2017), and includes organic matter decomposition and mineralization, plant uptake, sorption, oxidation-reduction, and fertilizer loading. This chapter presents a salinity equilibrium chemistry (SEC) module for UZF-RT3D, which includes the fate and transport of calcium (Ca), magnesium (Mg), sodium (Na), potassium (K), sulfate (SO_4), chloride (Cl), and bicarbonate (HCO_3) and associated chemical equilibrium reactions such as precipitation-dissolution of salt minerals (e.g. gypsum $CaSO_4$). In anticipation of model use in other regions worldwide, the salinity module source code has been designed for ease of including additional salt minerals that may be present in other groundwater systems.

The remainder of the chapter is structured as follows: Section 2 presents a conceptual model of salt ion fate and transport in an agricultural irrigated alluvial groundwater system; Section 3 presents the basic mass-balance equations of UZF-RT3D and the equilibrium chemistry for salt ion fate and transport; Section 4 presents the application of the model to a 500 km^2 stream-aquifer system in the highly-salinized Lower Arkansas River Valley (LARV) in southeastern Colorado to demonstrate model utility; and Section 5 provides summary and conclusions, including future research directions.

3.2. Salinity Fate and Transport in an Agricultural Groundwater System

The fate and transport of major salt ions in an irrigated region is depicted in Figure 3.1. The cycling of C and N are included due to their effect on S cycling and SO_4 chemical reduction, and the release of SO_4 from pyrite (FeS_2) in the presence of O_2 and NO_3. These conditions are not present in all aquifer systems, but pyrite is present in bedrock and outcropped marine shale in many regions worldwide.

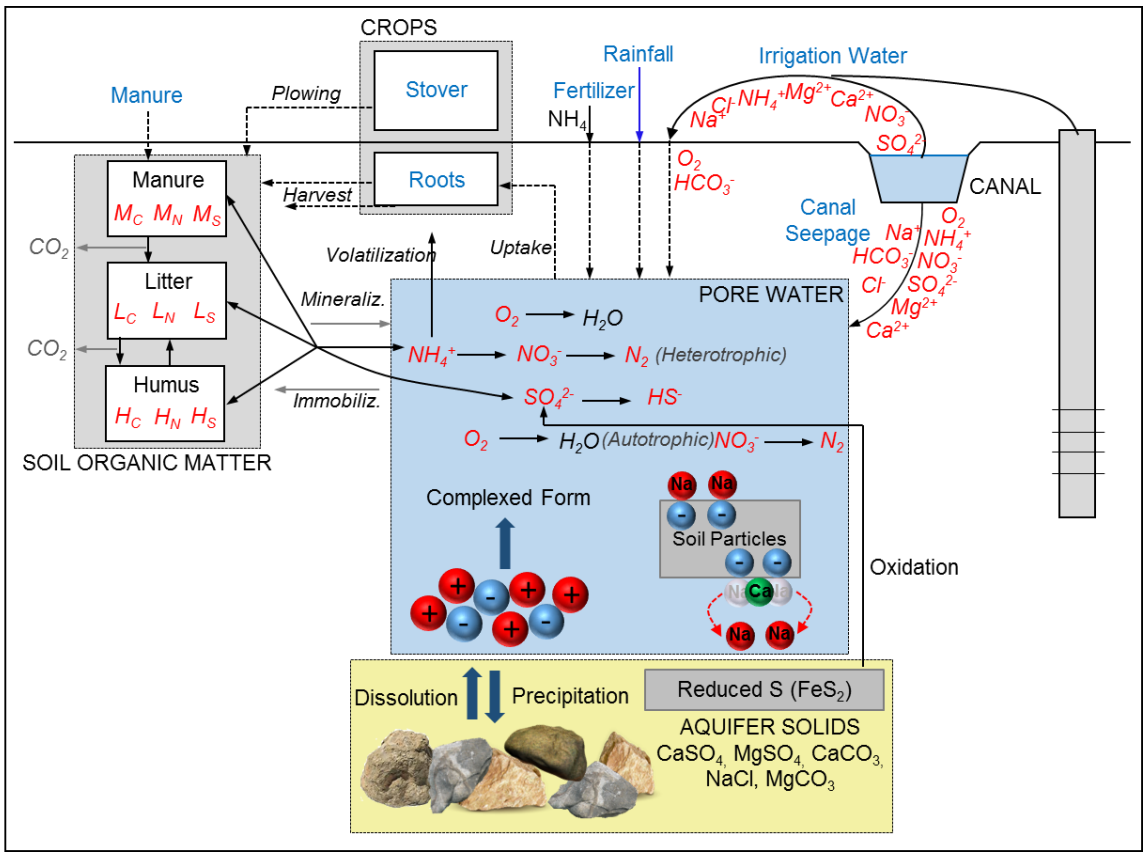

Figure 3.1. Nutrient cycling in soil and groundwater system in an agricultural area, including plant mass inputs/output, organic matter decomposition, mineralization/immobilization, oxidation-reduction reactions, precipitation-dissolution, complexation, and cation exchange.

Cycling of S mass occurs as organic S is incorporated into soil organic matter, composed of litter (fast-decomposing) and humus (slow-decomposing), via plowing, then mineralized to SO_4, and then taken up by crop roots during the growing season. S mass also can be added to the root zone via fertilizer. SO_4 can be chemically reduced via a microbially-mediated chemical reduction reaction (Frind et al., 1990), inhibited by the presence of O_2 and NO_3 due to the succession of terminal electron (e^-)-acceptor processes. Furthermore, SO_4 can be released from FeS_2 via autotrophic reduction of O_2 and NO_3 (Frind et al., 1990; Postma et al., 1991; Pauwels et al., 1998).

SO_4 mass, along with the mass of the other major anions (Cl, CO_3, HCO_3) and cations (Mg, Ca, Na), can be added to the subsurface via irrigation water and seeped surface water (canal

water, stream water). Irrigation water can be derived either from surface water or from groundwater via pumping. If salt minerals, e.g. $CaSO_4$, $CaCO_3$, and NaCl, are present in the soil and aquifer sediments, dissolution of the salt solids or precipitation out of the solution can occur, resulting in an increase or decrease in salt ion concentration in the groundwater and soil water. In addition, complexation of the dissolved species and cation exchange reactions can occur. Once in the groundwater system, the salt ions can be transported through the aquifer and to surface water discharge sites. If concentrations exceed saturation limits, then precipitation to salt solids can occur.

3.3. Model Development

This section describes the UZF-RT3D transport and chemical kinetics model, followed by a description of the new Salinity Equilibrium Chemistry (SEC) module.

3.3.1. Salinity Transport and Chemical Kinetics

The base solute reactive transport model is UZF-RT3D (Bailey et al., 2013b) ,which receives groundwater flow data from a MODFLOW-NWT (Niswonger et al., 2011) model that employs the Unsaturated-Zone Flow (UZF1) package (Niswonger et al., 2006), and solves the following system of advection-dispersion-reaction (ADR) equations for both dissolved-phase and solid-phase species in variably-saturated groundwater systems using a finite-difference approach (Bailey et al., 2013a):

$$\frac{\partial(C_k\theta)}{\partial t}R_k = -\frac{\partial}{\partial x_i}(\theta v_i C_k) + \frac{\partial}{\partial x_i}\left(\theta D_{ij}\frac{\partial C_k}{\partial x_j}\right) + q_f C_{f_k} + \theta r_f \qquad k = 1,2,...,m \tag{1a}$$

$$\frac{\partial(C_l\varepsilon)}{\partial t} = \alpha_l P_S + \varepsilon r_s \qquad l = 1,2,...,n \tag{1b}$$

where C_k is the concentration of the k^{th} solute [$M_f L_f^{-3}$], with f denoting the fluid phase; D_{ij} is the hydrodynamic dispersion coefficient [L^2T^{-1}]; v is the pore velocity [L_bT^{-1}] with b denoting the bulk phase; θ is the volumetric water content [$L_f^3 L_b^{-3}$]; q_f is the volumetric flux of water representing sources and sinks [$L_f^3 T^{-1} L_b^{-3}$] such as irrigation water, canal and seepage, groundwater discharge to the river, or pumped groundwater; C_f is the concentration of solute in the source or sink water [$M_f L_f^{-3}$]; r_f represents the rate of all reactions that occur in the dissolved phase [$M_f L_f^3 T^{-1}$]; R_j is the retardation factor for species j and is equal to $1+(\rho_b K_{dj})/\theta$, where ρ_b is the bulk density of the porous media [$M_b L_b^{-3}$]; P_S is the application rate of after-harvest stover mass [kg ha^{-1}]; α_l is the portion of the stover mass attributed to the solute; ε is the volumetric solid content [$L_s^3 L_b^{-3}$] and is equal to $1-\phi$, with ϕ representing porosity; and r_s is the reaction rate, with s denoting the solid phase. UZF-RT3D uses output from a MODFLOW-NWT (Niswonger et al., 2011) that uses the Unsaturated Zone Flow (UZF1) package (Niwsonger et al., 2006) for v and q_f.

Using the form of the ADR equation in Equation 1a, the transport of SO_4-S and Ca are written as follows, with the equations for the other major ions (Mg, Na, K, CO_3, HCO_3, Cl) similar to the Ca equation:

$$\frac{\partial\left(C_{SO_4-S}\theta\right)}{\partial t}R_{SO_4-S} = -\frac{\partial}{\partial x_i}\left(\theta v_i C_{SO_4-S}\right)+\frac{\partial}{\partial x_i}\left(\theta D_{ij}\frac{\partial C_{SO_4-S}}{\partial x_j}\right)+q_f C_{f_{SO_4-S}}+F_{SO_4-S}-U_{SO_4-S}+\varepsilon\left(r_{s,S}^{min}-r_{s,S}^{imm}\right) + \theta\left(r_{f,SO_4-S}^{auto}-r_{f,SO_4-S}^{het}\right) \quad (2a)$$

$$\frac{\partial\left(C_{Ca}\theta\right)}{\partial t}R_{Ca} = -\frac{\partial}{\partial x_i}\left(\theta v_i C_{Ca}\right)+\frac{\partial}{\partial x_i}\left(\theta D_{ij}\frac{\partial C_{Ca}}{\partial x_j}\right)+q_f C_{f_{Ca}}-U_{Ca} \quad (2b)$$

The SO_4 transport equation is unique from the others in that it includes mineralization/ immobilization (due to S cycling), chemical reduction, and autotrophic oxidation. Equations for S in the litter pool (L_S), in the humus pool (H_S), and in the manure pool (M_S) also are included in the UZF-RT3D model, but not shown here (see Tavakoli Kivi and Bailey, 2017). For the SO_4-S Eq. (2a), $F_{SO_4\text{-}S}$ is the inorganic fertilizer application of S [$M_f L_b^{-3} T^{-1}$]; $U_{SO_4\text{-}S}$ is the uptake rate [$M_f L_b^{-3} T^{-1}$]; *min* and *imm* signify mineralization and immobilization, respectively; and *auto* and *het* represent autotrophic and heterotrophic chemical reduction, respectively.

Due to the influence of O_2 and NO_3 on the fate and transport of SO_4-S, UZF-RT3D also solves mass-balance equations for NH_4, NO_3, and O_2, and includes C and N cycling in the soil-plant system, N fertilizer loading, uptake of NH_4 and NO_3, nitrification, NH_4 volatilization; heterotrophic denitrification; and autotrophic denitrification in the presence of FeS_2. These equations are summarized in Bailey et al. (2013a) and Bailey et al. (2015).

The microbial-mediated chemical reduction of O_2, NO_3, and SO_4-S are included in the model. Chemical reduction of SO_4-S is represented by the term r_{f,SO_4-S}^{het} in Equation (2a) and is simulated by the following rate law expression:

$$r_{f,SO_4-S}^{het} = \lambda_{SO_4-S}^{het} C_{SO_4-S}\left(\frac{CO_{2,prod}}{K_{CO_2}+CO_{2,prod}}\right)\left(\frac{I_{O_2}}{I_{O_2}+C_{O_2}}\right)\left(\frac{I_{NO_3}}{I_{NO_3}+C_{NO_3}}\right)\left(\frac{I_{SeO_4}}{I_{SeO_4}+C_{SeO_4}}\right)E \quad (3)$$

where λ_j is the base first-order rate constant for species j [T^{-1}]; K_j is the Monod half-saturation constant for species j [$M_f L_f^{-3}$]; I_{O_2}, I_{NO_3}, and I_{SeO_4} are the O_2, NO_3, and SeO_4 inhibition constants [$M_f L_f^{-3}$] signifying the species concentration at which lower-redox species can undergo

appreciable rates of reduction; $CO_{2,prod}$ is the total amount of CO_2 produced during decomposition of L_C, H_C, M_C and is used as an indicator of available organic C for microbial consumption, and *E* is an environmental reduction factor that accounts for soil moisture and soil temperature and acts to temper the reaction rates based on microbial activity (Birkinshaw and Ewen, 2000). Similar expressions are included for the chemical reduction of O_2 and NO_3, with denitrification inhibited by the presence of O_2.

3.3.2. Salinity Equilibrium Chemistry Module for UZF-RT3D

The Salinity Equilibrium Chemistry (SEC) module predicts major ion solute chemistry in a variably-saturated groundwater system. The chemical system considered in the SEC module is presented in Table 3.2 and includes eight aqueous components, ten complexed species, five solid species, and four exchange species. These components are selected due to their presence in the majority of soil-aquifer systems. Additional components can be included if needed for a particular study site. The module includes the major physical-chemical processes for salt ions: precipitation-dissolution of salt solids, complexation, and cation exchange.

Table 3.2. Name and group of species considered in the SEC module for UZF-RT3D.

Group	Species
Solid Species	$CaSO_4$,$CaCO_3$,$MgCO_3$,NaCl, $MgSO_4$
Complexed Species	$CaSO_4^0$, $MgSO_4^0$, $CaCO_3^0$, $CaHCO_3^+$, $MgCO_3^0$, $MgHCO_3^+$, $NaSO_4^-$, KSO_4^-, $NaHCO_3^0$, $NaCO_3^0$
Exchanged Species	Ca, Mg, Na, K
Aqueous Species	Ca^{2+}, Mg^{2+}, Na^+, K^+,SO_4^{-2}, CO_3^{2-}, HCO_3^-,Cl^-

3.3.2.1. Solution Chemistry Algorithm

There are two main algorithms that are thermodynamically equivalent for simulating equilibrium chemistry: the stoichiometric algorithm and the non-stoichiometric algorithm. Determining the concentration of ions at equilibrium using the stoichiometric algorithm requires

solving both mass balance and mass action equations simultaneously, and is used in models such as PHREEQC (Parkhust and Appelo, 1999, 2013), WATEQ (Truesdell and Jones, 1974), CHESS (der Lee et al., 2002), MINTEQL (Westall et al., 1976), and MINTEQA2 (Allison et al., 1991; Paz-Garcia et al., 2013). Non-stoichiometric algorithms, conversely, minimize Gibbs free energy subject to mass balance constraints (Narasimhan et al., 1986; Marion et al., 2010). Equilibrium is attained when Gibbs free energy of the system is minimized, with no further tendency to change.

The main advantage of the stoichiometric approach is that there is no restriction (the molal quantity of each component needs to be more than zero) for solving the equilibrium equations, whereas the non-stoichiometric algorithm requires transformation methods such as Lagrangian multipliers, thereby increasing the number of variables in the system. Another disadvantage of the non-stoichiometric approach is that free energy data are not as reliable as equilibrium constants (Nordstorm and Ball, 1984). In both cases, a set of non-linear equations is solved, with transformations to approximately linear equations performed since the analytical solution usually does not exist. A well-known approximation approach is the Newton-Raphson method (e.g. used in PHREEQC, CHESS). In this study, a stoichiometric algorithm has been used to determine the concentrations of each salt ion at equilibrium.

The Newton-Raphson method for solving a non-linear system of equations adopts an increment $\Delta\mathbf{x}$ and obtains the next iteration value, $\mathbf{x}_{new}$, for a given vector of unknowns by amending the current value $\mathbf{x}_{old}$:

$$\mathbf{x}_{new} = \mathbf{x}_{old} + \Delta\mathbf{x} \tag{4a}$$

with

$$\mathbf{f}(\mathbf{x}_{new}) = \mathbf{f}(\mathbf{x}_{old}) + \mathbf{J}(\Delta\mathbf{x}) \tag{4b}$$

where **f** is the residual function matrix and **J** is the Jacobian matrix of partial derivatives with respect to the *M* elements of **x**:

$$J = \begin{bmatrix} \frac{\partial f_1}{\partial x_1} & \cdots & \frac{\partial f_1}{\partial x_M} \\ \vdots & \ddots & \vdots \\ \frac{\partial f_M}{\partial x_1} & \cdots & \frac{\partial f_M}{\partial x_M} \end{bmatrix} \tag{5a}$$

Considering that the target is to obtain $\mathbf{f}(\mathbf{x}_{new}) \rightarrow 0$ within a specified tolerance:

$$\Delta\mathbf{x} = -\mathbf{J}^{-1}(\mathbf{x}_{old}) \tag{5b}$$

In the current problem, where **x** represents the set of major ion concentrations, there are a significant number of reactions in a complex system, with the Jacobian matrix needed in the process of transforming a nonlinear system of equations to a set of linear equations. This results in a sparse matrix which requires large amounts of computer memory and long run times for simulation. For each equilibrium sub-model (precipitation/ dissolution, complexation, and ion exchange) an efficient approach was used to reduce the computational burden of the SEC module. For instance, in the precipitation/dissolution sub-model, each ion concentration was obtained by directly solving a quadratic equation instead of inverting the Jacobian matrix, reducing the computations to second order equations.

Law of mass action

For a general chemical reaction type, the law of mass action determines the concentration of each ion within the system:

$$a\mathrm{A} + b\mathrm{B} \rightarrow c\mathrm{C} + d\mathrm{D} \tag{6}$$

where A, B, C, and D represent reactants and *a*, *b*, *c*, and *d* are constants. Every possible reaction for the component species listed in Table 3.2 must be written in the form of Eq. (6). At equilibrium, the concentrations of all reactants and products are related using the equilibrium constant *K*:

$$K = \frac{(\mathrm{C})^c(\mathrm{D})^d}{(\mathrm{A})^a(\mathrm{B})^b} \tag{7}$$

where parentheses denote solute activities. The dimensionless activity, i_A, for the i^{th} aqueous solute is computed by multiplying the activity coefficient γ_i by the molal concentration:

$$i_A = \gamma_i \cdot m_i / m_i^0 = \gamma_i \cdot m \tag{8}$$

where γ_i is the activity coefficient (dimensionless), m_i is the molality (mol/kg H_2O), and m_i^0 is the standard state (1 mol/kg $\mathrm{H_2O}$). There are different formulas to calculate activity coefficients of solutes, most of which depends on the "ionic strength" which defines the number of electrical charges in the solution. The measure of ionic strength is:

$$I = \frac{1}{2}\sum m_i . z_i^2 \tag{9}$$

where z_i is the charge number of ion *i*. Once the ionic strength is determined, using Debye-Huckle theory for a diluted solution (I<0.1), the activity coefficient for each ion will be specified as:

$$\log \gamma_i = -\frac{A_a z_i^2 \sqrt{I}}{1 + B_a a_i \sqrt{I}} \tag{10}$$

where A_a and B_a are temperature dependent constants (A_a = 0.5085 m^{-1} and $B_a = 0.3285\times10^{10}$ m^{-1} at 25^o C) and a_i is a measure of effective diameter of a hydrated ion *i*, with values listed in Table 3.3 for the ions considered in the SEC module.

For values of *I* between 0.1 to 0.5, the Davis equation is used to determine the activity coefficient:

$$\log \gamma_i = -Az_i^2 \left(\frac{\sqrt{I}}{1+\sqrt{I}} - 0.3I \right) \quad (11)$$

Table 3.3. The ion-size parameter a_i, (From Appelo and Postma 2005).

$a_i/(10^{-10}$ m)	Ion
3	K^+, Cl^-, NO_3^-
4-4.5	Na^+, HCO_3^-, SO_4^{2-}
4.5	CO_3^{2-}
6	Ca^{2+}
8	Mg^{2+}

Mass balance equations

Mass balance equations track the mass of each element in the system and are represented for the major aqueous components as:

$$Ca_T = [Ca^{2+}] + [CaSO_4^0] + [CaCO_3^0] + [CaHCO_3^+] \quad (12)$$

$$Mg_T = [Mg^{2+}] + [MgSO_4^0] + [MgCO_3^0] + [MgHCO_3^-] \quad (13)$$

$$Na_T = [Na^+] + [NaSO_4^-] + [NaCO_3^-] + [NaHCO_3^0] \quad (14)$$

$$K_T = [K^+] + [KSO_4^-] \quad (15)$$

$$SO_{4_T} = [SO_4^{2-}] + [CaSO_4^0] + [MgSO_4^0] + [NaSO_4^-] + [KSO_4^-] \quad (16)$$

$$Cl_T = [Cl^-] \quad (17)$$

where the subscript *T* denotes the total concentration of the aqueous component and brackets indicate the molality of the species within the solution. The total concentration of each species in

the solution is the summation of free ions and the complexed forms of that ion. The same types of equations are included for CO_3 and HCO_3.

Complexation reactions

The presence of complexes increases the solubility of minerals since complexation lowers the activity of the free ion (Appelo and Postma, 2005). The ten considered complexed species are shown in Table 3.2. Based on the law of mass action, the equilibrium constants are defined for the complexed species $CaSO_4^0$ and $CaCO_3^0$ as:

$$K_1 = \frac{(Ca^{2+})(SO_4^{2-})}{(CaSO_4^0)} \quad (19)$$

$$K_2 = \frac{(Ca^{2+})(CO_3^{2-})}{(CaCO_3^0)} \quad (20)$$

The equilibrium constants for the remaining eight complexed species are defined in the Supporting Material, and values for all ten equilibrium constants are listed in Table 3.4.

Table 3.4. Equilibrium constant values for complexed species (From Truesdell and Jones, 1974).

Equilibrium Constant	Value
K_1	0.004866
K_2	0.000599
K_3	0.078584
K_4	0.004699
K_5	0.001324
K_6	0.130586
K_7	0.12
K_8	0.054
K_9	0.562
K_{10}	0.1413

Cation exchange reactions

The original UZF-RT3D model (Bailey et al., 2013a) simulates sorption onto soil particles using the linear, Freundlich, or Langmuir sorption isotherms. However, the use of isotherms ignores the electrostatic effects of the charges. Cation exchange replaceability must be calculated considering electrostatic forces to determine the adsorbed ion to the soil particles and the released ion from particles to the solution, with the order of replaceability determined by Coulomb's law and found to be Na > K > Mg > Ca. The Gapon equation represents the cations reaction as an equivalent reaction:

$$X_{1/m\mathrm{M}} + 1/n\mathrm{N}^{n+} = X_{1/n\mathrm{N}} + 1/m\mathrm{X}^{m+} \tag{21}$$

where $X_{1/m\mathrm{M}}$ is exchangeable cation M on the surface (meq/100g), $X_{1/n\mathrm{N}}$ is exchangeable cation N on the surface (meq/100g), M and N are metal cations, and $m+$ and $n+$ are the charges of cations M and N respectively. Eq. (21) can be written in an equilibrium relationship, where K_s is the Gapon selectivity coefficient:

$$K_s = \frac{X_{1/n\mathrm{N}}(\mathrm{M}^{m+})^{1/m}}{X_{1/m\mathrm{M}}(\mathrm{N}^{n+})^{1/n}} \tag{22}$$

While cations can adsorb or detach from soil particles, each soil has a maximum capacity to adsorb free ions from solution. This capacity is referred to as the cation exchange capacity (CEC), which can be calculated by an empirical formula that considers the clay and organic C content of the soil (Appelo and Postma, 2005):

$$\mathrm{CEC} = 7\times(\%\mathrm{Clay}) + 35\times(\%\mathrm{C}) \tag{23}$$

where CEC is in mili-equivalents of ion per kg of soil and is assumed to be independent of temperature and pH, and the concentration of exchangeable species on the surface is much greater than the concentration in solution. Therefore:

$$CEC=X_{\frac{1}{2}Ca}+X_{\frac{1}{2}Mg}+X_{Na}+X_{K} \tag{24}$$

For the selected four ions in the module, the six Gapon equations are written as:

$$K_{s_1}=\frac{(Ca)^{\frac{1}{2}}X_{\frac{1}{2}Mg}}{(Mg)^{\frac{1}{2}}X_{\frac{1}{2}Ca}} \tag{25}$$

$$K_{s_2}=\frac{(Na)X_{\frac{1}{2}Ca}}{(Ca)^{\frac{1}{2}}X_{Na}} \tag{26}$$

$$K_{s_3}=\frac{(K)X_{\frac{1}{2}Ca}}{(Ca)^{\frac{1}{2}}X_{K}} \tag{27}$$

$$K_{s_4}=\frac{(K)X_{\frac{1}{2}Mg}}{(Mg)^{\frac{1}{2}}X_{K}} \tag{28}$$

$$K_{s_5}=\frac{(Na)X_{\frac{1}{2}Mg}}{(Mg)^{\frac{1}{2}}X_{Na}} \tag{29}$$

$$K_{s_6}=\frac{(Na)X_{K}}{(K)X_{Na}} \tag{30}$$

By rearranging Eqs (25)-(27) and substituting into Eq. (24), the exchangeable amount for Ca is determined by:

$$X_{\frac{1}{2}Ca}=CEC\div\left[\frac{(Mg)^{\frac{1}{2}}K_{1}}{(Ca)^{\frac{1}{2}}}+\frac{(Na)}{(Ca)^{\frac{1}{2}}*K_{2}}+\frac{(K)}{(Ca)^{\frac{1}{2}}*K_{3}}+1\right] \tag{31}$$

The same procedure can be applied to obtain relationships for the exchangeable amounts of Mg, Na, and K, which are given in Supporting Material. Values of the associated selectivity coefficients are listed in Table 3.5.

Table 3.5. Selectivity coefficient values for cation exchange reactions (From Robinns et al., 1980).

Gapon Selectivity Coefficient	Value
K_{s_1}	0.7
K_{s_2}	6
K_{s_3}	0.4
K_{s_4}	0.2
K_{s_5}	4
K_{s_6}	16

Precipitation-Dissolution Reactions

Due to the existence of solid minerals in the soils and aquifer materials, dissolution or precipitation of each salt must be considered in the SEC module. The stoichiometric reaction for a salt solid AB_s and the free ions A^+_{aq} and B^-_{aq} is:

$$AB_s \leftrightarrow A^+_{aq} + B^-_{aq} \tag{32}$$

If the solution is super-saturated then the concentration of A^+_{aq} and B^-_{aq} will decrease as AB_s precipitates out of solution. On the other hand, if the solution is under-saturated the concentration of the species will increase as AB_s dissolves into A^+_{aq} and B^-_{aq}.

Salt solids included in the present SEC module are $CaSO_4$, $CaCO_3$, $MgCO_3$, $MgSO_4$, and NaCl since they are common salts in many groundwater environments (see Table 3.2). The precipitation-dissolution chemical reactions for $CaSO_4$ and $CaCO_3$ are given as:

$$CaSO_4 \leftrightarrow Ca^{2+} + SO_4^{2-} \quad (33)$$

$$CaCO_3 \leftrightarrow Ca^{2+} + CO_3^{2-} \quad (34)$$

Similar reactions for the remaining three solid species are given in Supporting Material. The solubility product constants for $CaSO_4$ and $CaCO_3$ are defined as:

$$K_{sp_1} = \frac{(Ca^{2+})(SO_4^{2-})}{(CaSO_4)} \quad (35)$$

$$K_{sp_2} = \frac{(Ca^{2+})(CO_3^{2-})}{(CaCO_3)} \quad (36)$$

Solubility product constants for the remaining three solid species are defined in Supporting Material, and values of the solubility product constants for all five species are listed in Table 3.6.

Table 3.6. Solubility product values for salt solids used in the present model (From appendix 2 of Handbook of Chemistry and Physics, Haynes et al., 2016).

Salt Mineral Name	Solubility Product	Value
$CaSO_4$	K_{sp1}	4.9351×10^{-5}
$CaCO_3$	K_{sp2}	3.0702×10^{-9}
$MgCO_3$	K_{sp3}	4.7937×10^{-6}
$MgSO_4$	K_{sp4}	0.007244
NaCl	K_{sp5}	37.3

There are two main methods which can be used to implement precipitation-dissolution reactions in a computational module for equilibrium chemistry. In the first method, solids are added to the system one at a time: the solid with lower solubility precipitates first, and the direction of each reaction (precipitation or dissolution) is determined comparing the solubility limits of each specific solid. This method is used in models such as PHREEQC, MINTEQ, UNSATCHEM, and CHESS. In the second method, the concentration at equilibrium is determined by considering all of the ions that potentially could react with one another and precipitate out of the solution simultaneously, using the solubility product of each salt. Lucia et al., (2015) determined the concentration at equilibrium using this second method in an enhanced

oil recovery system. The first method is adopted for the SEC module due to the possibility for including additional salt solids, hence making the model more amenable for application to other study regions.

3.3.2.2. Verification of the SEC Module

Before applying the coupled model to the regional-scale study (Section 4), the SEC module was tested for accuracy by comparing model results with data presented by Lucia et al. (2015) in a study of C sequestration. The system considers a mixture of CO_3, Ca, and Mg with 0.0362, 0.0181, and 0.0362 molalities, respectively, which is representative of ion concentrations in most of the reservoirs in their study region, with the ion concentrations suggesting the precipitation of Ca or Mg salts. The result of this comparison is shown in Table 3.7, with a maximum difference between the two models of 0.04%.

Table 3.7. Comparison between the developed SEC module with Lucia et al. (2015).

Ion	Initial Concentration	Concentration at equilibrium (Lucia et al., 2015)	Concentration at equilibrium (This study: SEC module)
Ca^{2+}	1.8125×10^{-2}	1.40182×10^{-6}	1.40130×10^{-6}
Mg^{2+}	1.8125×10^{-2}	2.18876×10^{-3}	2.18855×10^{-3}
CO_3^{2-}	3.6251×10^{-2}	2.19016×10^{-3}	2.19035×10^{-3}

3.3.2.3. Implementing the SEC Module into UZF-RT3D

The SEC module is written in FORTRAN for ease of linking with UZF-RT3D and is divided into three sub-modules, one each for precipitation-dissolution, complexation, and cation exchange. The solution strategy and calculation steps are summarized in Figure 3.2. First, the concentration of each ion is provided to the Precipitation-Dissolution sub-module. Once the new equilibrium concentration has been determined by precipitation-dissolution, the Complexation sub-module is run and the concentration of free ions and complexed species is calculated. The updated concentrations of the ions then are provided to the Cation Exchange sub-module, which

updates the concentrations. Module calculations within each sub-module are repeated until the criterion for ionic strength is fulfilled.

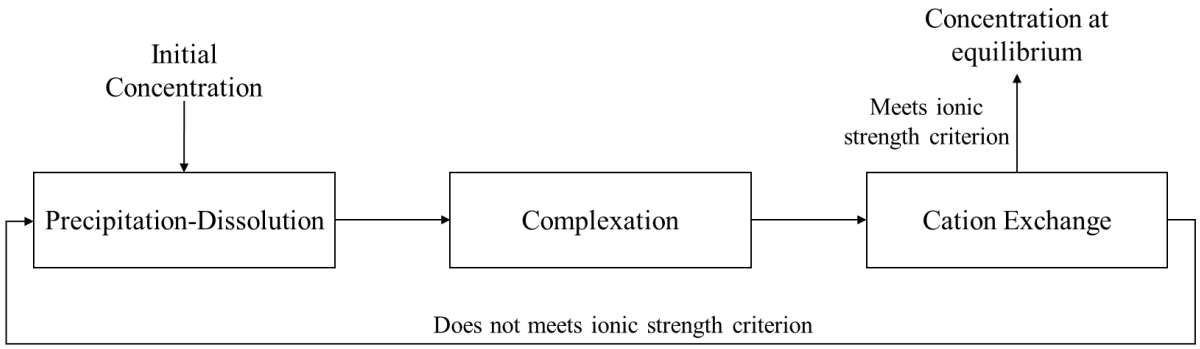

Figure 3.2. Information flow for equilibrium chemistry module.

The flow of data and calculations in the Precipitation-Dissolution sub-module are shown in Figure 3.3 with the five solids considered successively. To determine the direction of reaction (precipitation or dissolution), the saturation index (Q_{sp}), equal to the product of the ion pair concentrations, is calculated. If Q_{sp} is equal to K_{sp}, the solution is in equilibrium with respect to the solid and neither precipitation nor dissolution will take place. If Q_{sp} is less than K_{sp}, the solution is under-saturated with respect to the solid and dissolution will occur until Q_{sp} is equal to K_{sp}. If there is enough salt mineral mass for saturation to be reached, then only a portion of the salt mineral will be dissolved, otherwise all of the present salt mineral will be dissolved. If Q_{sp} is greater than K_{sp}, the solution is over-saturated with respect to the solid and precipitation will occur until equilibrium has been reached.

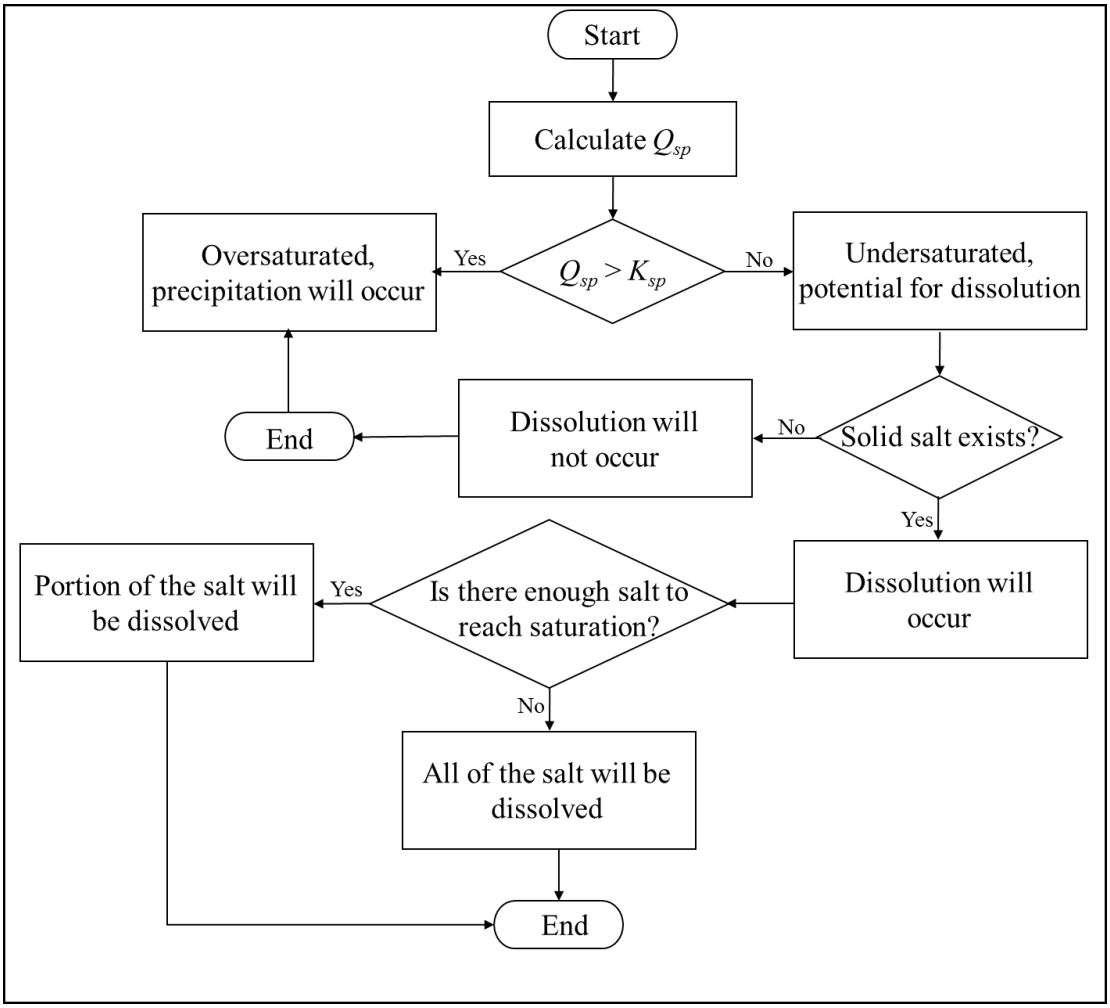

Figure 3.3. Flow chart for precipitation-dissolution sub-section of the salinity equilibrium chemistry module.

Coupling between the transport and chemical kinetic calculations of UZF-RT3D and the SEC module is performed using a sequential non-iterative approach (Barry el al., 2000; Carrayrou et al., 2008), in which the transport and chemical kinetic equations of UZF-RT3D are followed by internal iterations for equilibrium chemical reactions. The calculation steps of the coupled model, with inputs from MODFLOW-NWT, are shown in Figure 3.4.

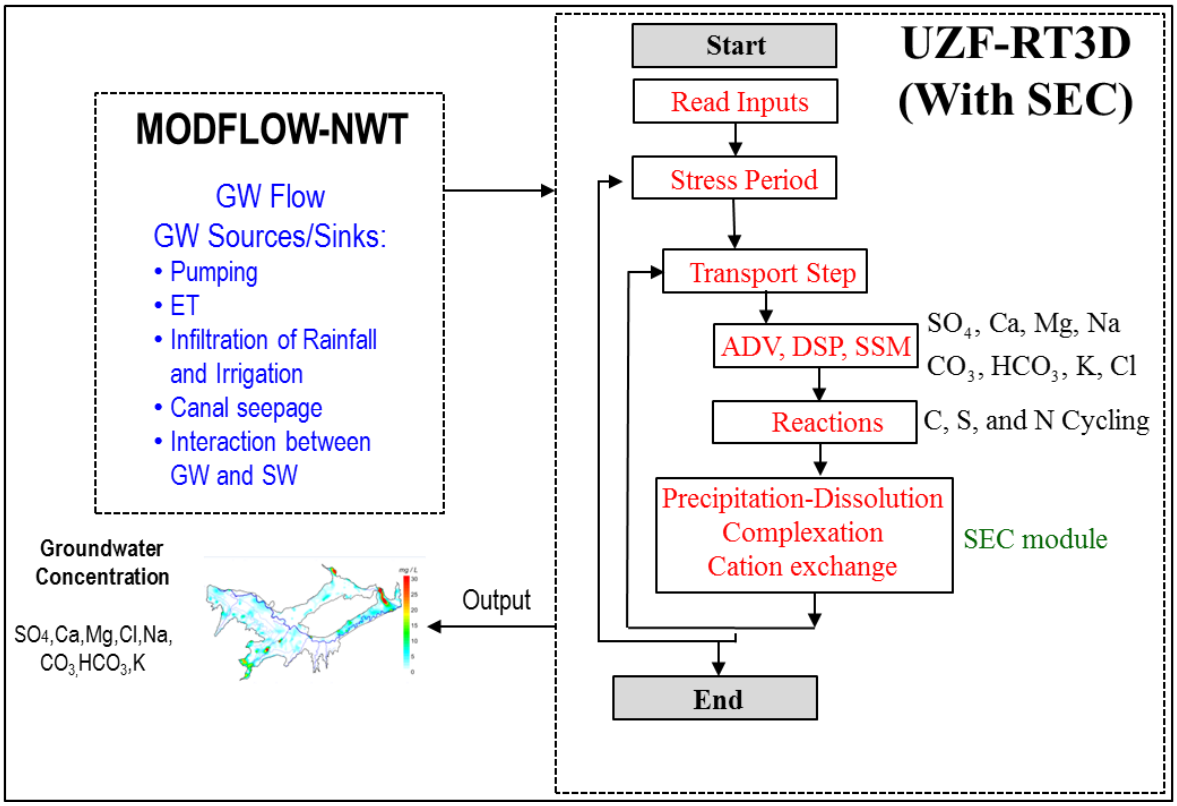

Figure 3.4. Coupling the equilibrium chemistry module with the UZF-RT3D transport model.

For each time step, UZF-RT3D first solves for concentration of each solute at each finite-difference grid cell according to advection, dispersion, source/sink mixing (solutes entering/leaving the aquifer via groundwater sources/sinks), and kinetic reactions, with the latter including the cycling of C, N, and S. Concentrations for each ion at each grid cell are then provided to the SEC module, with ion concentrations updated using the methods described in the previous section. The updated concentrations are then provided for the start of the next time step, with this coupling proceeding until the end of the simulation. In this coupling, the local equilibrium concept is adopted, in which the duration of the selected time step is assumed long enough for all interactions between chemical constituents to reach equilibrium (Rubin, 1983; Javadi & Al-Najjar, 2007; Al-Hamdan & Reddy, 2008).

3.4. Model Application at the Regional Scale

3.4.1. Study Region: Lower Arkansas River Valley, Colorado, USA

The UZF-RT3D model with the SEC module was applied to a 500 km^2 stream-aquifer system within the Lower Arkansas River Valley (LARV) in southeastern Colorado (Figure 3.5). For more than 130 years the region has been one of the most productive agricultural areas in the state of Colorado. Crops include alfalfa, melons, corn, beans, sorghum, wheat, grass, and vegetables. The climate is semi-arid, with average monthly rainfall ranging from 0.7 cm during the winter months (October-March) to 5.0 cm during the summer months (April-September). Irrigation is practiced from March to November, with irrigation water diverted from the Arkansas River via six irrigation canals or pumped from the alluvial aquifer.

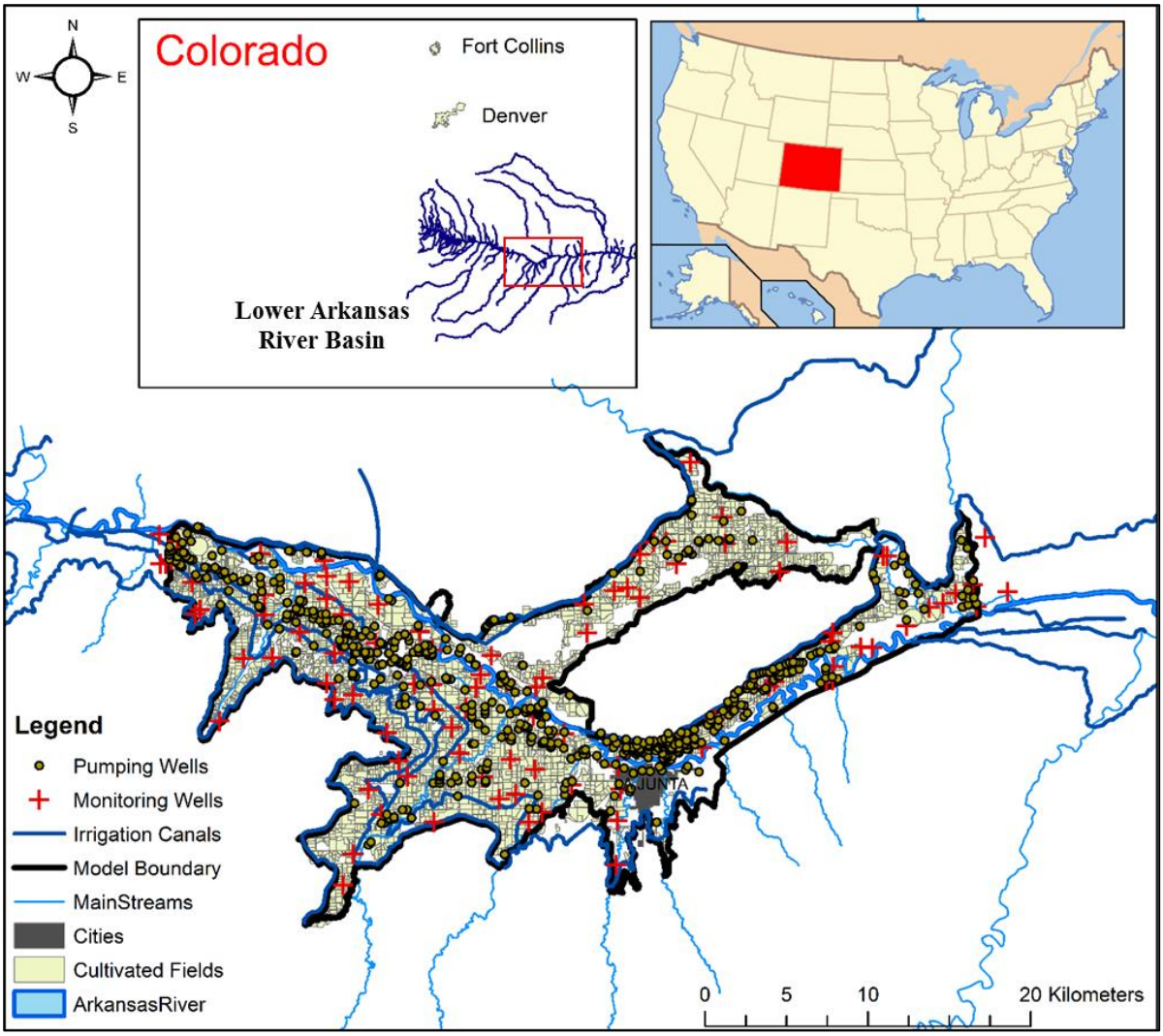

Figure 3.5. Location of the study region, showing the Arkansas River and its tributaries, irrigation canals, cultivated fields, monitoring wells, and pumping wells.

The region is impaired by high salinity in groundwater, surface water, and soil, caused by the existence of salt minerals, particularly gypsum ($CaSO_4$), waterlogging in the shallow subsurface (Konikow and Person, 1985; Hukkinen, 1993; Goff et al., 1998; Morway and Gates, 2012; Gates et al., 2002, 2016), and evaporative concentration. Figure 3.6 shows salt ion proportions from the analysis of 389 groundwater samples in the study region using a Piper Diagram (Piper, 1944), illustrating the hydro-geochemical facies of samples. The samples were collected between 2006 and 2009 from the monitoring wells shown in Figure 3.5. Results indicate that the majority of the

samples are type Ca-SO_4, due to the dominant presence of gypsum. Frequency histograms of C_{TDS}, $C_{SO_4\text{-}S}$, and C_{Ca} in groundwater samples are shown in Figure 3.7A, 3.7B, and 3.7C respectively. Comparing the spatio-temporal average C_{TDS} in the groundwater (2,732 mg/L) with the estimated maximum permissible C_{TDS} value for irrigation without crop yield reduction (~700 mg/L, See Figure 3.6) (Ayers and Westcot 1985) indicates the severity of salinization in the region. Also, the secondary EPA drinking water standard for C_{SO_4} is 250 mg/L, much less than the observed average of 630 mg/L (for $C_{SO_4\text{-}S}$) in the study region. Previous studies have estimated that high salinity in the groundwater and soil root zone have led to average crop yield reduction of up to 7% in the region (Gates et al., 2002; Morway and Gates, 2012).

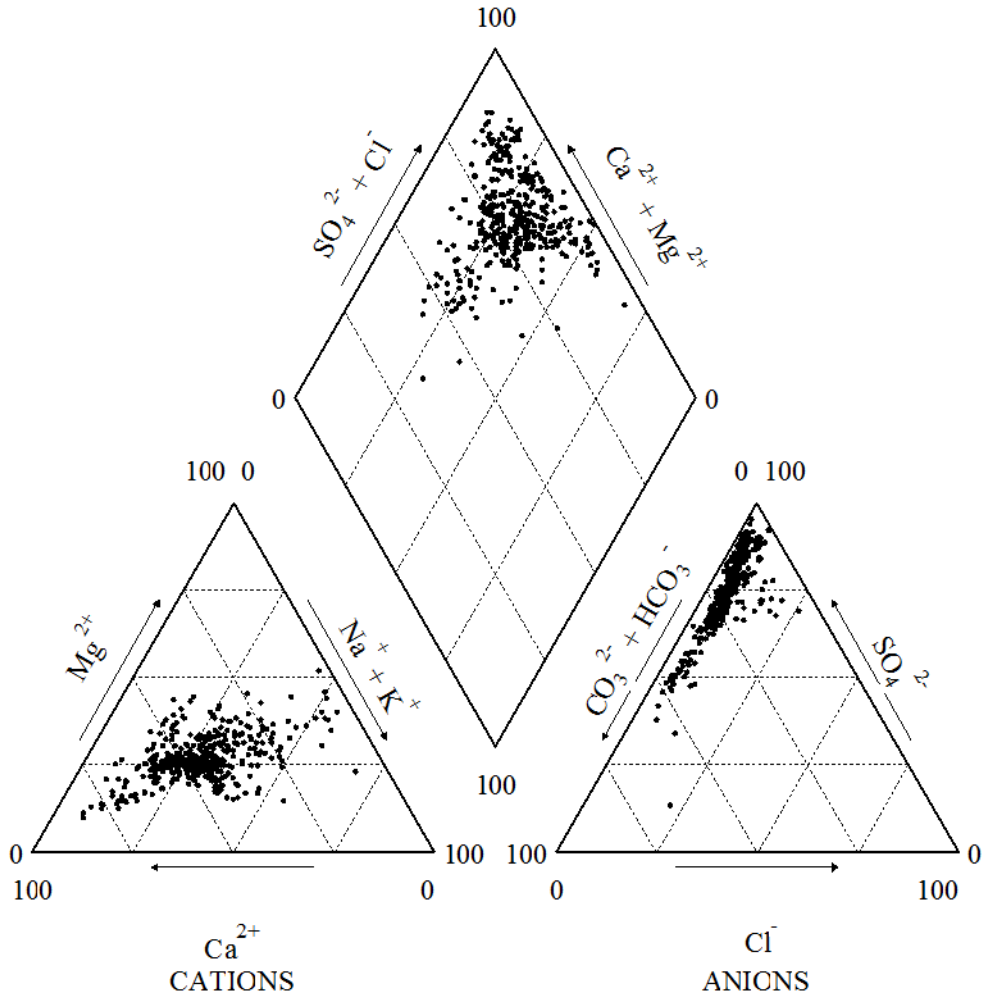

Figure 3.6. Piper diagram of ion concentrations in groundwater samples from the study region over the modeled period. Units are normalized and expressed as a percent of proportional mass per cation/anion.

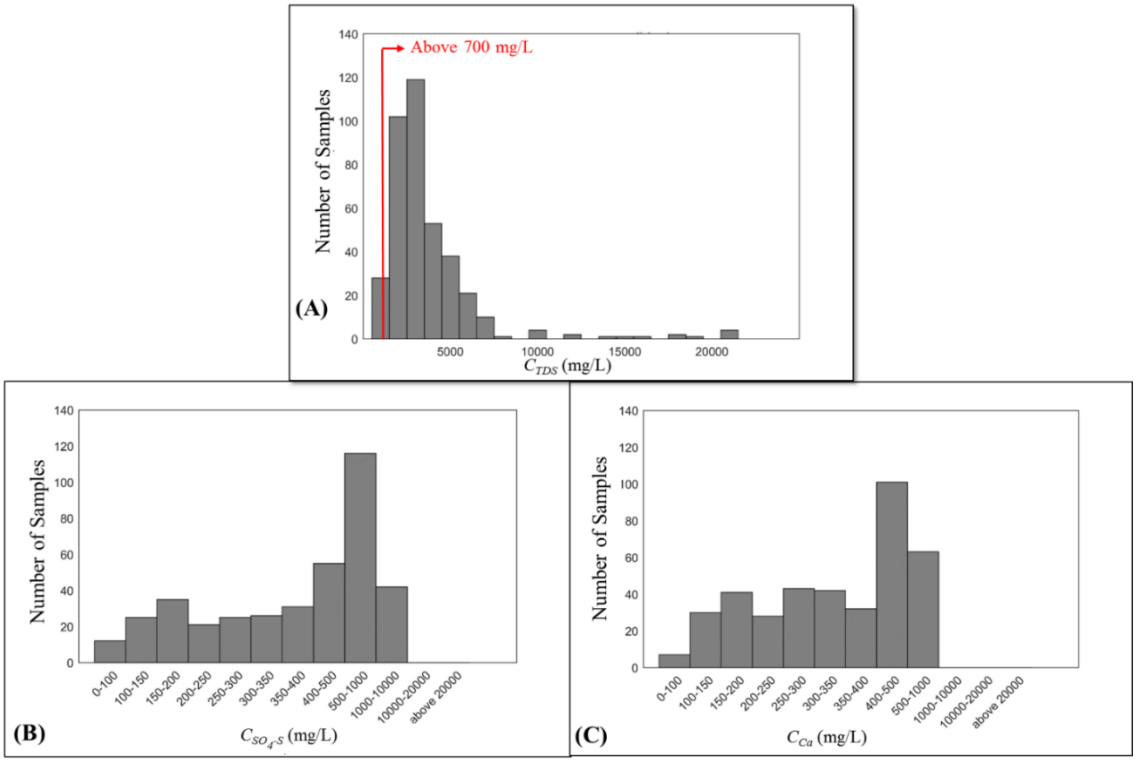

Figure 3.7. Frequency of (A) C_{TDS}, (B) $C_{SO_4\text{-}S}$, and (C) C_{Ca} in groundwater samples.

The groundwater flow patterns in the study region have been simulated by Morway et al. (2013), who used MODFLOW with the UZF1 package for unsaturated zone flow (Niswonger et al., 2006). The region is discretized into 250 m by 250 m grid cells horizontally and three layers vertically from ground surface to the shale bedrock (average depth is 15 m). The model considered infiltrated rainwater and irrigation water, groundwater pumping from 575 pumping wells (see Figure 3.5 for location), seepage from six irrigation canals, evapotranspiration from cropped and naturally-vegetated areas, and discharge to / seepage from the Arkansas River and its tributaries (Morway et al., 2013). The model was run for the period 1999-2007, which was extended in a later study through 2009 (Bailey et al., 2014). As example model input and output, the calibrated cell-by-cell values of hydraulic conductivity (m/d) are shown in Figure 3.8A, and the cell-by-cell average depth to water table during the simulation period is shown in Figure 3.8B.

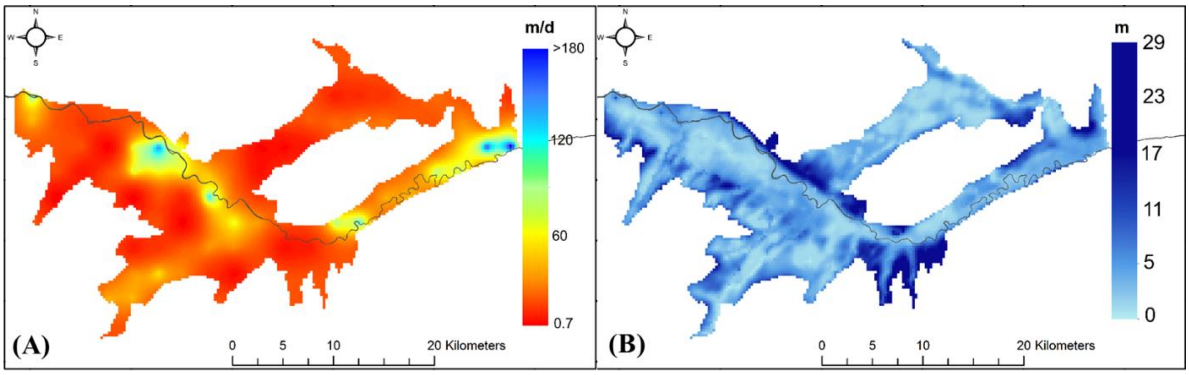

Figure 3.8. (A) Hydraulic conductivity (m/d) of the upper alluvium material, based on a tested groundwater flow model of the region (Morway et al., 2013), and (B) Average depth to the water table (m), as simulated by the flow model.

The UZF-RT3D / SEC model uses the flow patterns and sources/sinks from the MODFLOW model, with the same areal discretization but with six vertical layers spanning the depth between the ground surface and the shale bedrock. The top two layers are each 0.5 m in thickness to simulate solute chemistry and C, N, and S cycling in the root zone. The third layer is 1.0 m, and the thickness of the remaining three layers is divided evenly over the remaining depth to the shale bedrock. The model is run from January 1, 2006 to October 31, 2009 using daily time steps.

Concentration of the major ions in both surface water irrigation and groundwater irrigation is accounted for. For surface irrigation, with water derived from adjacent irrigation canals, the concentrations are specified using results from the analysis of canal water samples which were taken periodically in the river near the canal diversion during the simulation period (see Table S1 in Supporting Information in Appendix B for concentration values). For groundwater irrigation, concentration values of the ions are simulated by UZF-RT3D at the location of the well screen (layer 4 of the model). For areas where water from canals, tributaries, and the Arkansas River seeps into the aquifer, the salt ion concentrations in the surface water are estimated from field

samples collected during the simulation period (see Table S1 in Supporting Information in Appendix B for values).

Crop parameters are provided for each crop type (see Figure 3.9 for spatial distribution of crop type in 2006). These parameters govern the management and growth of each crop, and include the typical planting, harvesting, and plowing dates; fertilizer application and uptake; root growth and death; and C/N and C/S ratios. Parameters for organic matter decomposition, oxidation-reduction reactions, crop uptake, and linear sorption also are provided for C, N, and S cycling and for the chemical reduction of O_2, NO_3, and SO_4 in groundwater. These values are the same as those used in the S cycling and SO_4 transport model of Tavakoli Kivi and Bailey (2017), and are included in Supporting Information in Appendix B as Tables S2 and S3.

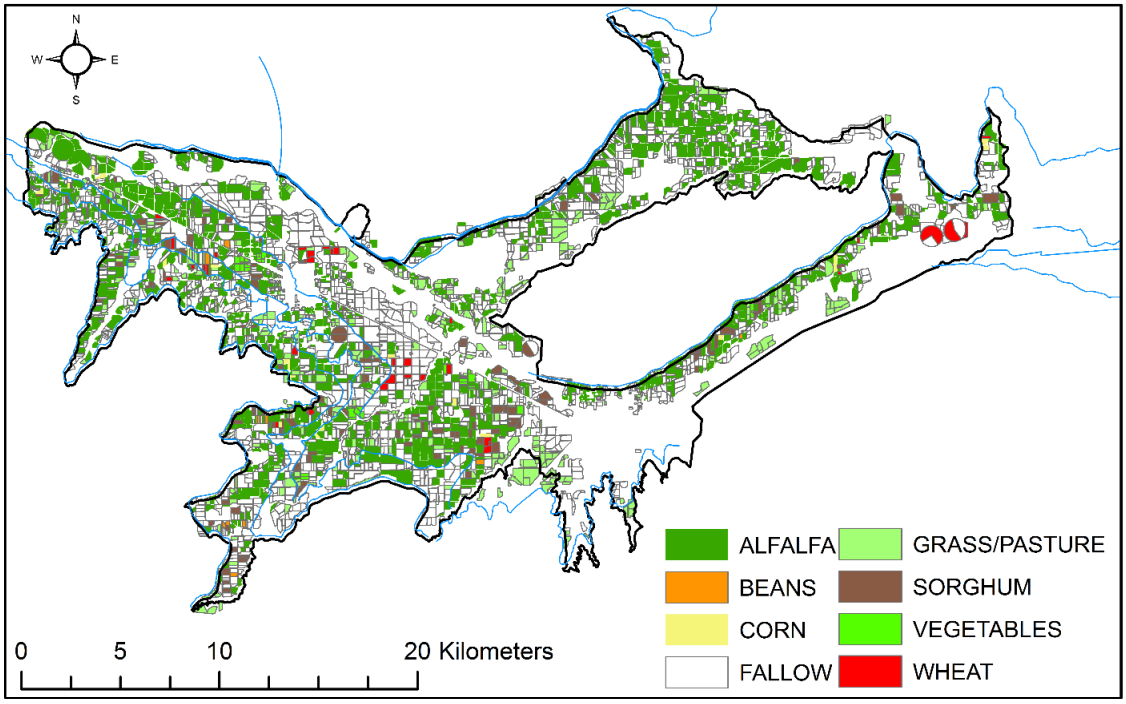

Figure 3.9. Crop type of each cultivated field during the 2006 growing season in the study region.

Parameters used in the SEC module are the same as those described in Section 3 (see Tables 3.3-3.7). The initial spatial distribution of salt minerals, $CaSO_4$ and $CaCO_3$, which is mapped to the individual grid cells, is based on a soil survey performed by the USDA's Natural Resources

Conservation Service (NRCS) (https://websoilsurvey.sc.egov.usda.gov/App/WebSoilSurvey.aspx). Data for $CaSO_4$ and $CaCO_3$ are expressed as a percent by weight, with values up to 45% and 8%, respectively, for the minerals.

3.4.2. Model Calibration and Testing

3.4.2.1. Comparing Model Results with Field Data

Estimation of model parameters in the coupled model involved analyzing solute concentrations and groundwater salt ion mass loadings during a spin-up simulation and during the 2006-2008 calibration period, with field data from 2008-2009 used as testing data. The spin-up simulation was included to achieve steady seasonal fluctuations of salt ion concentration in the aquifer and a steady fluctuation of groundwater salt ion mass loading to the Arkansas River, and was prepared by repeating the cropping and flow pattern for the year 2006 for 10 years using crop and chemical reaction parameters from Bailey et al. (2014).

The comparison of model results with measured values during the calibration and testing periods was conducted in a manner advocated by Konikow (2011), with the objective of reproducing major trends and spatio-temporal statistics rather than time series of concentrations at point locations of measurement (e.g. monitoring wells), the scale of a model grid cell being 10^7 to 10^8 times larger than that of a measurement location within the cell. With this objective, model results were tested against observed spatio-temporal averages of concentration for each salt ion, with spatial averages occurring by irrigation command area (see Figure 3.10) due to the unique water rights priority, irrigation, and cultivation histories of each command area. Results also are compared using the frequency distribution of concentration for each salt ion. These comparisons are performed for each salt ion in the saturated zone of the aquifer.

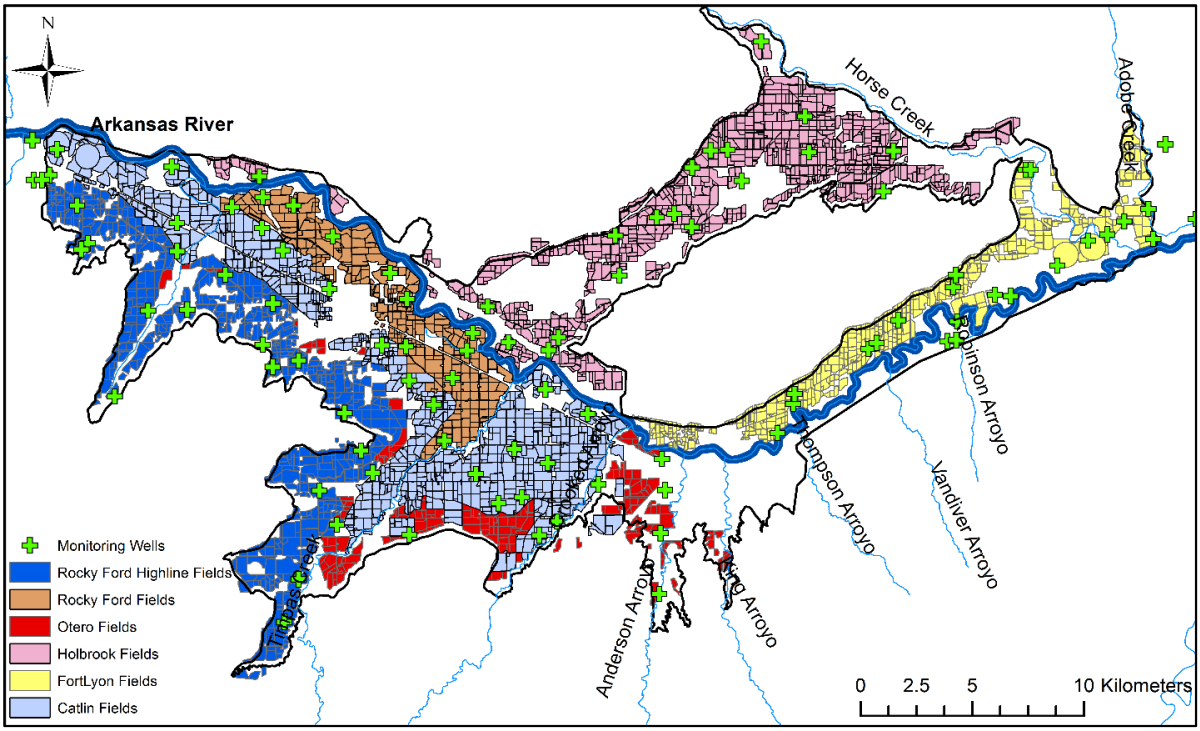

Figure 3.10. Division of the study region into canal command areas with fields receiving irrigation water from the Rocky Ford Highline, Rocky Ford, Otero, Holbrook, Fort Lyon, and Catlin canals.

For the soil root zone, the frequency distribution of C_{TDS} is compared between the model and values derived from more than 54,000 measurements of soil electrical conductivity (EC) in many fields scattered across the study region (Morway and Gates 2012). The EC values (dS/m) are converted to C_{TDS} (mg/L) using a relationship that exists between EC and C_{TDS} in groundwater samples collected in the saturated zone (Gates et al., 2016). For the model, C_{TDS} for each grid cell in the top 2 layers of the model is computed by summing the simulated concentrations of the ions. Since the soil EC values were estimated using a saturated paste extract, only model results from cells with a near-saturation water content (above 95%) were included in the frequency distribution comparison.

In addition to using groundwater solute concentrations for model testing, stochastic river mass-balance calculations were performed, using a method similar to Mueller-Price and Gates (2008), for the stream system to determine the approximate daily mass loadings of SO_4 and TDS

to the Arkansas River that are not accounted for by measured loading from the tributaries. It is assumed that a substantial portion of the unaccounted-for mass loading, especially during the non-irrigation season, can be attributed to mass loading from the aquifer to the Arkansas River, and thereby provides an additional test for model results.

3.4.2.2. Parameter Estimation Methodology

Estimation of parameters in the SEC module was performed using a joint manual and automated calibration approach to achieve a satisfactory match between observed and simulated target variables. Target variables include spatially-averaged $C_{SO_4\text{-}S}$, C_{Ca}, C_{Mg}, C_{Na}, C_{Cl}, C_{HNO_3} and C_{TDS} in the saturated zone; spatially-averaged C_{TDS} of soil water in the root zone; the relative frequency distribution of all major salt ions in the saturated zone; the relative frequency distribution of C_{TDS} in soil water in the root zone; and groundwater mass loading of SO_4 and TDS to the Arkansas River.

A variant of the Brier Score (BS) (Brier 1950), which compares the relative frequency distribution of two sample sets and commonly is used to evaluate probability distribution performance, is computed in this study for a relative frequency histogram of n_b classes, or bins, as:

$$\mathrm{BS} = \left(\frac{1}{n_b}\right)\sum_{1}^{n_b}\left(f_i - o_i\right)^2 \qquad (37)$$

where f_i is the relative frequency of simulated values in the i^{th} bin and o_i is the relative frequency of observed values in the i^{th} bin. The value of $(BS)^{1/2}$ ranges between 0 and 1, providing a measure here of the average discrepancy between simulated and observed relative frequency, with values of $(BS)^{1/2}$ closer to 0 indicating a better match.

As a first step in the calibration process, the solid salt content in the soil profile was adjusted using initial values from NRCS soil survey data to yield C_{TDS} in the soil root zone that is similar

to the observed soil sampling data. Preliminary simulations also indicated that model results are strongly dependent on the solubility product K_s for each salt represented in the model, which are governed by temperature and pH. Since the temperature in the root zone and in the deep layers of the aquifer differs seasonally, a value of K_s was assigned to each of the saturated and unsaturated zones for each salt mineral. Once the salt distribution was determined, the PEST (Parameter Estimation) software (Doherty, 2007) was used to refine the solubility products of each salt solid. PEST adjusts selected parameters in sequential simulation runs to minimize the objective function, which is the sum of the squared weighted residuals between the observed and simulated values:

$$\Phi = \sum_{i}^{n_v} w_i (o_{v_i} - m_{v_i})^2 \tag{38}$$

where Φ is the objective function, n_v is the number of target variables, w_i is the weight assigned to the ith target variable, and o_{v_i} and m_{v_i} are the observed and simulated values of the i^{th} target variable, respectively. The value of w_i for each target variable is calculated as the product of an uncertainty weight and a unit discrepancy weight. The uncertainty weight, was calculated as the inverse of an estimated coefficient of variation (CV) reflective of the relative uncertainty in the observations of the target variable. The unit discrepancy weight, was determined by unifying the sum of the square of each observed variable value.

An iterative approach using both the spin-up simulation and the 2006-2008 simulation was used in the model calibration procedure due to the dependence of initial concentrations in 2006 on the long-term spin-up simulation. Initial K_s values for the SEC module were assigned from the literature (Table 3.6). The overall procedure is as follows:

a. Establish a preliminary set of initial conditions for the 2006-2008 simulation using a 30 year spin-up simulation;

b. Use PEST to provide an estimate of K_s values according to command area;

c. Re-run the spin-up simulation with the new set of K_s values to establish new initial conditions, with comparisons made to estimated SO_4 and TDS mass loading to the Arkansas River. The spin-up simulation was re-run using K_s values until the groundwater salinity mass loadings at the end of the spin-up simulation matched well with the range of observed daily groundwater salinity mass loadings during the 2006-2008 period;

d. A further adjustment was made comparing the model results to observed values within the test period by manually adjusting the K_s values to achieve the best match between simulated and observed salt ion concentrations in the saturated zone.

Values of K_s were assigned to each canal command area for both the soil root zone and the saturated zone and were estimated using PEST considering the target values. Parameter values resulting from the UZF-RT3D/SEC calibration process are shown in Table 3.8, all of which fall within the range of values reported in the literature.

Table 3.8. Calibrated solubility product for salt solids using PEST.

Solubility Product	Unsaturated zone	Saturated zone
K_{sp_1}	4.9300×10^{-5}	3.5691×10^{-5}
K_{sp_2}	3.0700×10^{-9}	3.7037×10^{-9}
K_{sp_3}	4.7900×10^{-6}	4.7937×10^{-6}
K_{sp_4}	0.0070	0.0071
K_{sp_5}	37	37.2

3.4.3. Calibration and Testing Results

Figures 3.11(A), 3.11(B), and 3.11(C) show the cell-by-cell computed $C_{SO_4\text{-}S}$, C_{Ca}, and C_{TDS} values in groundwater, averaged over the 2006-2009 simulation period. High levels of $C_{SO_4\text{-}S}$ and C_{TDS} occur principally in the Rocky Ford Highline canal command area and in the Holbrook canal command area (see Figure 3.10). Typically, areas of high C_{Ca} coincide with areas of high $C_{SO_4\text{-}S}$ indicative of the presence of gypsum. The areas of highest concentration often are far from the Arkansas River, indicating that mass loadings of TDS to the river are lower than what could be expected if the plumes of high-concentration groundwater move towards the river over the coming years. Figure 3.12 shows a spatial comparison between the simulated and observed $C_{SO_4\text{-}S}$ and C_{TDS} values in groundwater averaged over the 2006-2009 period. The observed values for 2006-2009 period were averaged for each monitoring well and the Kriging method was used to construct the contour plot of observed values for the study region. Although the purpose of the calibration was not to reproduce exact values at each grid cell, model results demonstrate the capability of the model to reproduce overall observed spatial patterns of groundwater salinity. In particular, the zones of observed high salinity in the Rocky Ford Highline and Holbrook canal command areas have been simulated by the model.

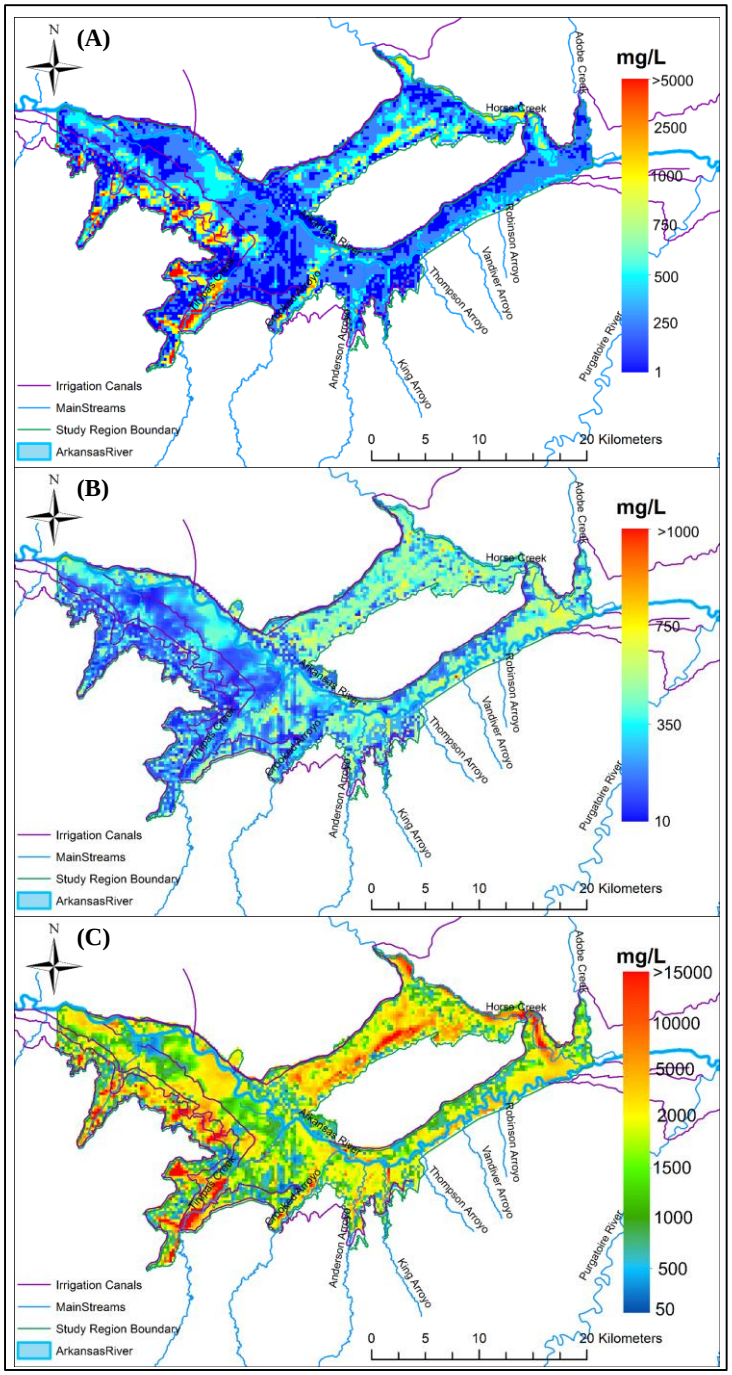

Figure 3.11. Raster plots of (A) average simulated $C_{SO_4\text{-}S}$ (mg/L), (B) average simulated C_{Ca} (mg/L), and (C) average simulated C_{TDS} (mg/L) in the middle alluvium (layer 4 of the model).

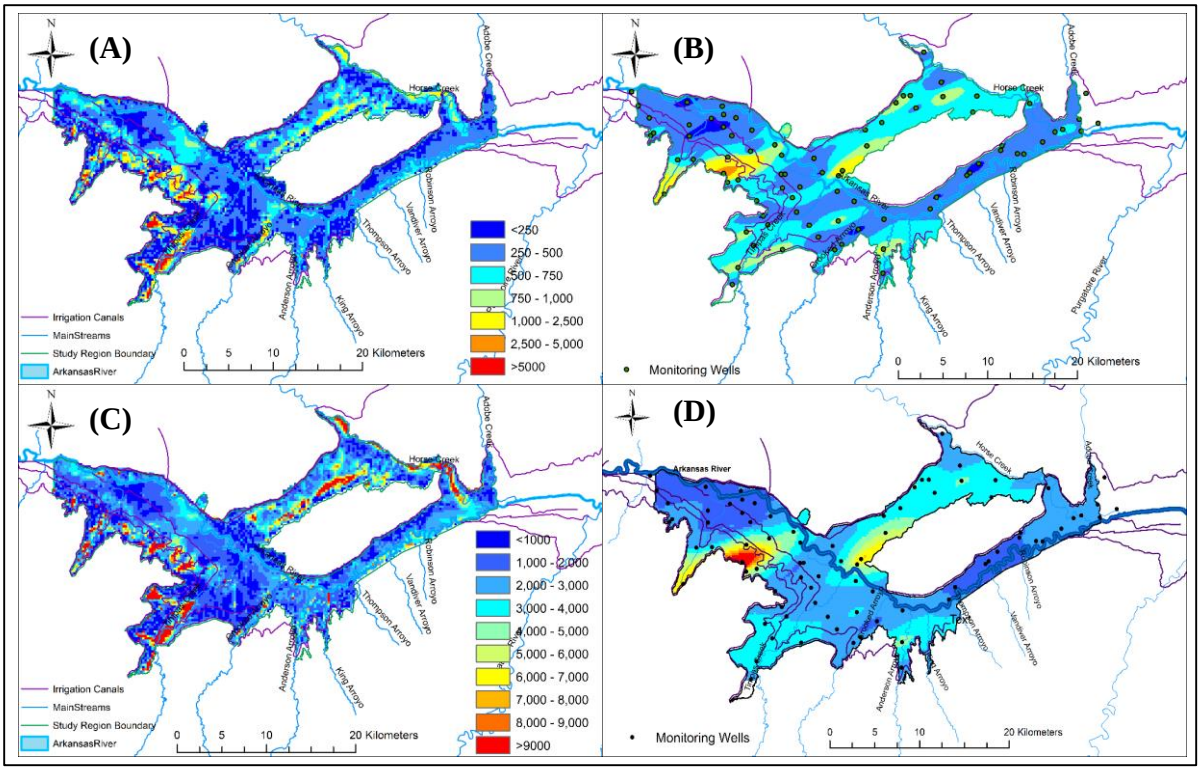

Figure 3.12. Raster plots of (A) average simulated $C_{SO_4\text{-}S}$ (mg/L), (B) average observed $C_{SO_4\text{-}S}$ (mg/L), (C) average simulated C_{TDS} (mg/L), and average observed C_{TDS} (mg/L) in the middle alluvium (layer 4 of the model).

The comparison between the simulated and observed average values within each canal command area for $C_{SO_4\text{-}S}$, C_{Ca}, C_{Mg}, and C_{TDS} in groundwater are shown in Figure 3.13 for both the calibration and testing periods. Whiskers on the plotted observed values represent ± standard deviation of an assumed normal distribution with CV = 0.43, estimated following the method described in Bailey et al (2014) to account for uncertainty due to measurement error and scale discrepancy. Considering this uncertainty, model results are favorable compared to the observed values. Interestingly, simulated and observed values for $C_{SO_4\text{-}S}$ and C_{TDS} have a better match for the testing period. The spatio-temporal average of simulated values of $C_{SO_4\text{-}S}$ within a grid cells in layer 4 over the entire region is 512 mg/L for the calibration period and 510 mg/ L for the testing period, compared with respective average observed values of 655 mg/L and 509 mg/L.

Layer 4 is chosen as the target layer since the groundwater monitoring wells typically are screened at a depth corresponding to the elevation represented by layer 4 in the model. For C_{TDS}, average simulated values in layer 4 are 2,822 mg/L and 2,845 mg/L for the calibration and testing periods, respectively, while average observed values are 3,003 mg/L and 2,813 mg/L for the calibration and testing periods.

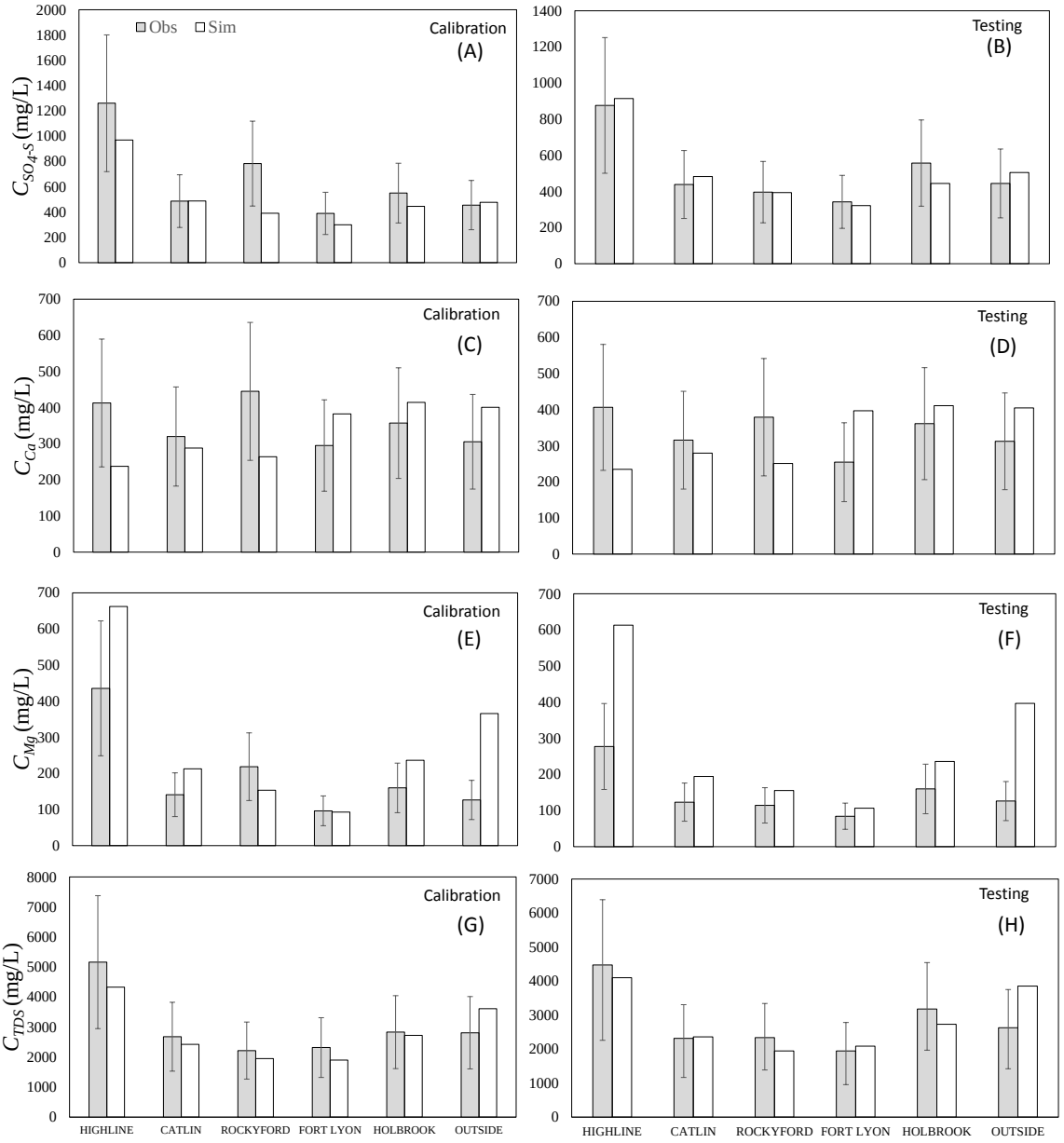

Figure 3.13. Comparison between simulated average and observed average $C_{SO_4\text{-}S}$, C_{Ca}, C_{Mg}, and C_{TDS} respectively for each command area for the calibration period (A, C, G, E) and for the testing period (B, D, F, H).

Figure 3.14 and 3.15 show relative frequency histograms for simulated values of $C_{SO_4\text{-}S}$, C_{Ca}, C_{Mg}, C_{Na}, C_{Cl}, and C_{HCO_3} in groundwater in layer 4 and for observed values. Although the previous comparison was made between the average values over the command region, these plots demonstrate the model's ability to reproduce the distributions of concentrations across the

region and over the model calibration and testing periods. Eleven bins are used to create the relative frequency histograms, up to a value of 20,000 mg/L, with a twelfth bin representing values above 20,000 mg/L.

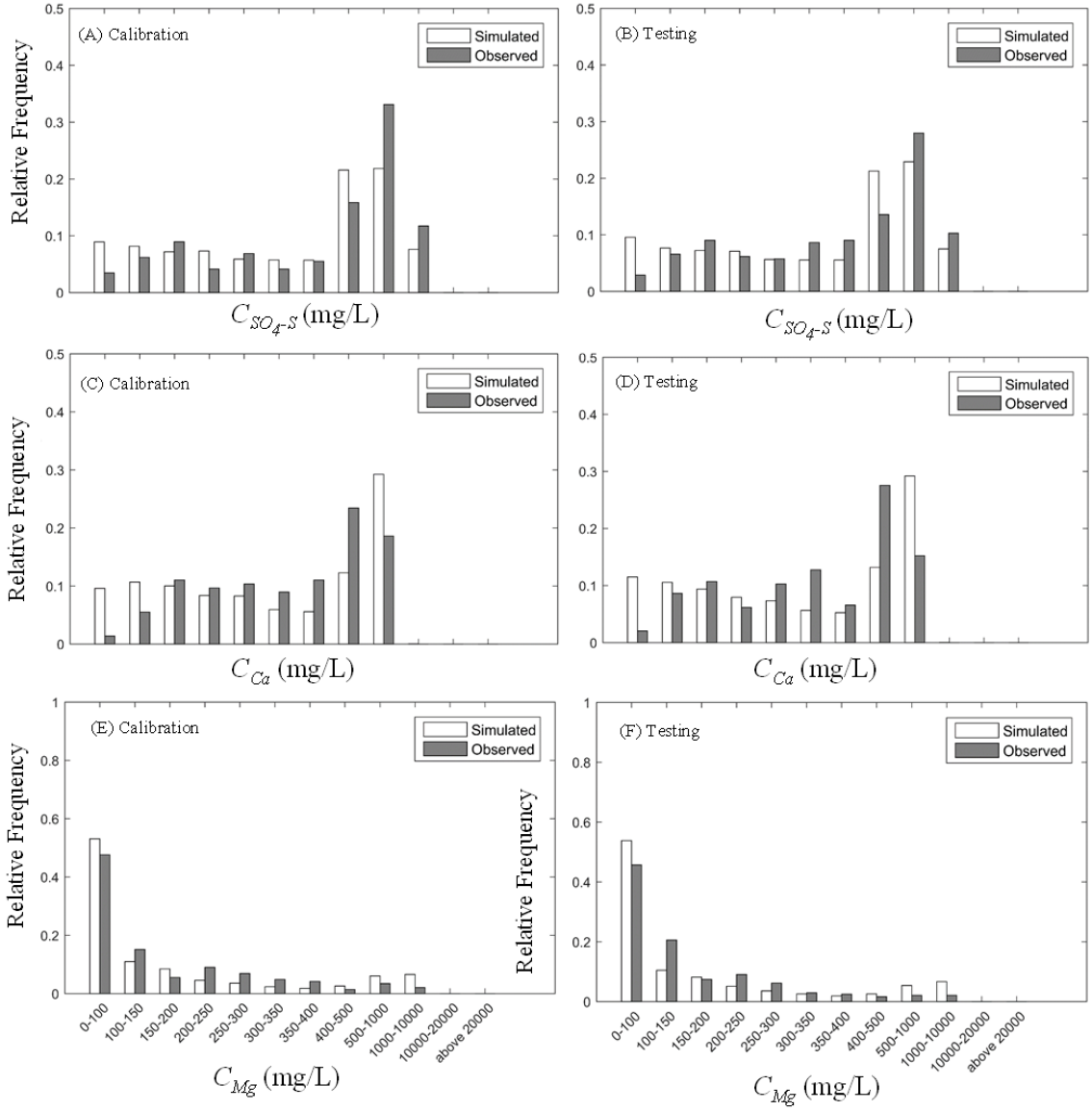

Figure 3.14. Comparison of relative frequency histograms for simulated and observed $C_{SO_4\text{-}S}$, C_{Ca}, and C_{Mg} for the calibration period (A, C, E) and the testing period (B, D, F).

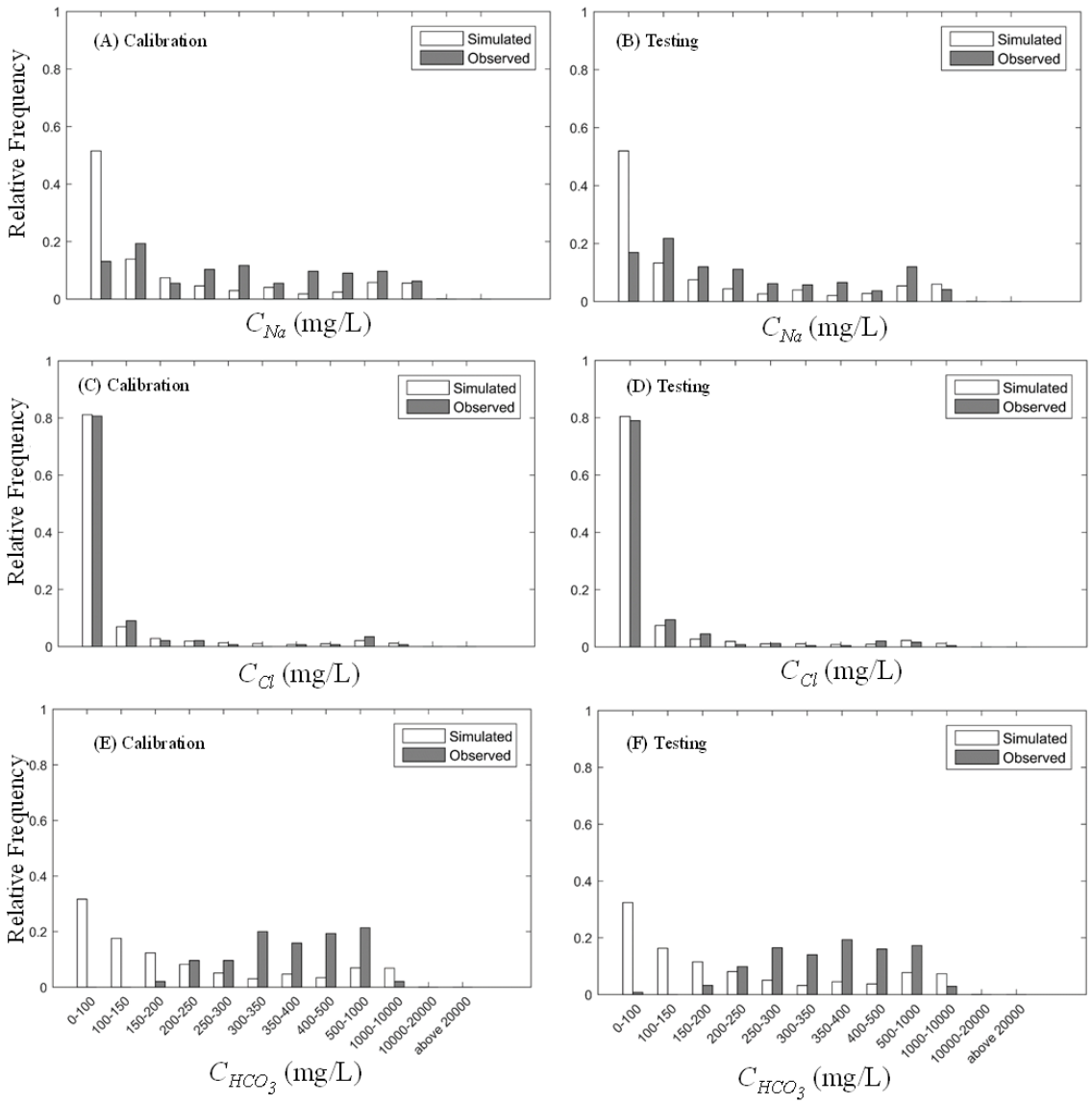

Figure 3.15. Comparison of relative frequency histograms for simulated and observed C_{Na}, C_{Cl}, and C_{HCO_3} or the calibration period (A, C, E) and the testing period (B, D, F).

The values of $(BS)^{1/2}$ for C_{SO_4}-s, C_{Ca}, and C_{Mg} in groundwater for the calibration period are 0.04, 0.06, and 0.03, and for the testing period are 0.04, 0.07, and 0.04, respectively, indicating the model accurately replicates not only the averages of each concentration but also the distributions of the observed data. The $(BS)^{1/2}$ values for C_{Na}, C_{Cl}, and C_{HCO_3} for the calibration period are 0.12, 0.01, and 0.14, respectively, and for the testing period are 0.11, 0.01, and 0.13.

The $(BS)^{1/2}$ score for simulated C_{HCO_3} and C_{Na} reveals poorer model performance for these specific ions. The main source of HCO_3 in groundwater is the dissolution of $CaCO_3$, which is also a source of CO_3. The SEC module currently does not fully accommodate the C cycle in a closed system; instead, the simple dissolution formula for $CaCO_3$ in Eq. (34) is used (Millero, F.J., 2001). As a result, the model under-predicts C_{HCO_3}. The main source of Na is dissolution of NaCl. In the LARV, as shown in Figure 3.6, most of the groundwater samples are Ca-SO_4 type; thus, under-predicting C_{HCO_3} and C_{Na} does not compromise the validity of this and similar applications in terms of total salinity transport and storage. By including the full C cycle and considering the partial CO_2 pressure, C_{HCO_3} would be calculated as a secondary component in $CaCO_3$ dissolution.

Although not used in parameter estimation, time series of measured and simulated values of $C_{SO_4\text{-}S}$ and C_{Ca} are shown in Figure 3.16 for three monitoring wells in the study region. Poor matches (see Well 204 for C_{Ca}) can result in these point-by-points comparisons, in part due to the large discrepancy between the model grid scale and the observation scale. Nevertheless, in general the model yields values of similar magnitude to the field data. If desired, cell-by-cell chemical reaction parameters could be calibrated, albeit with great computational effort, to yield better matches with point measurements. However, the purpose of the model is to reproduce general spatial and temporal trends and distributions.

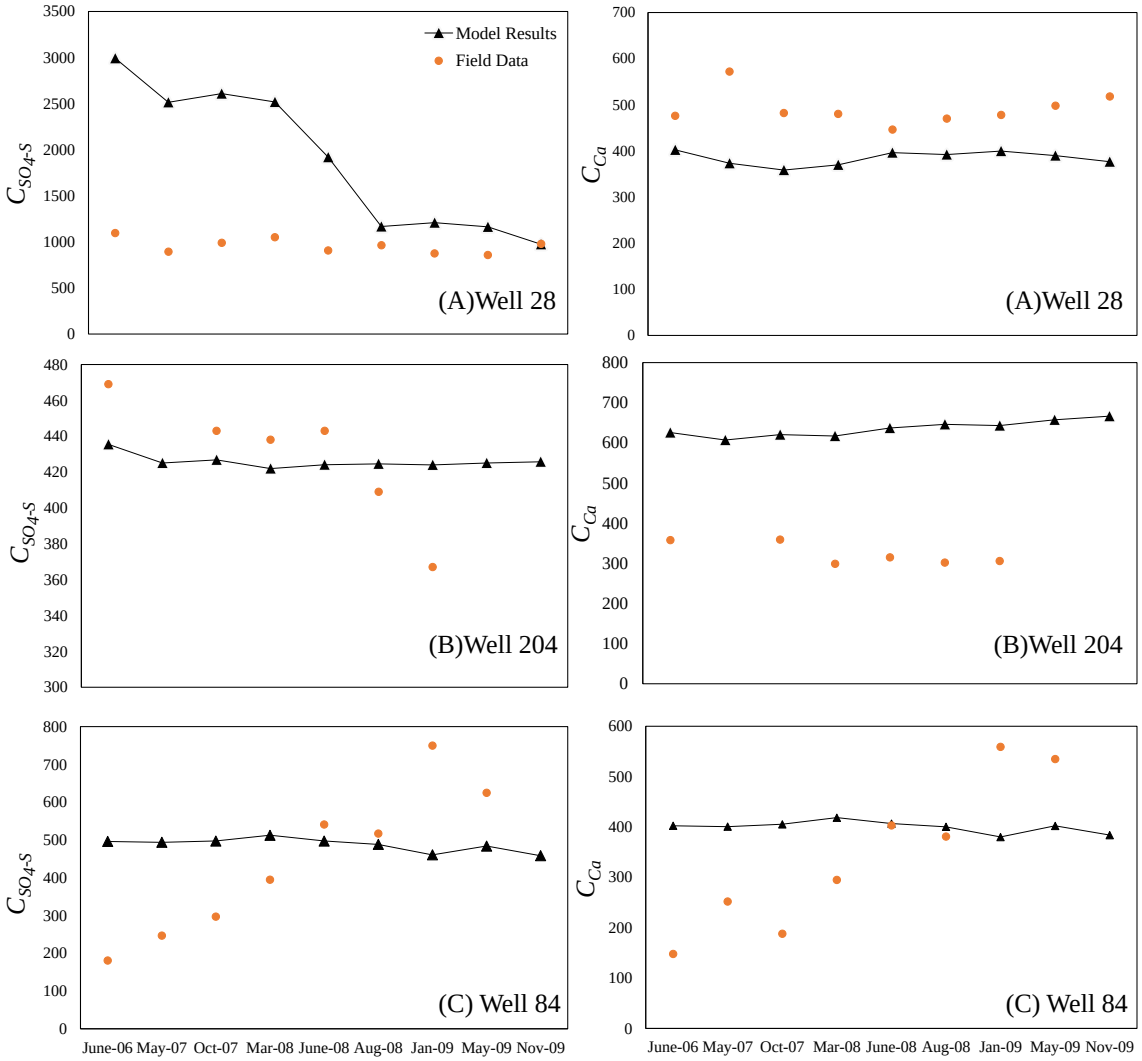

Figure 3.16. Comparison of simulated $C_{SO_4\text{-}S}$ and C_{Ca} values in grid cells contacting (A) Well 28, (B) Well 204, and (C) Well 84 and values measured in the corresponding wells, demonstrating a variety in model results with point measurements.

Figure 3.17 shows the simulated cell-by-cell values of C_{TDS} in the root zone (top 1 m) soil water, averaged over the 2006-2009 simulation period. High soil salinity (> 10,000 mg/L) occurs in many areas in the region, principally in the fields irrigated by the Catlin and Rocky Ford Highline canals (see Figure 3.10), and along Timpas Creek and Crooked Arroyo and certain reaches of the Arkansas River. The severity of the problem in regards to potential impact on crop yield is apparent when compared to permissible limits of C_{TDS} to avoid yield reduction for alfalfa

and corn, the dominant crops in the LARV. Assuming an average soil water content at 40% of saturation in irrigated fields over the region, threshold C_{TDS} values of 4,300 mg/L and 5,100 mg/L can be estimated for corn and alfalfa, respectively (Grieve et al, 2012; Gates et al 2016). The average value of C_{TDS} computed over the region and over the simulation period was 4,993 mg/L, suggesting that a substantial area is suffering from crop yield reduction. These results are comparable with the conclusions of Morway and Gates (2012) for this same region, with 22% of locations surveyed exceeding the crop-yield threshold. Also, higher C_{TDS} values are expected in areas with shallow groundwater where more salt enters the root zone by upflux from saline groundwater when the water table rises (Morway and Gates 2012). Comparing the water table depth plot (Figure 3.8B) with the location of high C_{TDS} in Figure 3.17 complies to the same conclusion. The average value of simulated C_{TDS} for cells with near-saturated soil conditions (see Section 4.2.1) is 4,034 mg/L, which matches favorably with the average observed C_{TDS} of 4,180 mg/L in soil saturated extract samples. The relative frequency histograms of simulated and observed C_{TDS} values for near-saturated soil conditions are shown in Figure 3.18. The value of $(BS)^{(1/2)}$ is 0.03, indicating that the model can be employed to satisfactorily estimate soil salinity over a regional scale, allowing subsequent estimation of impacts on crop yields.

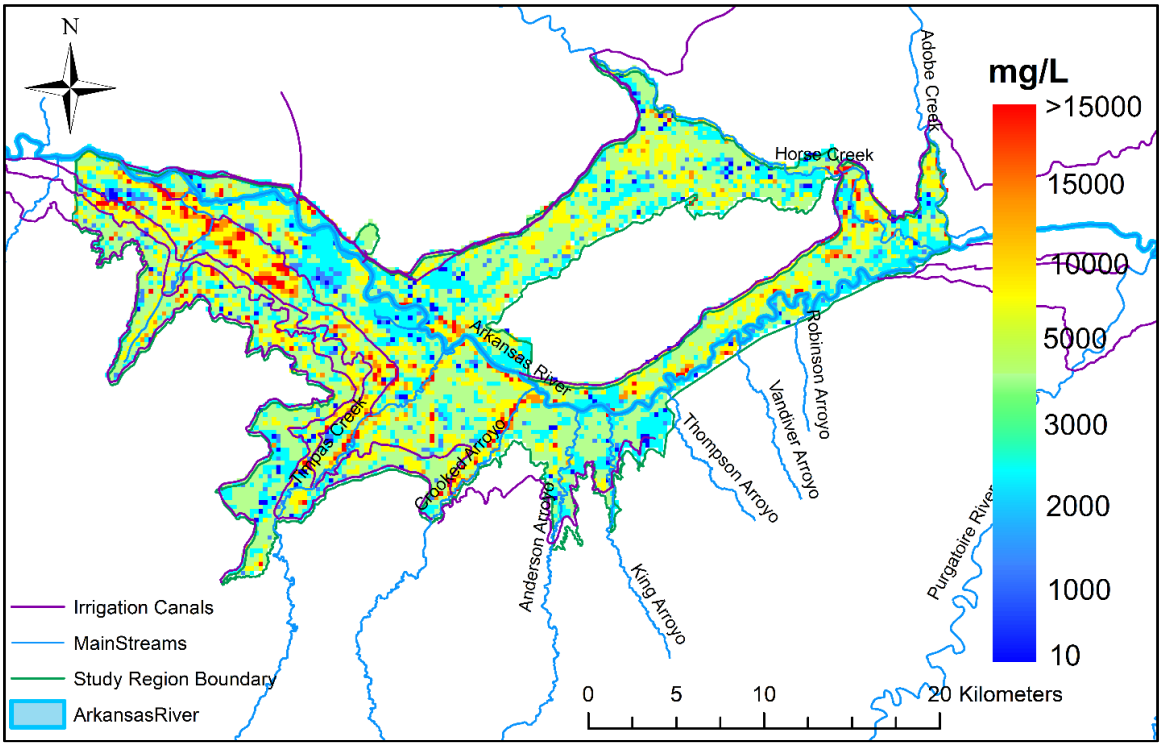

Figure 3.17. Raster plots of C_{TDS} (mg/L) in the root zone, as simulated by the UZF-RT3D/SEC model.

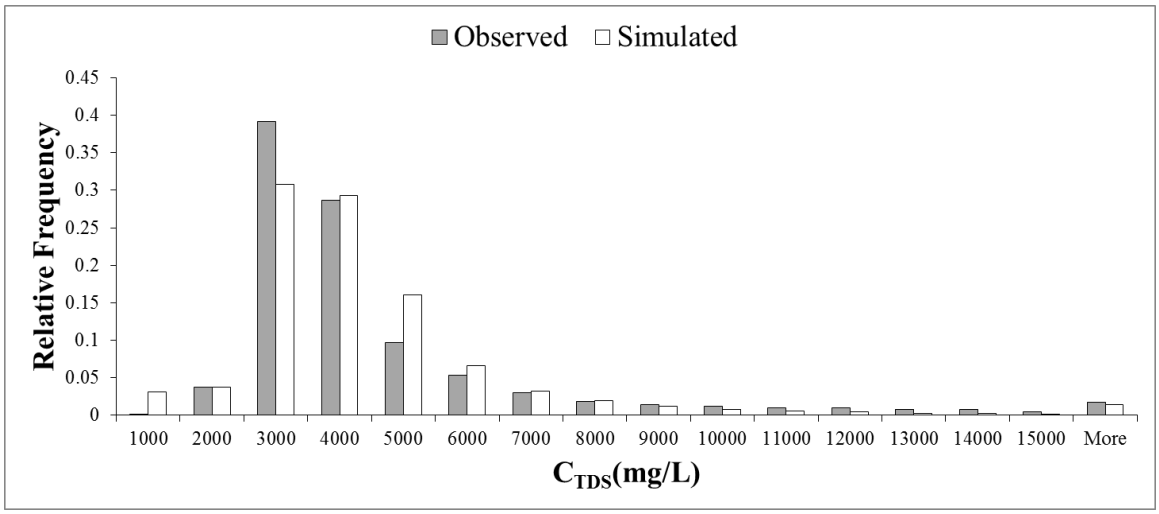

Figure 3.18. Comparison of frequency histogram of simulated and observed C_{TDS} in the soil root zone.

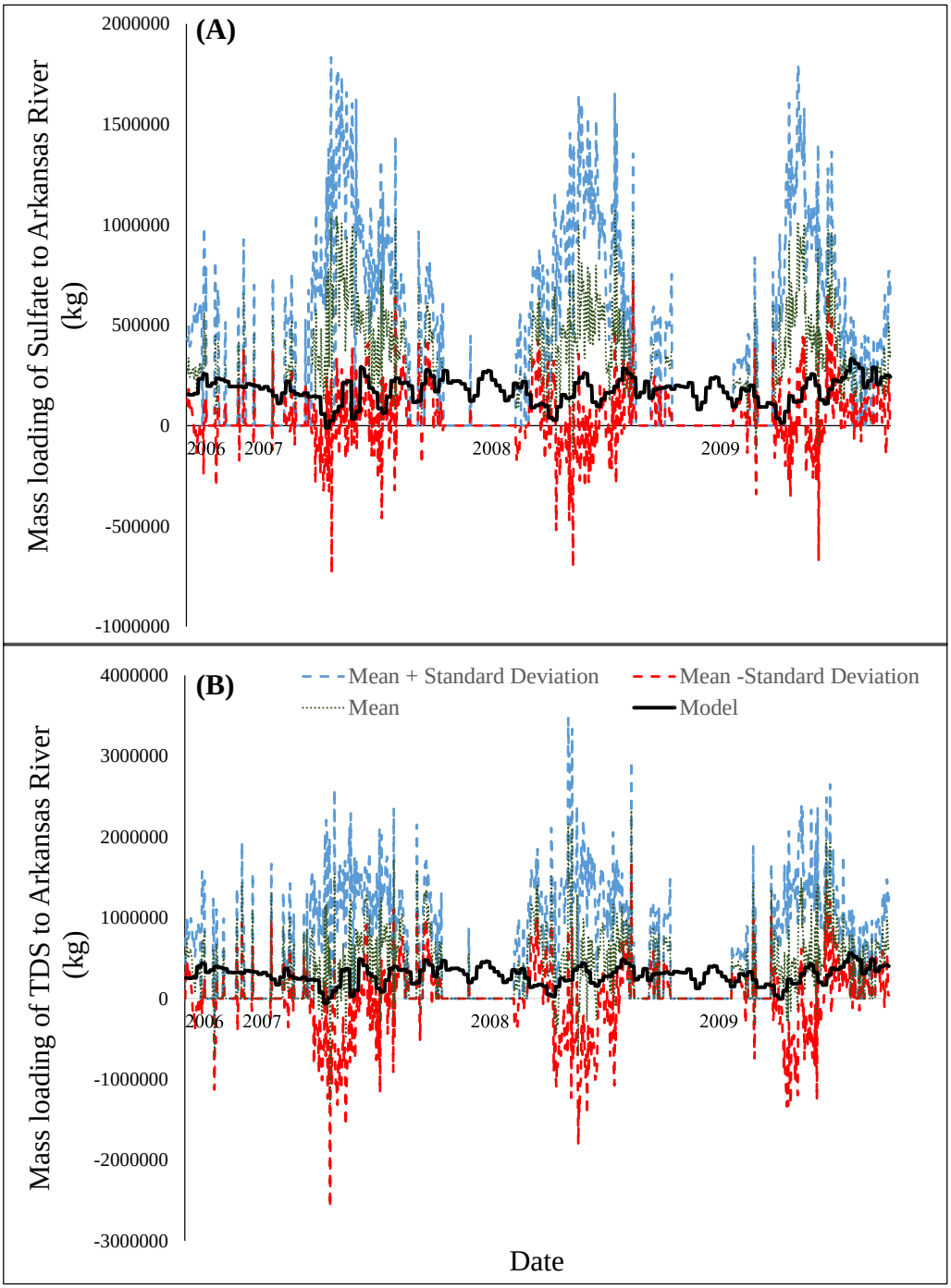

Figure 3.19. Simulated (A) SO_4 and (B) TDS groundwater mass loading to the Arkansas River for each day during the 2006-2009 simulation period. Statistics of stochastic mass balance estimates of total unaccounted-for mass loading are also shown.

The simulated daily average SO_4 and TDS mass loadings from groundwater to the Arkansas River (kg/day) are shown in Figure 3.19, with a comparison to statistics of the stochastic river mass balance estimates of total unaccounted-for mass loading. The model-predicted groundwater mass loading to the river typically is well within the stochastic mean minus one standard deviation and is below the stochastic mean. This is to be expected since the stochastic mass balance results represent both groundwater mass loading and loading from unaccounted-for surface water returns to the river.

3.5. Summary and Conclusions

The UZF-RT3D variably-saturated multi-species reactive transport model was amended to include equilibrium chemical reactions for application in salt-affected agricultural groundwater systems. The developed Salinity Equilibrium Chemistry (SEC) module includes precipitation-dissolution, complexation, and cation exchange equilibrium reactions for the major cations and anions (calcium, magnesium, sodium, potassium, sulfate, chloride, bicarbonate, and carbonate). The module is imbedded into the UZF-RT3D modeling code to allow the fate and reactive transport of these ions to be simulated in both the unsaturated and saturated zones of an aquifer system. The resulting UZF-RT3D/SEC model also includes cycling of C, N, and S in the plant-soil system, with redox reactions and sorption included for dissolved oxygen, ammonium, nitrate, and sulfate.

The model is applied to a 500 km^2 irrigated groundwater system along the Lower Arkansas River alluvial aquifer system in southeastern Colorado, with model results tested against a large dataset of observed salt concentrations and estimates of groundwater salt ion mass loading to the river. Results indicate that including the SEC module results in simulated salt ion concentration values that approach the high observed concentrations in the study region, addressing a

deficiency noted by Tavakoli Kivi and Bailey (2017) in their earlier modeling of sulfur and the sulfate ion in the Arkansas River Valley using UZF-RT3D. Of key importance is the ability of the model to predict not only groundwater salt concentrations but also mass loadings to the river network, which affect downstream irrigated areas, and also to predict soil salinity, which can be used to determine impact on crop yield. The fully-calibrated model can be used to investigate best management practices for salt remediation in the Colorado's Lower Arkansas River Valley and shows potential for application to similar salt-affected regions worldwide.

REFERENCES

Allison, J., Kevin, J., 1991, MINTEQA2: A geochemical assessment model for environmental systems: Version 3.0 User's manual, Technical Report, 600/3-91/021.

Al-Hamdan, A.Z., Reddy, K.R., 2008, Electrokinetic remediation modeling incorporating geochemical effects, Journal of Geotechnical and Geoenvironmental Engineering, 134, pp. 91–105.

Appelo, C.A.J., Postma, D. and Geochemistry, G., 2005, Geochemsitry, Groundwater and Pollution. Taylor & Francis Group.

Ayers, R.S., and D.W. Westcot. 1985, Water Quality for Agriculture, FAO Irrigation and Drainage Paper 29 rev 1. FAO, UN, Rome 174pp.

Bailey, R.T., Gates, T.K., Halvorson, A.D., 2013a, Simulating variably-saturated reactive transport of selenium and nitrogen in agricultural groundwater systems, J. Contam. Hydrology, 149, 27-45.

Bailey, R.T., Morway, E.D., Niswonger, R., and Gates, T.K., 2013b, Modeling variably saturated multispecies reactive groundwater solute transport with MODFLOW-UZF and RT3D. Groundwater, 51(5), 752-761.

Bailey, R.T., Gates, T.K., Ahmadi, M., 2014, Simulating reactive transport of selenium coupled with nitrogen in a regional-scale irrigated groundwater system, Journal of Hydrology, 515, 29-46.

Bailey, R.T., Gates, T.K., and E.C. Romero, 2015, Assessing the effectiveness of land and water management practices on nonpoint source nitrate levels in an alluvial stream-aquifer system. Journal of Contaminant Hydrology 179, 102-115.

Barry DA, Bajracharya K, Crapper M, Prommer H, Cunningham CJ., 2000, Comparison

of split-operator methods for solving coupled chemical non-equilibrium reaction/groundwater transport models. Math Comput Simul , 53(1–2):113–27.

Birkinshaw, S.J., Ewen, J., 2000, Nitrogen transformation component for SHETRAN catchment nitrate transport modelling. J. Hydrol. 230, 1–17.

Blanco, R.I., Naja, G.M., Rivero, R.G. and Price, R.M., 2013. Spatial and temporal changes in groundwater salinity in South Florida. Applied geochemistry, 38, pp.48-58.Brassard, P., Bodurtha, P., 2000, A feasible set for chemical speciation problems, Computers & Geosciences, 26 (3), pp. 277–291.

Brier, G. W. 1950. Verification of forecasts expressed in terms of probability. Monthly Weather Rev., 78(1-3).

Burkhalter, J. P., and Gates, T. K. 2005. "Agroecological impacts from salinization and waterlogging in an Irrigated river valley". Journal of Irrigation and Drainage Engineering, 131(2): 197 - 209.

Carrayrou J, Mose R, Behra P., 2008, Operator-splitting procedures for reactive transport and comparison of mass balance errors. J Contam. Hydrol., 68(3–4):239–68.

Chen, W., Hou, Z., Wu, L., Liang, Y., and Wei, C. 2010. "Evaluating salinity distribution in soil irrigated with saline water in arid regions of northwest China. Agric. Water Mgmt., 97(12), 2001 – 2008.

Doherty, J., 2007, PEST User Manual, fifth edition, Watermark Numerical Computing, Brisbane, Queensland, Australia.

Ebrahimi, M., Kazemi, H., Ehtashemi, M., Rockaway, T., 2016, Assessment of groundwater quantity and quality and saltwater intrusion in the Damghan basin, Iran, Chemie der Erde – Geochemistry, vol: 76 (2) pp: 227-241.

Farid, I., Zouari, K., Rigane, A., Beji, R., 2015, Origin of the groundwater salinity and geochemical processes in detrital and carbonate aquifers: Case of Chougafiya basin (Central Tunisia), Journal of Hydrology, vol: 530 pp: 508-532

Fipps, G. (2003), Irrigation water quality standards and salinity management strategies. Texas AgriLife Extension Service, B-1667.

Frind, E.O., Duynisveld, W.H.M., Strebel, O., Boettcher, J., 1990, Modeling of multicomponent transport with microbial transformation in groundwater: The Fuhrberg case, Water Resources Research, Vol. 26, NO. 8, 1707-1719.

Gates, T.K, Steed, G.H., Niemann, J.D., Labadie, J.W., 2016, Data for Improved Water Management in Colorado's Arkansas River Basin, Hydrological and Water Quality Studies, Colorado State University.

Gates, T.K., Burkhalter, J.P., Labadie, J.W., Valliant, J.C., Broner, I., 2002, Monitoring and modeling flow and salt transport in a salinity-threatened irrigated valley, Journal of Irrigation and Drainage Engineering, Vol. 128, No. 2, 88-99.

Goff, K., M.E. Lewis, M.A. Person, and L.F. Konikow. 1998. Simulated effects of irrigation on salinity in the Arkansas River Valley in Colorado. Ground Water 36:76-86.

Gonçalves, M. C., J. Šimůnek, T. B. Ramos, J. C. Martins, M. J. Neves, and F. P. Pires, 2006, Multicomponent solute transport in soil lysimeters irrigated with waters of different quality, Water Resour. Res., 42, W08401, doi:10.1029/2006WR004802, 17 pp.

Grieve, C. M., Grattan, S. R., and Maas, E. V. 2012. Plant salt tolerance. Chap. 13 in Wallender, W. W., and Tanji, K. K., Agricultural salinity assessment and management, 2nd ed. Manuals and Reports on Engineering Practice No. 71, Amer. Soc. Civil Engineers, Reston, VA.

Harrington, N., Cook, P., 2014, Groundwater in Australia, National Centre for Groundwater Research and Training, Australia.

Haynes, W.M., 2016, Handbook of Chemistry and Physics, CRC Press, Boca Raton, FL.

Herczeg, A.L., Dogramaci, S.S., Leanet, F.W.J., 2001, Origin of dissolved salts in a large, semi-arid groundwater system: Murray Basin, Australia, Marine Freshwater Research, 52, 41-52.

Hukkinen, J. 1993. Institutional distortion of drainage modeling in Arkansas River Basin. J Irrigation and Drain Eng. 119:743-755.

Huyakorn, P.S., J.B. Kool, and Y.S. Wu. 1991. VAM2D-Variably saturated analysis model in two dimensions.Version 5.2 with hysteresis and chained decay transport. Documentation and user's guide. NUREG/CR-5352, Rev. 1. U.S. Nuclear Regulatory Commission, Washington, DC.

Jacques, D. and J. Simhek, 2005. Multicomponent - Variable Sat- urated Transport Model, Description, Manual, Verification and Examples, Waste and Disposal. SCKoCEN, BLG-998, Mol, Belgium.

Jacques, D., J. Simhek, D. Mallants, and M. Th. van Genuchten, 2003. The HYDRUS-PHREEQC Multicomponent Transport Model for Variably-Saturated Porous Media: Code Verification and Application. In: MODFLOW and More 2003: Understanding Through Modeling, E. Poeter, Ch. Zheng, M. Hill, and J. Doherty (Editors). Int. Ground Water Modeling Center, Colorado School of Mines, FOG Collins, Colorado, pp, 23-27.

Jalali, M., 2007. Salinization of groundwater in arid and semi-arid zones: an example from Tajarak, western Iran. Environmental Geology, 52(6), pp.1133-1149.

Jamshidzadeh, Z., Mirbagheri, S.A., 2011, Evaluation of groundwater quantity and quality in the Kashan Basin, Central Iran, Desalination, 270 (1–3), pp. 23–30.

Javadi, A., Al-Najjar, M., 2007, Finite element modeling of contaminant transport in soils including the effect of chemical reactions, Journal of Hazardous Materials, 143 (3), pp. 690–701.

Jeevanandam, M., Kannan, R., Srinivasalu, S., Rammohan, V., 2007, Hydrogeochemistry and Groundwater Quality Assessment of Lower Part of the Ponnaiyar River Basin, Cuddalore District, South India, Environmental Monitoring and Assessment, Volume 132, Issue 1, pp 263–274.

Konikow, L.F., 2011, The secret to successful solute-transport modeling, GroundWater 49 (2), 144–159.

Konikow, L.F., and M. Person. 1985. Assessment of long-term salinity changes in an irrigated stream aquifer system. Water Resources Research 21:1611-1624.

Latif, M., Ahmad, M.Z., 2009, Groundwater and soil salinity variation in a canal command area in Pakistan, Irrigation and Drainage, 58: 456-468.

Lin, Y.W., Garcia, L., 2008, Development of a Hydro-Salinity Simulation Model for Colorado's Arkansas Valley, Journal of Irrigation and Drainage Engineering, Vol. 134, 757-767.

Lorenzen, G., Sprenger, C., Baudron, P., Gupta, D. and Pekdeger, A., 2012. Origin and dynamics of groundwater salinity in the alluvial plains of western Delhi and adjacent territories of Haryana State, India. Hydrological Processes, 26(15), pp.2333-2345.

Lucia, A., Henley, H., Thomas, E., 2015, Multiphase equilibrium flash with salt precipitation in systems with multiple salts, Chemical Engineering Research and Design, V. 93, 662-674

Mahmood, K., Morris, J., Collopy, J. and Slavich, P., 2001. Groundwater uptake and sustainability of farm plantations on saline sites in Punjab province, Pakistan. Agricultural Water Management, 48(1), pp.1-20.

Marion, G.M., Mironenko, M.V., Roberts, M.W., 2010, FREZCHEM: A geochemical model for cold aqueous solution, Computers and Geosciences, 36, 10-15.

Millero, F.J., 2001, The physical chemistry of natural waters, Wiley

Misra, A.K. and Mishra, A., 2007. Study of quaternary aquifers in Ganga Plain, India: focus on groundwater salinity, fluoride and fluorosis. Journal of Hazardous Materials, 144(1), pp.438-448.

Morway, E.D., Gates, T.K., 2012, Regional assessment of soil water salinity across an intensively irrigated river valley, Journal of Irrigation and Drainage Engineering, Vol. 138, No. 5, 393-405.

Morway, E.D., Gates, T.K. and Niswonger, R.G., 2013. Appraising options to reduce shallow groundwater tables and enhance flow conditions over regional scales in an irrigated alluvial aquifer system. Journal of hydrology, 495, pp.216-237.

Mueller Price, J., & Gates, T.K., 2007, Assessing uncertainty in mass balance calculation of river nonpoint source loads. Journal of Environmental Engineering, 134(4), 247-258.

Narasimhan, T. N., A. F. White, and T. Tokunaga, 1986, Groundwater contamination from an inactive uranium mill tailings pile, 2, Application of a dynamic mixing model, Water Resour. Res., 22(13), 1820-1834.

Niswonger, R.G., Prudic, D.E., Regan, R.S., 2006. Documentation of the unsaturated zone flow (UZF1) Package for Modeling Unsaturated flow Between the Land Surface and the Water Table with MODFLOW-2005, U.S. Geological Survey Techniques and Methods 6-A19.

Niswonger, R.G., Panday, Sorab, and Ibaraki, Motomu, 2011. MODFLOW-NWT, A Newton Formulation for MODFLOW-2005: U.S. Geological Survey Techniques and Methods 6-A37, 44p.

Nordstrom, D.K., Ball, J.W., 1984, Chemical models, computer programs and metal complexation in natural water C.J.M Kramer, J.C Duinker (Eds.), Complexation of Trace Metals in Natural Waters, Martinus Nijhoff/W. Junk, pp. 149-162.

Oosterbaan, R. J., 2005, SAHYSMOD (version 1.7a), Description of principles, user manual and case studies, International Institute for Land Reclamation and Improvement, Wageningen, Netherlands, 140.

Parkhust, D.L., Appelo, C.A.J., 2013, Description of Input and Examples for PHREEQC Version 3- A Computer Program for Speciation, Batch-Reaction, One-Dimensional Transport, and Inverse Geocehmical Calculations, Chapter 43 of Section A, Groundwater, Book 6, Modeling Techniques.

Parkhurst, D.L., Kipp, K.L., Engesgaard, Peter, and Charlton, S.R., 2004, PHAST—A program for simulating ground-water flow, solute transport, and multicomponent geochemical reactions: U.S. Geological Survey Techniques and Methods 6–A8, 154 p.

Parkhust D., Appelo, 1999, User's guide to PHREEQC (Version-2)-a computer program for speciation, batch-reaction, one-dimensional transport, and inverse geochemical calculations, USGS, Report 99(4259), 326.

Pauwels, H., W. Kloppmann, J.-C. Foucher, A. Martelat, and V. Fritsche, 1998, Field tracer test for denitrification in a pyrite-bearing schist aquifer. Applied Geochemistry. 13:767-778.

Paz-García J., Johannesson, B., Ottosen, L., Ribeiro, A., Rodríguez-Maroto, J., 2013, Computing multi-species chemical equilibrium with an algorithm based on the reaction extents, Computers & Chemical Engineering, Vol: 58 pp: 135-143.

Pereira, L. S., Goncalves, J. M., Dong, B., Mao, Z. and Fang, S. X. 2007. "Assessing basin irrigation and scheduling strategies for saving irrigation water and controlling salinity in the upper Yellow River Basin, China." Agric. Water Mgmt., 93(3), 109 – 122.

Postma, D., Boesen, C., Kristiansen, H., and F. Larsen, 1991, Nitrate reduction in an unconfined sandy aquifer: water chemistry, reduction processes, and geochemical modeling. Water Resources Research 27(8), 2027-2045.

Piper, A.M., 1944, A graphical procedure in the geochemical interpretation of water-analysis. Eos. Tran, Am., Geophys. Union 25 (6), 914-928

Qureshi, A.S., McCornick, P.G., Qadir, M. and Aslam, Z., 2008. Managing salinity and waterlogging in the Indus Basin of Pakistan. Agricultural Water Management, 95(1), pp.1-10.

Rasouli, F., Pouya, A.K. and Šimůnek, J., 2013. Modeling the effects of saline water use in wheat-cultivated lands using the UNSATCHEM model. Irrigation science, 31(5), pp.1009-1024.

Robbins, C.W., Jurinak, J.J. and Wagenet, R.J., 1980, Calculating Cation Exchange in a Salt Transport Model 1. Soil Science Society of America Journal, 44(6), pp.1195-1200.

Rubin, J., 1983, Transport of reacting solutes in porous media: Relation between mathematical nature of problem formulation and chemical nature of reactions, Water Resources Research, 19 (5), pp. 1231–1252.

Schoups, G., Hopmans, J.W., Young, C.A., Vrugt, J.A., Wallender, W.W., Tanji, K.K., and S. Panday (2005), Sustainability of irrigated agriculture in the San Joaquin Valley, California. Proceedings of the National Academy of Sciences of the United States of America, 102(43), 15352-15356.

Shammas, M.I., Jacks, G., 2007, Seawater intrusion in the Salalah plain aquifer, Oman, Journal of Environmental Hydrology, Volume 15 Paper 19.

Sherif, M., Mohamed, M., Kacimov, A., Shetty, A., 2011, Assessment of groundwater quality in the northeastern coastal area of UAE as precursor for desalination, Desalination Volume 273, Issues 2–3, Pages 436–446.

Singh, A., Panda, S.N., 2012, Integrated salt and water balance modeling for the management of waterlogging and salinization; I: Validation of SAHYSMOD, Journal of Irrigation and Drainage Engineering, Vol. 138, 955-963.

Singh, N. T. 2005. Irrigation and soil salinity in the Indian subcontinent: Past and present. Lehigh Univ. Press, Bethlehem, PA.

Šimůnek, J., M. Šejna, and M. Th. van Genuchten, 2012, The UNSATCHEM Module for HYDRUS (2D/3D) Simulating Two-Dimensional Movement of and Reactions Between Major Ions in Soils, Version 1.0, PC Progress, Prague, Czech Republic, 54 pp.

Šimunek, J., Šejna, M ., Van Genuchten, MT, 2005, HYDRUS-1D, version 4.14, code for simulating the one-dimensional movement of water, heat, and multiple solutes in variably saturated porous media, Tech. rep., University of California Riverside.

Šimůnek, J., and D. L. Suarez, 1994, Two-dimensional transport model for variably saturated porous media with major ion chemistry, Water Resources Research, 30(4), 1115-1133.

Tafteh, A. and Sepaskhah, A.R., 2012. Application of HYDRUS-1D model for simulating water and nitrate leaching from continuous and alternate furrow irrigated rapeseed and maize fields. Agricultural Water Management, 113, pp.19-29.

Tweed, S.O., Leblanc, M., Webb, J.A. and Lubczynski, M.W., 2007. Remote sensing and GIS for mapping groundwater recharge and discharge areas in salinity prone catchments, southeastern Australia. Hydrogeology Journal, 15(1), pp.75-96.

Tavakoli Kivi, S., and Bailey, R. T. 2017. Modeling sulfur cycling and sulfate reactive transport in an agricultural groundwater system. Agric. Water Mgmt., 185(1), 78 – 92.

Truesdell, A.H., Jones, B.F., 1974, WATEQ-a computer program for calculating chemical equilibrium for natural waters, US Geological Survey.

Tuteja, N.K., Beale, G., Dawes, W., Vaze, J., Murphy, B., Barnett, P., Rancic, A., Evans, R., Geeves, G., Rassam, D., Miller, M., 2003, Predicting the effects of landuse change on water and salt balance—a case study of a catchment affected by dryland salinity in NSW, Australia, Journal of Hydrology, 283, 67-90.

van der Lee, J., Windt, L.D., 2002, CHESS Tutorial and CookBook, Version 3.0, Technical Report.

Wagenet, R.J., and J.L. Hutson. 1987, LEACHM-Leaching estimation and chemistry model. Center Environ. Res., Cornell Univ., Ithaca, NY.

Wang, Y., Deng, C., Liu, Y., Niu, Z., and Li, Y. 2018. "Identifying change in spatial accumulation of soil salinity in an inland river watershed." Sci. Total Environ., 621, 177 – 185.

Westall, J., Zachary, J., Morel, F., 1976, MINEQL: a computer program for the calculation of chemical equilibrium composition of aqueous systems.

Yeh, G.T., Tripathi, V.S., Gwo, J.P., Cheng, H.P., Cheng, J.C., Salvage, K.M., Li, M.H., Fang, Y., Li, Y., Sun, J.T., Zhang, F., Siegel, M.D., 2004, HYDROGEOCHEM 5.0: A Three-

Dimensional Model of Fluid Flow, Thermal Transport, and HYDROGEOCHEMical Transport through Variably Saturated Conditions, Oak Ridge National Laboratory.

CHAPTER 4

PRELIMINARY ASSESSMENT OF BEST MANAGEMENT PRACTICES FOR REMEDIATION OF SALINITY IN A REGIONAL STEAM-AQUIFER AGRICULTURAL SYSTEM

4.1. Introduction

High salt concentration in the shallow crop root zone and in groundwater underlying agricultural areas around the world has been a serious issue for millennia. High salt concentration in the root zone affects crop yield primarily by depressing osmotic potential in the soil pores and thereby reducing evapotranspiration (ET). High salt concentration in the underlying saturated zone accentuates this condition, as shallow groundwater and associated salt ion mass can move upward into the soil profile due to negative pressure gradients, or as highly-saline groundwater is pumped and used as irrigation. In addition, the mass of salt ions can be transported via groundwater to nearby rivers, which affects the quality of downstream agricultural areas where highly-saline water is diverted for irrigation, which continues the concentrating use-reuse cycle. To respond to this issue, identifying best management practices (BMPs) that could assist in remediating high salt concentrations becomes important for each affected agricultural region.

Numerous studies have used field and numerical modeling techniques to explore and identify remediation BMPs for chemical species, especially for nutrients such as nitrogen (N) (Logan, 1990; Zhang et al., 1996; Alva et al., 1998; Bethune et al., 2004; Rong et al., 2011). For agricultural watersheds, typically the reduction in solute mass loadings from the aquifer to the stream (Sharpley et al., 1994; Royer et al., 2006; Bailey et al., 2015), effect on soil salinity

(Qadir et al., 2004; Sharma et al., 2004; Mandare et al., 2008), and impacts on crop yield have been used as indicators of improvement and remediation. The implementation of various management strategies, such as irrigation scheduling and improving the quality of canal water, were assessed by Mandare et al., (2008) in the States of Punjab and Haryana, India by comparing impacts on soil salinity and crop yield. In addition, the effect of growing appropriate salt-tolerant plants and reusing the drained disposed water on improving crop production has been studied (Qadir et al., 2004). Due to the high salinity of drained water in agricultural areas, the effect of reusing drainage water, crop rotation, and pre-irrigation on crop yield has been illustrated in arid and semi-arid regions of India (Sharma et al., 2004).

In this chapter, the groundwater salinity transport model (UZF-RT3D/SEC) presented in Chapter 3 is used to assess the effectiveness of various BMPs for the Upstream Study Region (USR) in the LARV, Colorado. The specific BMPs analyzed are 1) reducing applied irrigation depths across all irrigated fields and 2) partially sealing the six earthen irrigation canals in the study region. The effectiveness of the BMPs is quantified according to the decrease in root zone salinity, the decrease in the groundwater salinity in the saturated zone of the aquifer, and the loading of total dissolves solids (TDS) to the Arkansas River via groundwater. A preliminary investigation of effect on crop yield also is carried out.

4.2. Methodology

This section outlines the method for implementing and quantifying the effect of BMPs in the USR using the calibrated and tested UZF-RT3D/SEC model for the study region. The effect of the BMPs on root zone salinity, and hence on crop yield, may require only a few years to be exhibited. However, due to the long travel time of groundwater, several decades may be required

for management practices implemented at the field scale to markedly affect changes in groundwater loadings to rivers and tributaries. Therefore, multi-decadal simulations will be used to assess BMPs.

To establish the required multi-decadal simulation time for the BMP analysis, the groundwater flow simulation using MODFLOW (Morway et al., 2013), originally run for the years 1999-2007, was repeated four times, with the end of each simulation used as the initial conditions for the subsequent simulation, resulting in a 38-year simulation period. For the preliminary UZF-RT3D/SEC model simulation, it was assumed that the 2006-2009 cultivation pattern is repeated during the 38-year simulation. The base crop and chemical reaction parameter values used in the model are the same as those used in the calibrated and tested 2006-2009 model (Tavakoli-Kivi et al., 2018; see Chapter 3). The salt solid concentration at the end of the calibration period is used as the initial condition for the 38-year simulation. Furthermore, the calibrated solubility product of each salt solid for the saturated and unsaturated zone is used to establish a Baseline simulation, against which BMP simulation results are compared.

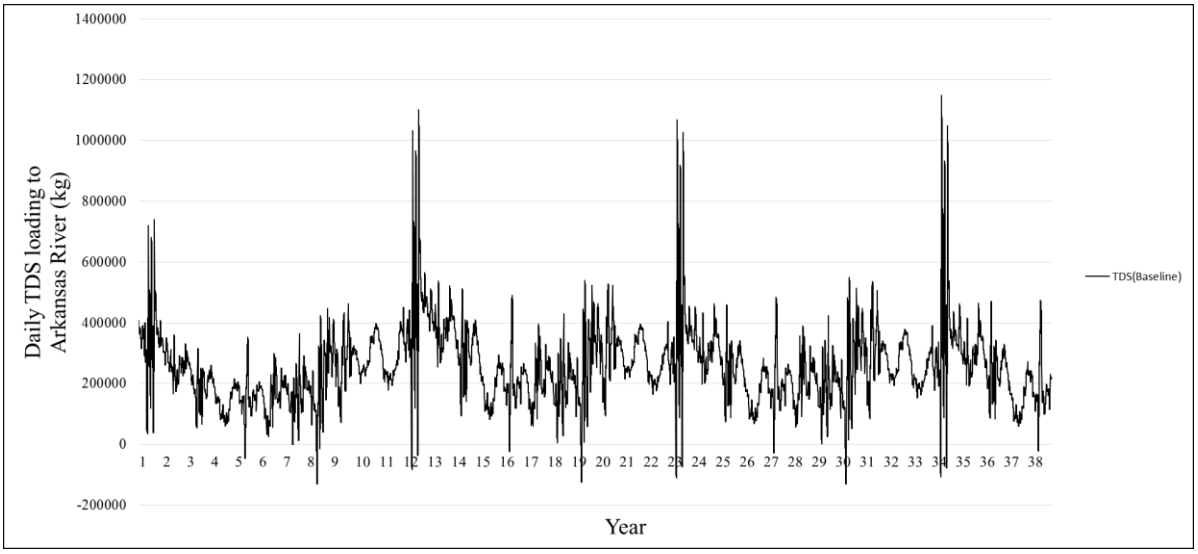

Figure 4.1. Time series of total daily TDS mass loading to the Arkansas River and tributaries during the 38-year Baseline simulation.

The results of the Baseline scenario using the baseline groundwater flow simulation, the cropping pattern and values as reported, initial salt solid concentration, and calibrated solubility products are shown in Figures 4.1 and 4.2. Figure 4.1 shows the time series of total daily TDS mass loading to the Arkansas River and tributaries during the 38-year Baseline simulation. Figure 4.2 shows the average daily TDS for the root zone over each canal command area and for the uncultivated area in the USR during the 38-year simulation, with TDS determined by summing the concentrations of all salt ions. For the majority of the command areas (A, B, C, E), TDS concentration averaged across the grid cells contained within the command area decreases steadily during the 38-year period. As described in chapter 3, 10 to 20 years of spin-up simulation ran for stabilizing the initial condition in saturated zone. Hence, this time period of spin-up simulation might be inadequate to establish initial conditions for unsaturated zone. The average TDS concentration in the Fort Lyon command area (D) has no observable trend, and the uncultivated area experiences an increase in TDS. It should be noted that these Baseline results do not necessarily predict conditions during the next 38 years in the USR, since groundwater and salt sources/sinks and weather patterns are based on historical data. The usefulness in these results is in comparison with BMP simulation results. The effectiveness of each BMP will be assessed by comparing the simulated root zone TDS concentration, groundwater TDS, and groundwater mass salt loading with Baseline simulation results.

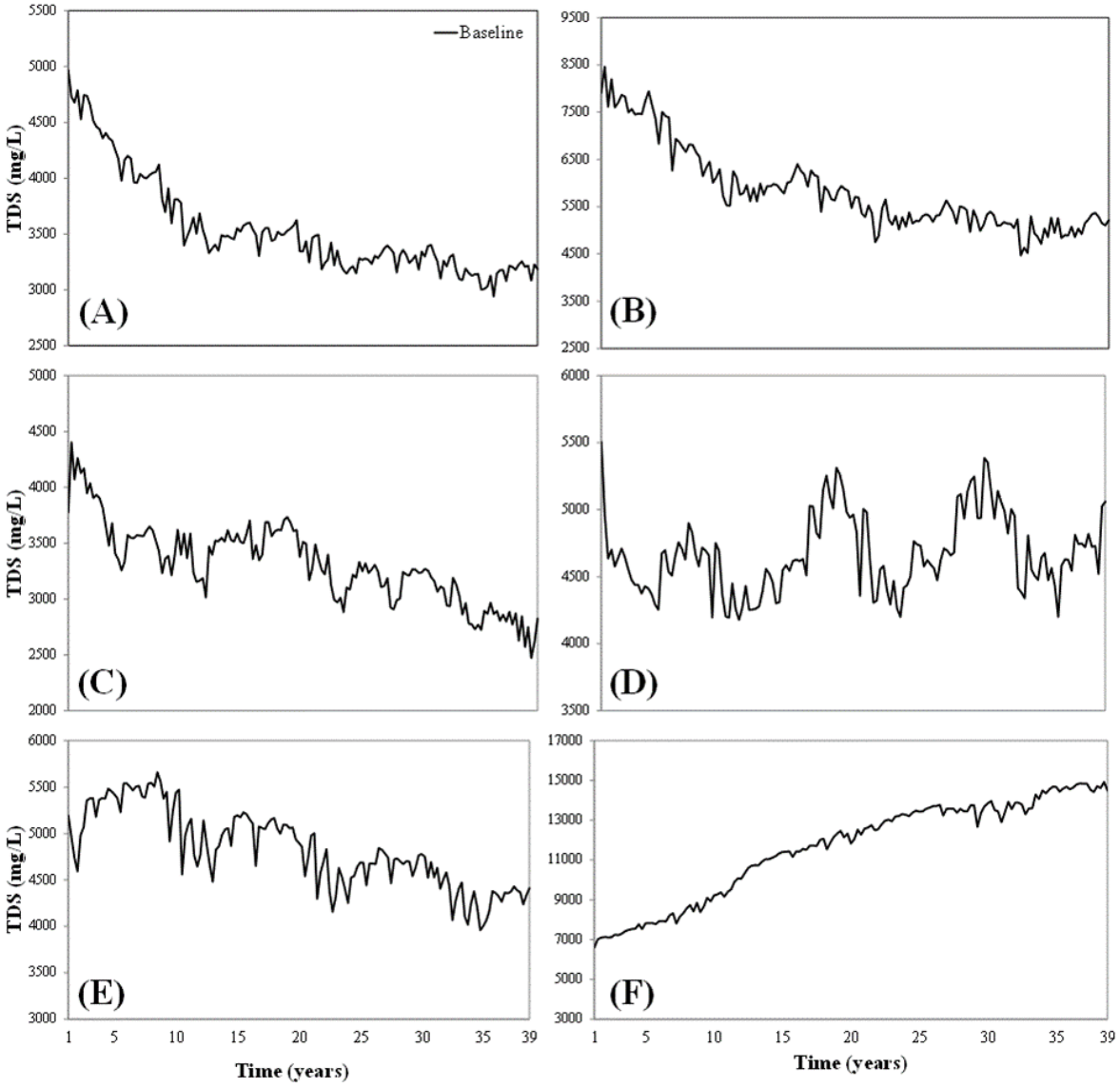

Figure 4.2. Time series of total daily TDS in the root zone for (A) Rocky Ford Highline, (B) Catlin, (C) RockyFord, (D) FortLyon, (E) Holbrook, and (F) Outside during the 38-year Baseline simulation.

A full BMP analysis would consider land fallowing, canal sealing, and reduced irrigation. In addition to these water BMPs, land BMPs like reduced fertilizer application and enhanced riparian buffers also should be taken into account (Shultz et al 2018). In this study, only two water BMPs, reduced irrigation (RI) and canal sealing (CS), are explored to assess impact on salt concentration and loadings. The impact of land fallowing and land BMPs, both alone and in combination, will be assessed in future studies. These practices not only decrease the mass input

of each solute but also depress the local and regional groundwater gradient which results in lower groundwater discharge to nearby stream networks. By sealing the canals (CS) or applying less irrigation water (RI), the rates of infiltration and seepage decrease, resulting in less solute mass added to the subsurface. Simultaneously, reducing the infiltration rates, or decreasing the volume of applied water, changes the behavior of flow within the soil profile throughout the subsurface system.

RI and CS BMPs were implemented by modifying input files of the MODFLOW-UZF model, with flow results then used by the UZF-RT3D/SEC model. The process of implementing reduced irrigation for the USR is explained in detail in Morway et al. (2013). Reduced irrigation was simulated by decreasing applied amounts on cultivated fields by 10% (RI10), 20% (RI20), and 30% (RI30), with each level assessed using a unique simulation. Canal sealing is assumed to be accomplished by applying a granular linear anionic polyacrylamide along the entire length of each canal, a tested and reliable procedure in the LARV (Susfalk et al., 2008). Scenarios of canal sealing to bring about 40% (CS40), 60% (CS60), and 80% (CS80) seepage reduction, as compared with Baseline conditions, were created by lowering the conductance value of canal segments in the River package of the MODFLOW-UZF model.

Thus in total, six BMP simulations are run. All six are assessed by comparing changes of TDS in the root zone, changes of TDS in groundwater, alterations to the mass loading of TDS to the river and tributaries, and shifts in relative crop yield.

4.3. Results and Discussion

4.3.1. Changes in Unsaturated Zone TDS

The comparison of TDS in the root zone between the CS BMPs and the Baseline condition is shown in Figure 4.3 for each command region in the USR. Overall, the three CS BMPs are predicted to lower the TDS in the root zone in increasing order of intensity, meaning that the

TDS under the CS80 generally is lower than the CS60 scenario, etc. Figure 4.4 shows the percent decrease of TDS concentration in the root zone for the BMP simulations as compared with the Baseline. The total percent decrease of TDS in the root zone under CS40 in comparison to the more aggressive CS80 is similar or greater (shown in Figure 4.4(B) and 4.4(C)) in the Catlin and Rocky Ford command areas, due to the water priority right of these regions which means that these two regions has priority of accessing water from canals results in availability of enough water throughout the entire year. In another words, by sealing the canals the flow behavior might not impact as expected due to the water availability. Another explanation is that the CS practice is more subject to localized effects as compared to RI, since canals are line sources of water and salt mass to the subsurface whereas fields are spread throughout the landscape as aerial sources of water and salt. Positive values indicate a decrease in TDS concentration, whereas negative values indicate an increase in TDS concentration. Under the Rocky Ford Highline Canal the TDS reduces by 2.1%, 2.8%, and 3.6% for CS40, CS60, and CS80, respectively. The highest percent decrease occurs under the Fort Lyon Canal which is 16.2% for the CS80 scenario. For uncultivated area (Figure 4.4F), TDS decreases by 5%, 5.4%, and 6.6% for CS40, CS60, and CS80 respectively.

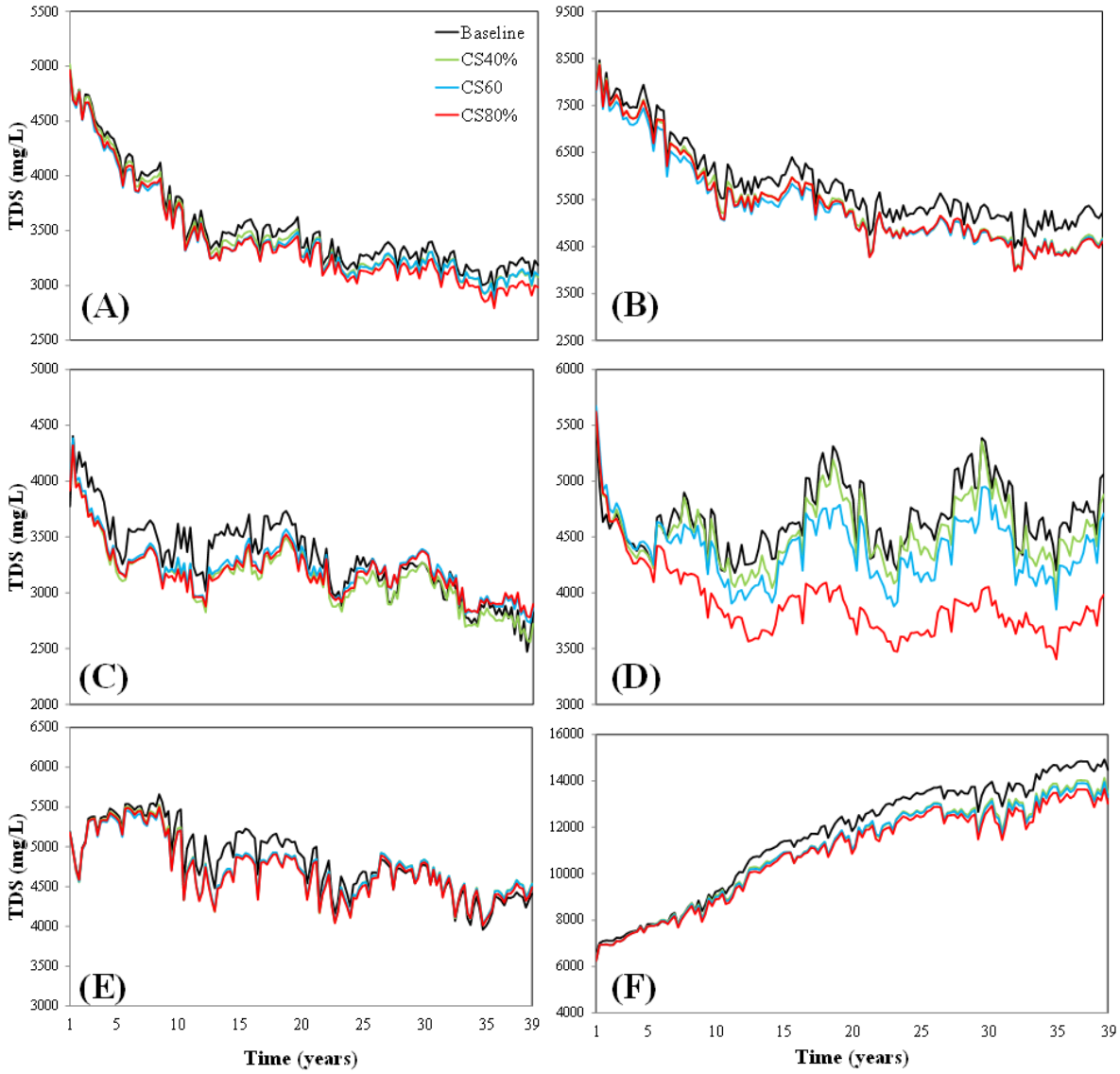

Figure 4.3. Comparison of time series of average daily TDS in the root zone between simulated Baseline and Canal sealing (40%, 60%, and 80%) scenarios for (A) Rocky Ford Highline, (B) Catlin, (C) RockyFord, (D) FortLyon, (E) Holbrook, and (F) Outside during the 38-year simulation.

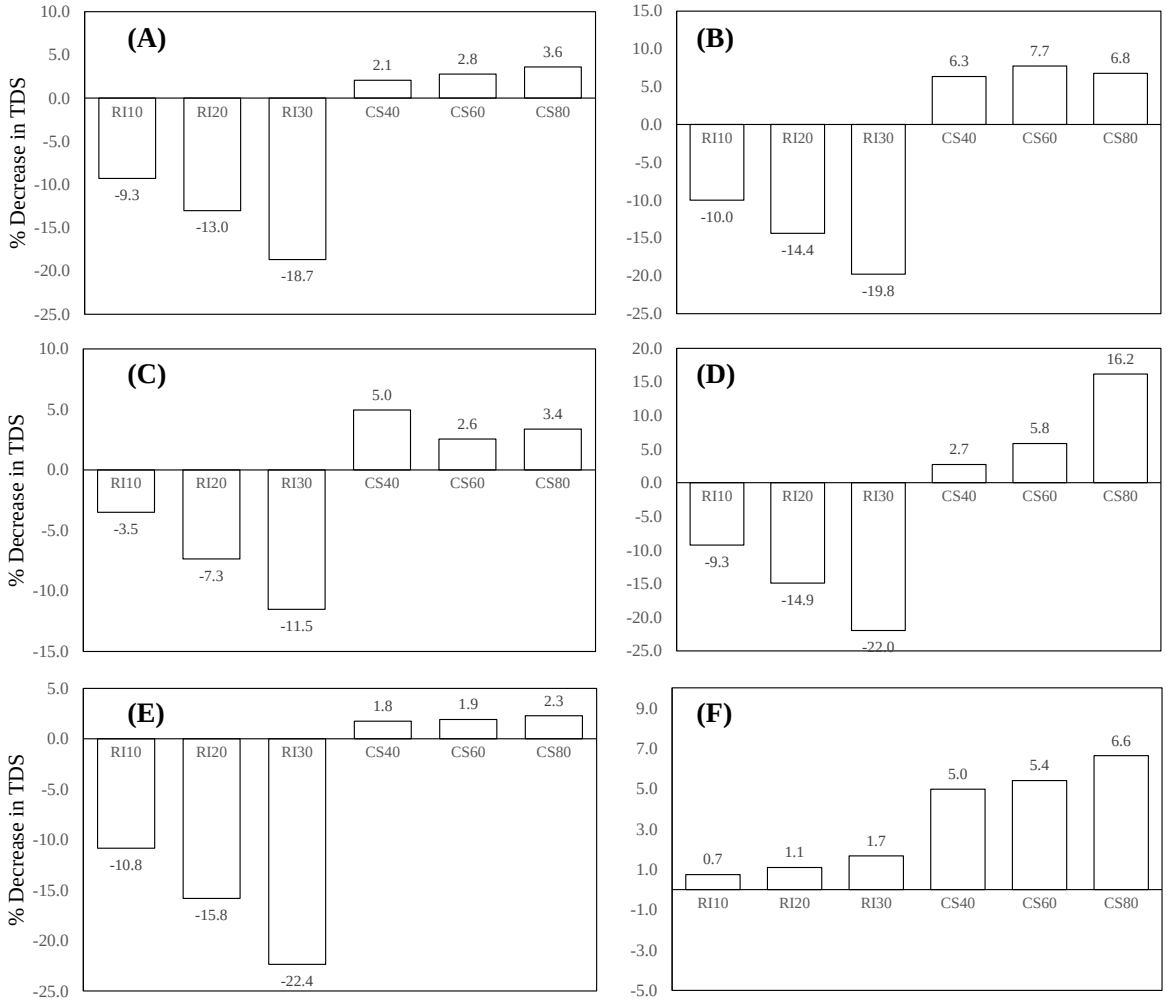

Figure 4.4. Simulated reduction in spatio-temporal averaged TDS in the root zone from Baseline simulation for Reduced irrigation (10%, 20%, and 30%) and Canal sealing (40%, 60%, and 80%) scenarios for (A) Rocky Ford Highline, (B) Catlin, (C) Rocky Ford, (D) Fort Lyon, (E) Holbrook, and (F) Outside during the 38-year simulation period.

The comparison of TDS in the root zone between the RI BMPs and the Baseline condition is shown in Figure 4.5 for the command areas and for the uncultivated region. As seen in the results for each command area the overall TDS in the root zone increases for all of the three RI practices except for in the uncultivated area. As the level of reduction in applied irrigation increases, the availability of water in the root zone drops as well as the leaching of salts to the deeper zone of the aquifer. Hence, the TDS in the root increases as expected. One of the major mechanisms for decreasing the salt concentration in the root zone occurs when salts are leached out as water

percolates from the upper layer of soil to the underlying aquifer. By reducing the applied irrigation water, this deep percolation which potentially could flush salt ion mass to deeper soil zones is diminished. Less deep percolation also leads to a drop in the groundwater table and consequently in saline upflux. Nevertheless, in many areas the net effect of a decrease in applied irrigation water is an increase in root zone salinity.

The total TDS in the unsaturated zone is simulated to increase by roughly 10%, 15%, and 20% for RI10, RI20, and RI30 respectively for the canal command areas in the USR (Figure 4.4), with the exception of the Rocky Ford command area where the simulated increase was a bit less. For the uncultivated area implementing each BMP resulted in lower TDS in the root zone by 0.7%, 1.1%, and 1.7% for RI10, RI20, and RI30 respectively (Figure 4.4F) since this area is not affected by irrigation directly and water content in the root zone will not be altered significantly during each scenario.

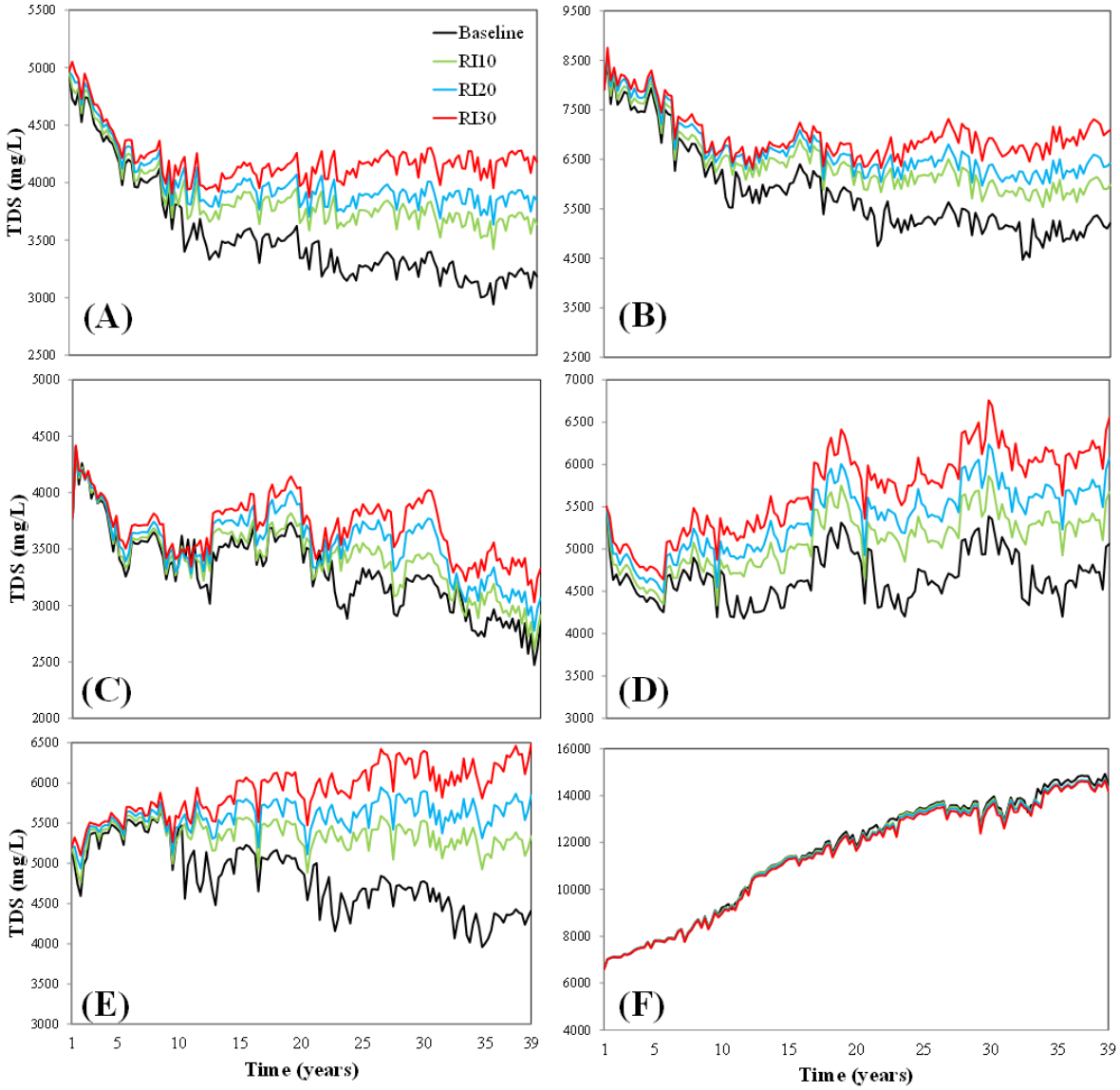

Figure 4.5. Comparison of time series of average daily TDS in the root zone between simulated Baseline and Reduced irrigation (10%, 20%, and 30%) scenarios for (A) Rocky Ford Highline, (B) Catlin, (C) RockyFord, (D) FortLyon, (E) Holbrook, and (F) Outside during the 38-year simulation.

4.3.2. Changes in Groundwater TDS

The comparison of TDS in the saturated zone with the Baseline scenario, averaged across all command areas in the USR, is shown in Figure 4.6. Comparison of time series is shown for three RI and three CS BMPs in Figure 4.6(A) and 4.6(B), respectively. Figure 4.7 summarizes the percent decrease of TDS in groundwater by calculating the average of simulated TDS within the entire region and comparing with the average of the Baseline simulation. Positive values

indicate a decrease in TDS concentration, whereas negative values indicate an increase in TDS concentration. The simulated average TDS in the saturated zone increases 1.4%, 3.7%, and 8.1% for RI10, RI20, and RI30 respectively. Contrarily, TDS in the saturated zone decreases by 0.2%, 3.5%, and 7.3% for CS40, CS60, and CS60 respectively.

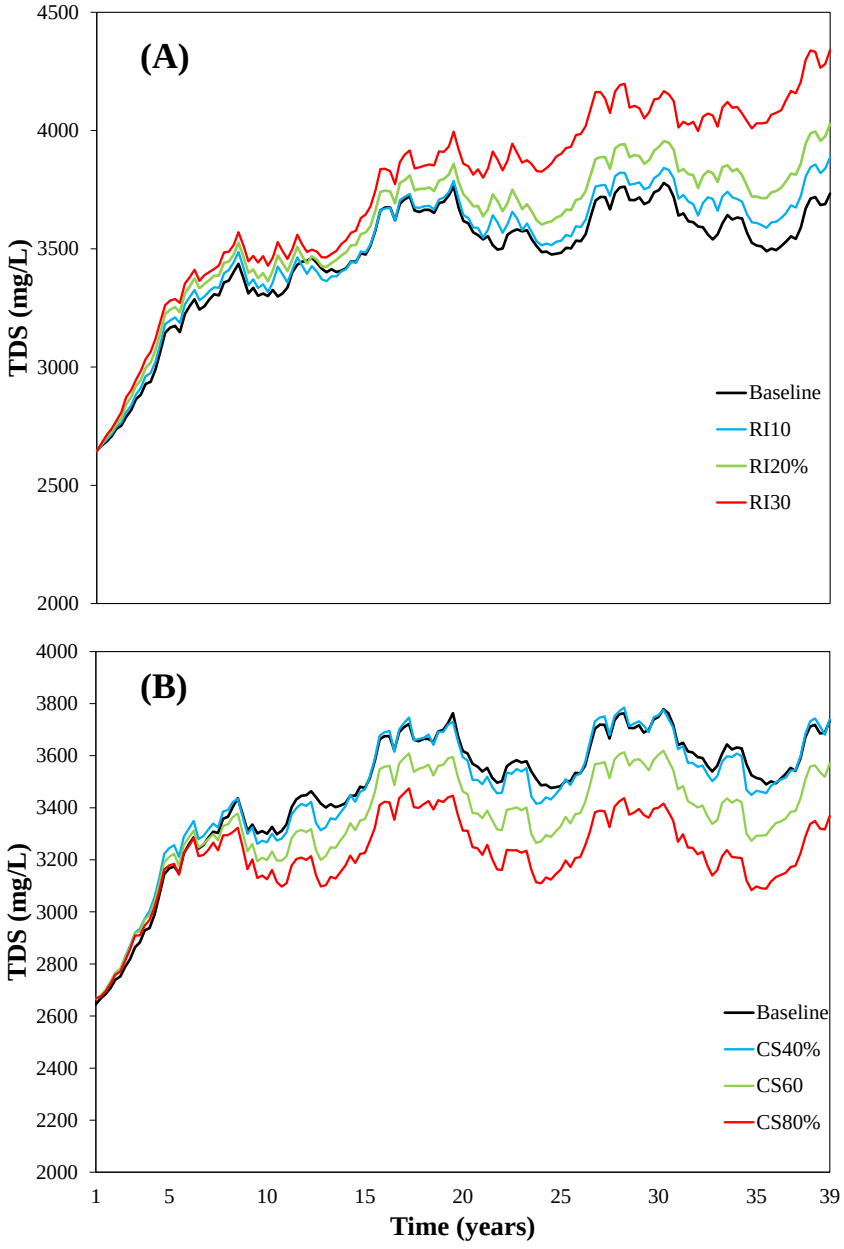

Figure 4.6. Comparison of time series of average daily TDS in saturated zone between simulated Baseline and (A) Reduced irrigation (10%, 20%, and 30%) scenarios and (B) Canal sealing (40%, 60%, and 80%) during the 38-year simulation.

Predicted increases in the groundwater TDS under RI may be due to increases in salt ion concentration in flow which leaches from the unsaturated zone to the saturated zone. As described before, TDS increases in the unsaturated zone under RI scenarios. The leached water carries higher concentration in comparison with the Baseline scenario, resulting in higher concentration in groundwater TDS. As seen in Figure 4.6, the RI10 and CS40 scenarios have minimum impact on average TDS. Both the RI and CS scenarios decrease the volume of the water which enters the deeper layer of the aquifer in comparison to the Baseline condition. As the water content decreases, TDS concentration increases accordingly, albeit the TDS mass decreases. This behavior can be seen for all RIs scenarios. Specifically the most aggressive one (RI30), which reduced the TDS by 8.1% in groundwater. The change of water content is not strong enough in CS scenarios in comparison to RI scenarios since the decrease in water volume entering the deeper aquifer, as described before, is more localized. Furthermore, the change of water content affects the precipitation/dissolution reaction in the SEC module. As concentration of each solute changes in groundwater solution, based on availability of salt solids and the solubility limit, the concentration of each solute could decrease if they precipitate out of solution or could increase if the corresponding salt solid dissolves into the solution.

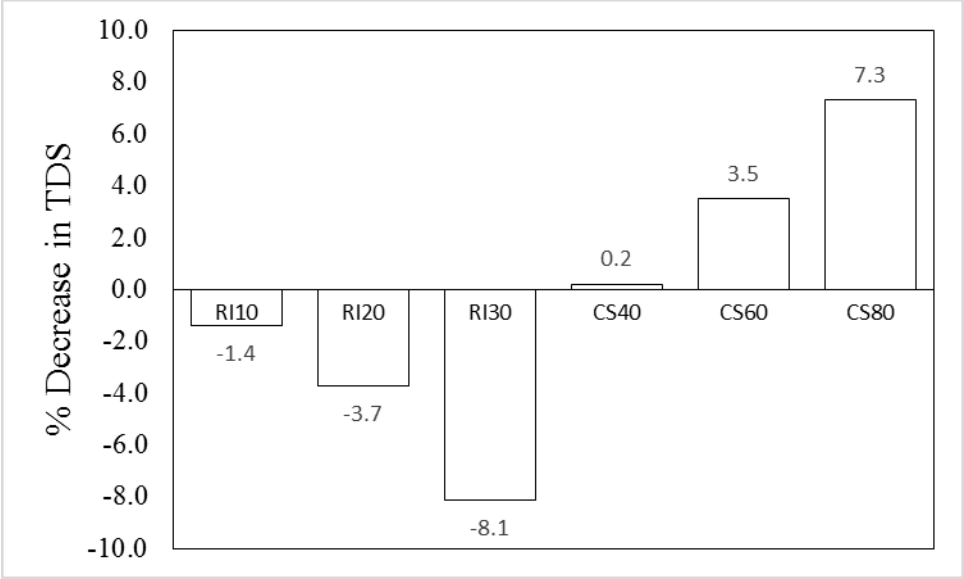

Figure 4.7. Percent decrease in TDS in saturated zone for reduced irrigation (10%, 20%, and 30%) and canal sealing (40%, 60%, and 80%) BMP simulation scenarios.

4.3.3. Changes in TDS mass loadings to streams

Mass loading of TDS to the river system from the aquifer occurs along the Arkansas River and along the tributaries. The time series comparison of TDS mass loading for the Baseline simulation and RI (10%, 20%, and 30%) and CS (40%, 60%, and 80%) scenarios are shown in Figure 4.8 and 4.9, respectively, for the 38-year simulation period averaged over all points of groundwater discharge to the stream on a daily basis. Positive values indicate groundwater salt loading to the river system and negative values indicate salt loading from the river to the groundwater. Although the results indicate that the overall mass loading to the river system is decreased under implementation all of the six scenarios, mass loading to the river under these scenarios is increased during some years, occurring periodically (i.e Year 11, 22). One possible explanation of this could be due to water application and reduction of seepage during the wet years, reducing the mass loading from the canals to the aquifer (Bailey et al., 2015). As the volume of water decreases during these years, the concentration of TDS increases which results in higher mass loading from the aquifer to the river.

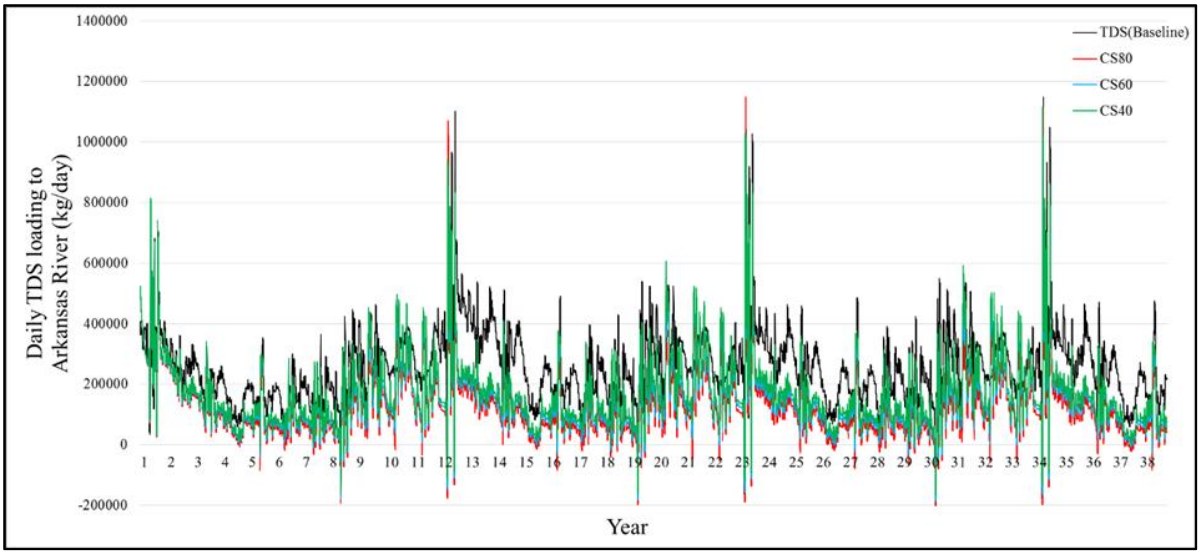

Figure 4.8. Comparison of time series of total daily TDS mass loading to the Arkansas River and tributaries during the 38-year simulation between Baseline simulation and Canal sealing (40%, 60%, and 80%) scenarios.

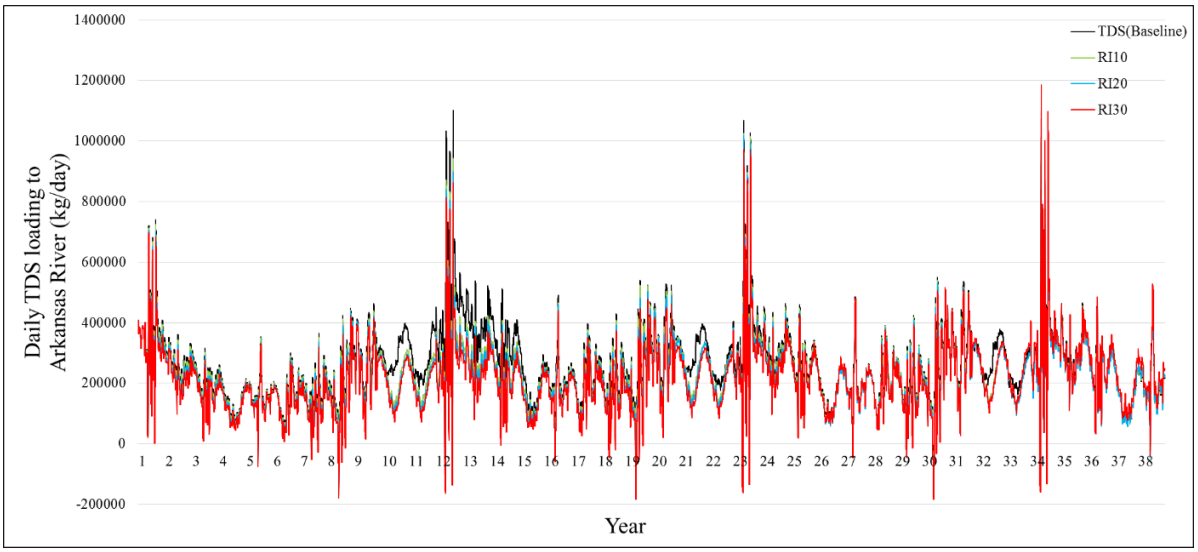

Figure 4.9. Comparison of time series of total daily TDS mass loading to the Arkansas River and tributaries during the 38-year simulation between Baseline simulation and Reduced irrigation (10%, 20%, and 30%) scenarios.

Figure 4.10 presents the cumulative TDS loading from the aquifer to the river for the Baseline simulation and the six BMP simulations showing the total mass of approximately 3.5E+9 kg in the Baseline condition and the varying decreased loadings from the BMP scenarios. Figure 4.11 summarizes the overall spatio-temporal average percent decreases in TDS loading from the

aquifer to the river over the 38-year simulation period. The RI30 and CS80 BMPs were found to be most effective within each group at decreasing groundwater salt loading to the river. For RI scenarios, the TDS mass loading to the river decreases by 10%, 14%, and 16% for the RI10, RI20, and RI30 respectively. Likewise, the TDS mass loading for CS scenarios is decreased by 33%, 40%, and 50% for the CS40, CS60, and CS60. The decrease in salt mass loading is caused by two factors: first, BMPs decrease the water table elevation through the region, thereby decreasing the groundwater head gradient from the irrigated areas to the river and thus decreasing the rate of return flow to the river and tributaries. In addition, for some BMPs salt ion concentration in the saturated zone is decreased, resulting in a lower salt mass per volume of groundwater discharging to the river system. Generally speaking, results demonstrate that the mass loading to the river could be significantly decreased through implementation of BMPs within the study region.

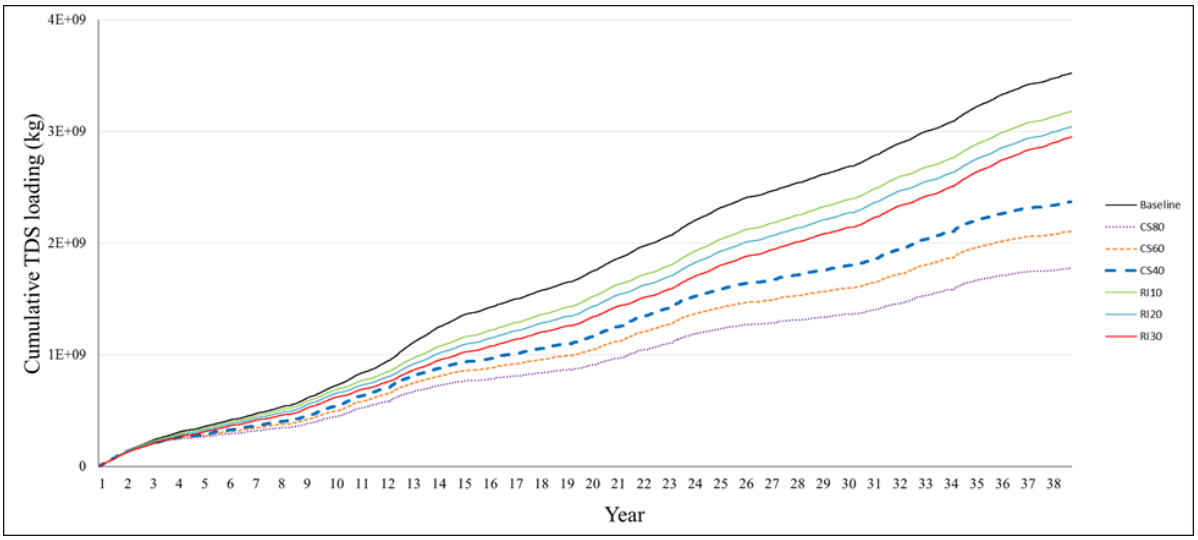

Figure 4.10. Cumulative mass loading of TDS from the aquifer to the Arkansas River during the 38-year simulation for Baseline simulation, reduced irrigation (10%, 20%, and 30%), and canal sealing (40%, 60%, and 80%) BMPs.

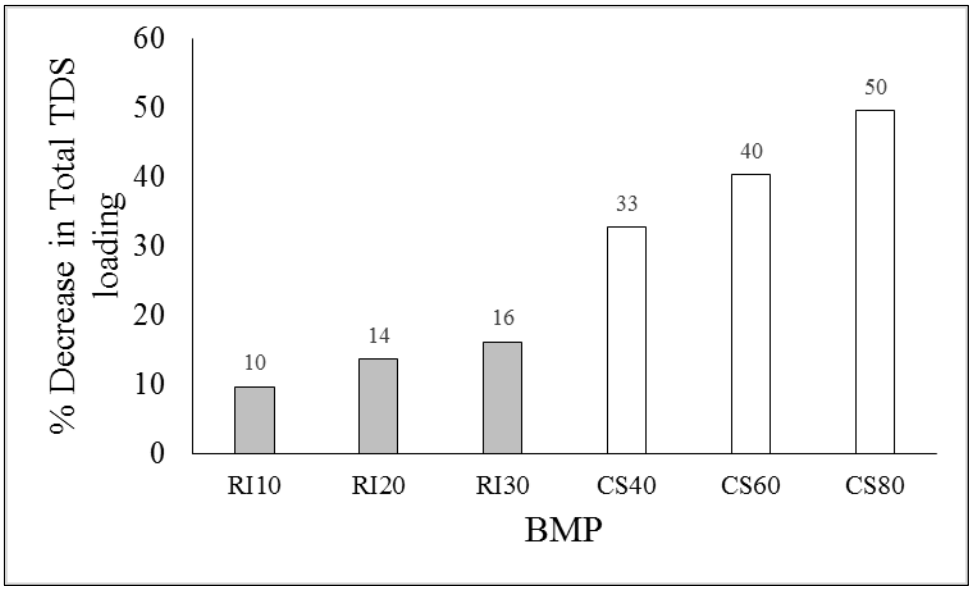

Figure 4.11. Percent decrease from the Baseline in TDS loading to the Arkansas River for reduced irrigation (10%, 20%, and 30%) and canal sealing (40%, 60%, and 80%) BMP simulation scenarios.

4.3.4. Effect of Unsaturated Zone Salinity on Crop Yield

To estimate the comprehensive impact of BMPs on crop yield, the effect of changes in both soil water content and soil water salinity should be taken into account. In this section, only the effect of soil salinity is considered by relating the electrical conductivity of the soil water to crop yield using the response function presented by Mass (1990). This function is given as:

$$Y_r = 100 - S_{YR} (EC_e - EC_{eT}) \quad (1)$$

where Y_r is relative yield (relative to potential crop yield), EC_e is the electrical conductivity of a saturated-soil extract taken from the root zone (dS/m), EC_{eT} is the threshold saturated extract soil water salinity (dS/m) above which yield of a given crop declines, and S_{YR} is the rate of crop-yield reduction in percent per dS/m for the given crop. Table 4.1 gives the values of EC_{eT} and S_{YR} for crops in the USR of the LARV. The value of Y_r is an estimate of the crop yield under the given conditions as a percentage of potential crop yield which would result if all crop growth factors, including soil salinity, were at an ideal level. In this study, the effect of simulated root-

zone salinity was assessed on the dominant crop for each computational cell over the entire region for a preliminary assessment. Using a relationship introduced by Gates et al. (2016) (see chapter 3) the TDS computed for each time step within the irrigation season (mid-March to mid-November) of the last year of the simulation period within the root zone (layer 1 and 2 of the model) of each grid cell in the UZF-RT3D/SEC model was converted to soil water EC, for the Baseline and for each implemented BMP. The corresponding value of EC_e for each cultivated field and each time step was then determined by multiplying the simulated EC by the ratio of porosity to simulated water content of each cell. Finally, values of EC_e for each computational cell were averaged over all of the time steps of the last irrigation season of the simulation period. These average values of EC_e were used in Eq. (1) to estimate the relative crop yield for each grid cell for the last irrigation season of the simulation.

Table 4.1 Salt tolerance of crops (from Grieve, C.M., Grattan, S.R., Maas, E.V., from Agricultural salinity Assessment and Management, 2012, Edited by Wesley W. Wallender, Kenneth, K., Tanji)

Crop	S_{YR}	EC_{eT}
Alfalfa	7.3	2
Bean	19	1
Corn	12	1.7
Melon	10	1
Onion	16	1.2
Pasture	8.4	2
Pumpkin	16	3.2
Sorghum	16	6.8
SpringGrain	7	8
Squash	16	3.2
Sunflower	5.5	4.8
Vegetable	9.9	2.5
Wheat	7.1	6

Figure 4.12 presents the estimated effect of root-zone salinity on the relative crop yield under the Baseline condition for the USR. The spatial average relative crop yield over the region is 86%. There are areas with very high simulated salinity resulting in zero crop productivity, likely

due in part to averaging soil water content over the spatial area of each grid cell rather than for specific irrigated fields. Hence, a finer-resolved groundwater flow model likely would result in more accurate crop yield determinations.

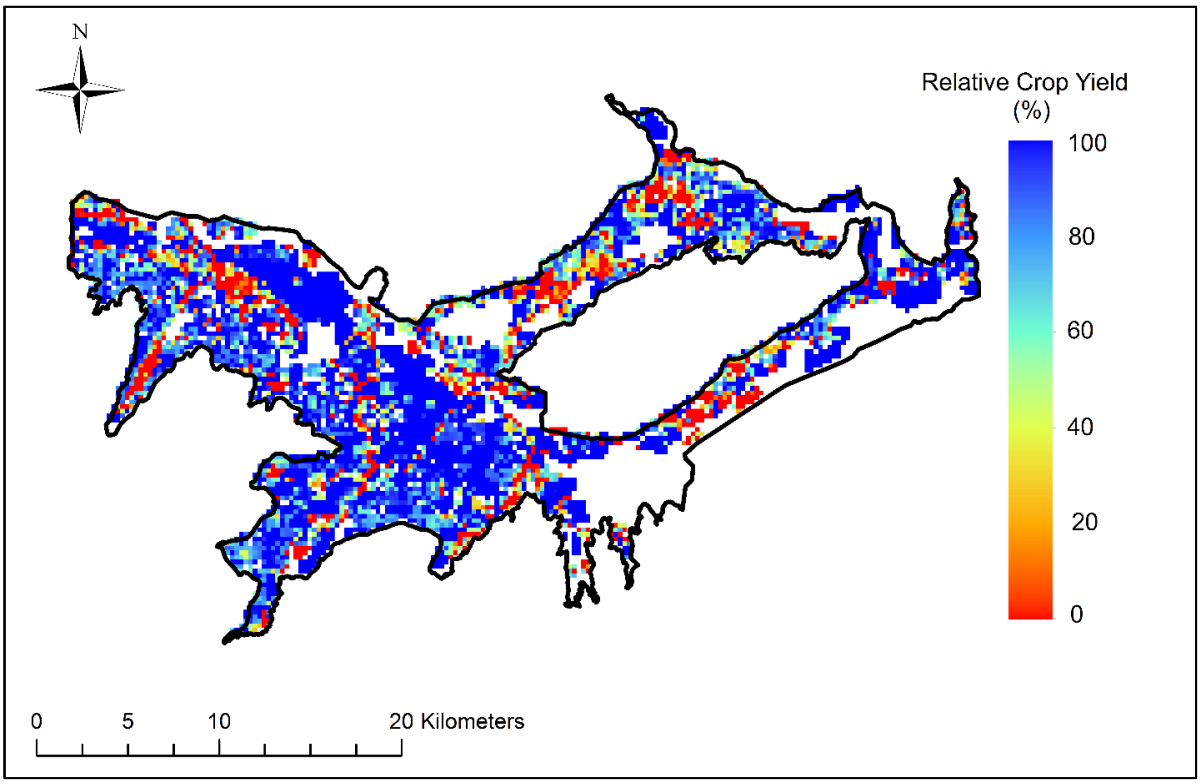

Figure 4.12. Relative crop yield under the Baseline condition for each cell for the last year of simulation period.

Figure 4.13 shows the spatial distribution of percentage point increase in relative crop yield from the Baseline for all six BMPs. Positive values indicate that the estimated relative crop yield increases, while negative values mean relative crop yield decreases in comparison with the Baseline scenario. As expected, the average relative crop yield increases under CS scenarios due to the lower spatial average TDS simulated in the root zone. The average relative crop yield increases by 1.5, 1.9, and 2.7 percentage points for CS40, CS60, and CS80 respectively for the simulation period over the entire region. Unlike CS practices, as the spatial average TDS in the root zone increases for the RI scenarios, the average relative crop yield decreases in comparison

to Baseline condition. As shown in Figure 4.13(D), (E), and (F) the average relative crop yield decreases by 2.0, 2.9, and 4.6 percentage points for RI10, RI20, and RI30 scenarios respectively. It is important to note that these are preliminary estimates of impact of salinity on crop yield. It is interesting to note that the under the RI30 scenario, although the average relative crop yield is estimated to drop by 4.6 percentage points, there are areas where the relative crop yield increases, indicating that each BMP is likely to have differing effects from field to field and pointing toward the need to target BMP applications to favorable locations. The reasons for these spatial variations in relative crop yield are explored and discussed more in detail in the next section.

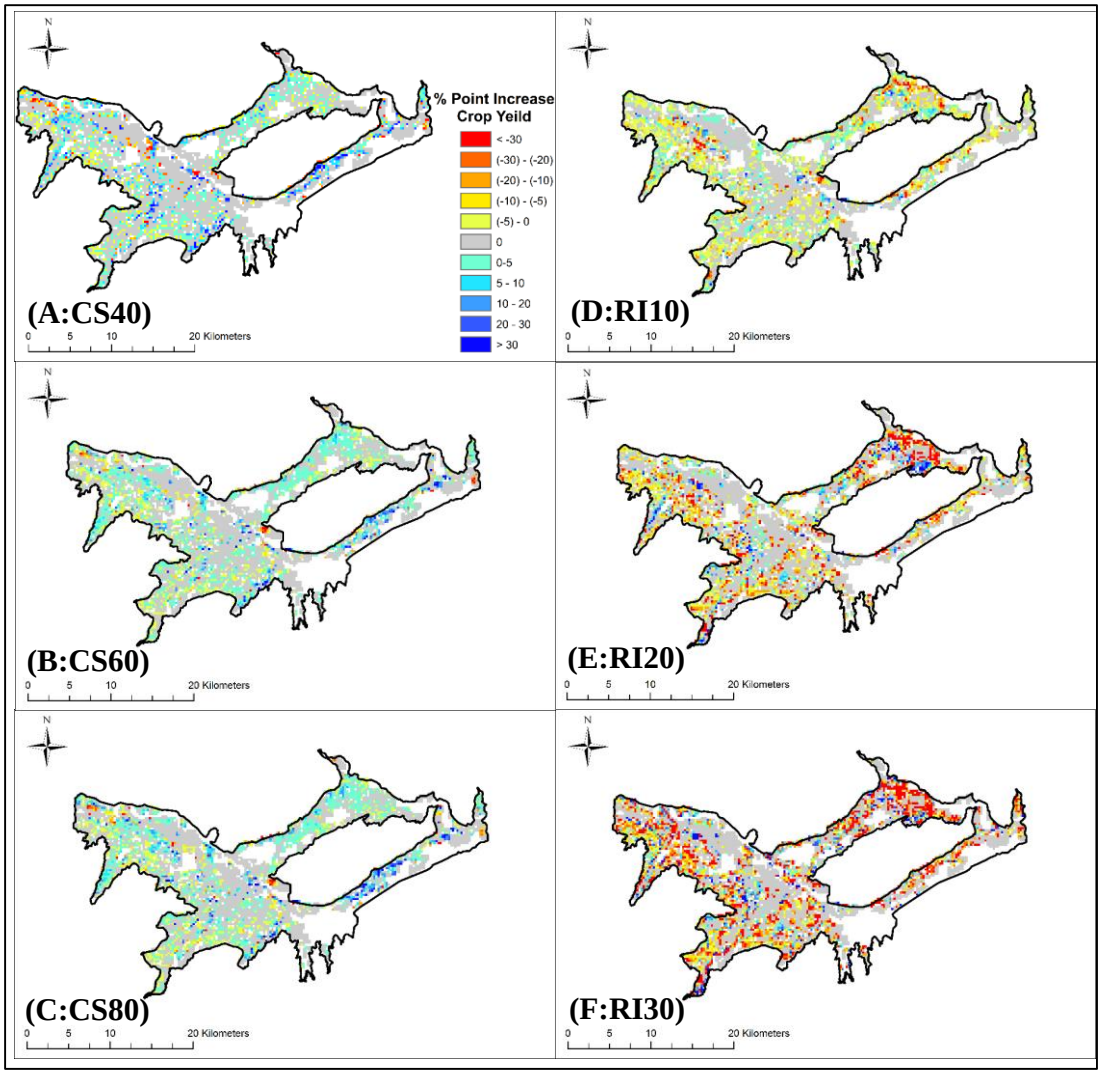

Figure 4.13. Spatial distribution of difference percentage point increase in relative crop yield from the Baseline condition for the last year of simulation period for (A) CS40, (B) CS60, (C) CS80, (D) RI10, (E) RI(20), and (F) RI(30).

4.3.5. Effect of Management Practices on Water and Salt Movement

As shown in Figure 13, implementing RI and CS BMPs produces different results throughout the modeled study region. The RI BMPs, due to a lowering of water content from less irrigation and an associated increase in soil salinity, results in a decreased crop yield for most of the area. However, crop yield increases in a few areas. For the CS BMPs, the opposite is predicted to occur, with increased crop yield simulated for the vast majority of the region except for a few areas. This section explores reasons for the spatial variability of soil salinity and associated crop

yield response. Since the developed model was applied to a large agricultural region, assessing reasons for this variability can assist in implementing the most efficient BMP for each local cultivated area. Also, understanding how BMP adoption would increase or decrease soil or groundwater salinity provides assistance to explore the right BMP for remediation strategies.

The major water and salt sources and movements within the shallow soil-aquifer system before and after implementing the RI and CS BMPs are depicted in Figures 14A and 14B, respectively. For a soil profile, salt enters from above via irrigation water and from below via upflux, with leaching carrying the salt mass through the profile. Figure 4.14A compares the water table level and magnitude of applied irrigation, leaching, and upflux both before and after implementing an RI scenario. In this scenario, the applied irrigation on cultivated fields is lowered (by red arrows), typically leading to less leaching as compared to the Baseline since deep percolation, which flushes salt ion mass to deeper soil zones, is diminished. This also results in a lowering of the water table, and hence less salt is in turn transported to the unsaturated zone via groundwater upflux. Thus, although in most areas the decrease in leaching leads to an increase in soil salinity and reduction in crop yield, in some areas this is countered by the decrease in salt upflux which results from the regional lowering of the water table. For fields where under Baseline conditions irrigation applications are excessive, with associated shallow water tables and excessive upflux, RI scenarios can lessen excessive deep percolation while still maintaining adequate salt leaching, yet drop the water table and diminish salt upflux. Hence, the RI BMPs would be most effective in areas of with Baseline conditions of excessive irrigation applications, perhaps under canals with high water rights priorities and ample available water, and with very shallow water tables.

On the other hand, CS only modifies (decreases) infiltration rates in the vicinity of canals yet lowers the water table regionally. Irrigation is applied to fields according to usual rates, resulting in the same amount of leaching and associated salt flushing through the cultivated areas. However, generally a reduction in canal seepage lowers the groundwater table throughout the region, and hence less salt is carried up to the unsaturated zone via upflux, thereby decreasing the TDS in the unsaturated zone. Assessing the changes in salt storage and transport in the soil profile under different BMPs can guide the selection of the most effective practice for each cultivated field due to localized pre-BMP conditions (e.g. depth of water table, availability of irrigation water).

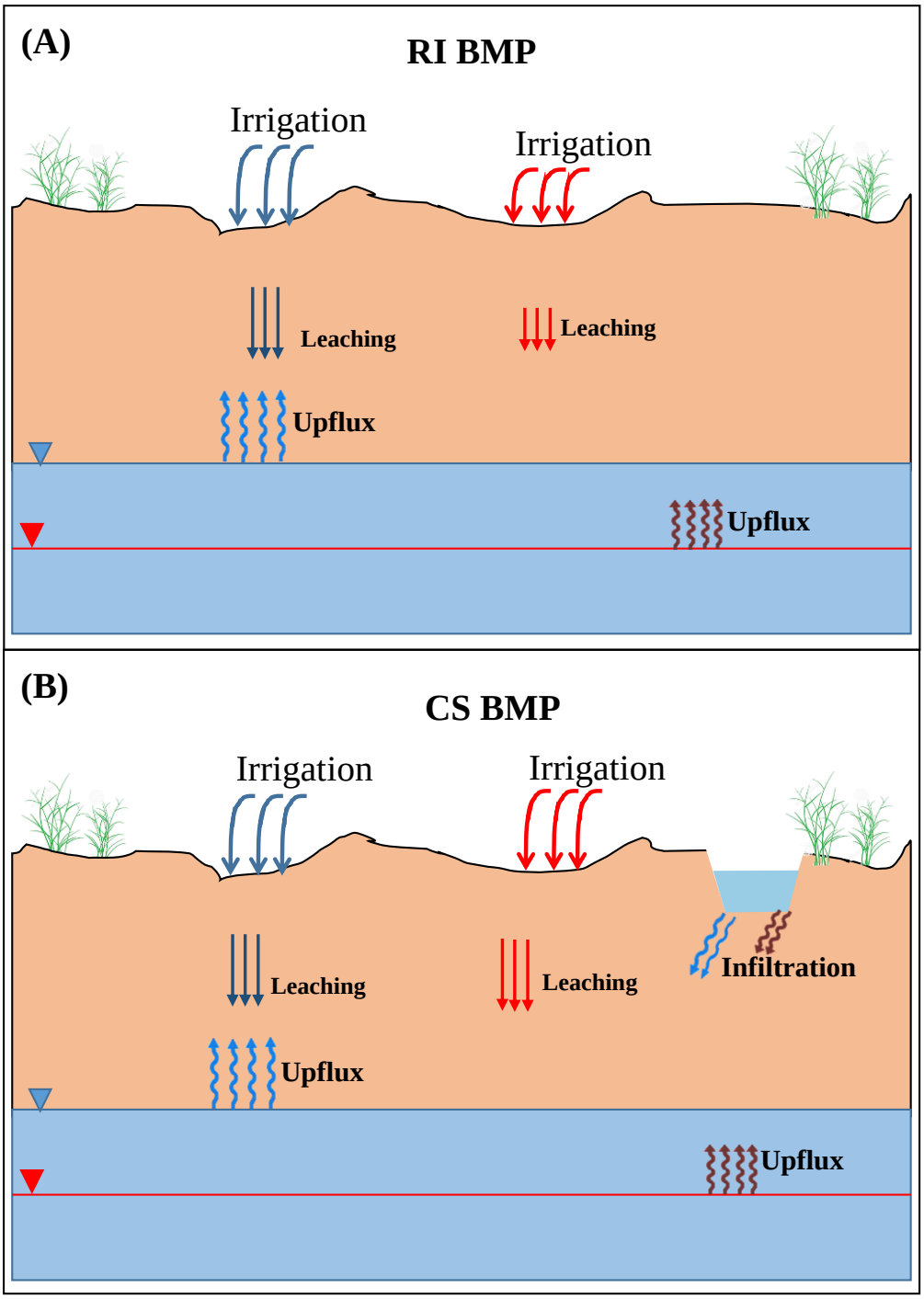

Figure 4.14. Comparison water table and magnitudes of irrigation, leaching, infiltration, and upflux before (blue arrows) and after (red arrows) implementing (A) RI and (B) CS.

4.4. Conclusion

This chapter summarizes the potential impact of RI and CS management practices on TDS in the root zone and in the groundwater, on TDS mass loading from groundwater to nearby steams, and on crop yield if broadly implemented over an agricultural region (500 km^2) which has been irrigated for more than a century in southeastern Colorado. The effectiveness of each BMP has been determined using a multi-decadal simulation by a calibrated and tested model.

Overall, results demonstrate that implementing BMPs potentially will have a significant impact on TDS concentration and salt mass loading. These results provide a first step in identifying regional remediation strategies for salinity. Since each cultivated crop has a different salt tolerance, future study should consider implementing each BMP to either reduce soil salinity below the threshold of existing crops or select cropping patterns for the simulated salinity across the region that minimizes impacts on crop productivity. Furthermore, as mentioned, to be able to estimate the overall impact of BMPs on crop yield, both simulated root zone water content and salinity needs to be considered jointly. Moreover, the impact of salinity over the irrigation seasons within the entire simulation period on crop yield has to be considered rather than evaluating just the impact of salinity over the irrigation season in the last year. Lastly, the effect of salinity should be considered not only on crop yield approximations but also in determining the ET and effect on the flow model. As the soil water salinity changes through the time steps of the model, due to the dependency of ET on salinity, ET values need to be modified through every time step within the model domain.

REFERENCES

Alva, A.K., Paramasivam, S. and Graham, W.D., 1998, Impact of nitrogen management practices on nutritional status and yield of Valencia orange trees and groundwater nitrate. Journal of Environmental Quality, 27(4), pp.904-910.

Bailey, R.T., Romero, E.C. and Gates, T.K., 2015, Assessing best management practices for remediation of selenium loading in groundwater to streams in an irrigated region. Journal of Hydrology, 521, pp.341-359.

Bethune, M., Gyles, O.A. and Wang, Q.J., 2004, Options for management of saline groundwater in an irrigated farming system. Australian Journal of Experimental Agriculture, 44(2), pp.181-188.

Gates, T.K, Steed, G.H., Niemann, J.D., Labadie, J.W., 2016, Data for Improved Water Management in Colorado's Arkansas River Basin, Hydrological and Water Quality Studies, Colorado State University.

Grieve, C.M., Grattan, S.R., Maas, E.V., 2012, from Agricultural salinity Assessment and Management, Edited by Wesley W. Wallender, Kenneth, K., Tanji

Logan, T.J., 1990, Agricultural best management practices and groundwater protection. Journal of Soil and Water Conservation, 45(2), pp.201-206.

Maas, E. V., 1990, "Crop salt tolerance." Agricultural salinity assessment and management, ASCE Manuals and Reports on Engineeering Practice No. 71, K. K. Tanji, ed., ASCE, New York, 262–304.

Mandare, A.B., Ambast, S.K., Tyagi, N.K. and Singh, J., 2008, On-farm water management in saline groundwater area under scarce canal water supply condition in the Northwest India. Agricultural water management, 95(5), pp.516-526.

Morway, E.D., Gates, T.K. and Niswonger, R.G., 2013, Appraising options to reduce shallow groundwater tables and enhance flow conditions over regional scales in an irrigated alluvial aquifer system. Journal of hydrology, 495, pp.216-237.

Morway, E.D. and Gates, T.K., 2012, Regional assessment of soil water salinity across an intensively irrigated river valley. Journal of Irrigation and Drainage Engineering, 138(5), pp.393-405.

Qadir, M. and Oster, J.D., 2004, Crop and irrigation management strategies for saline-sodic soils and waters aimed at environmentally sustainable agriculture. Science of the total environment, 323(1-3), pp.1-19.

Rong, Y. and Xuefeng, W., 2011, Effects of nitrogen fertilizer and irrigation rate on nitrate present in the profile of a sandy farmland in Northwest China. Procedia Environmental Sciences, 11, pp.726-732.

Royer, T.V., David, M.B. and Gentry, L.E., 2006, Timing of riverine export of nitrate and phosphorus from agricultural watersheds in Illinois: Implications for reducing nutrient loading to the Mississippi River. Environmental Science & Technology, 40(13), pp.4126-4131.

Sharma, D.P. and Tyagi, N.K., 2004, On-farm management of saline drainage water in arid and semi-arid regions. Irrigation and drainage, 53(1), pp.87-103.

Sharpley, A.N., Chapra, S.C., Wedepohl, R., Sims, J.T., Daniel, T.C. and Reddy, K.R., 1994, Managing agricultural phosphorus for protection of surface waters: Issues and options. Journal of environmental quality, 23(3), pp.437-451.

Shultz, C. D., Gates, T. K., and Bailey, R. T. 2018. Finding best management practices to lower selenium and nitrate in groundwater and streams in an irrigated river valley. Journal of Hydrology, In Review.

Susfalk, R., Sada, D., Martin, C., Young, M.H., Gates, T., Rosamond, C., Mihevc, T., Arrowood, T., Shanafield, M., Epstein, B. and Fitzgerald, B., 2008, Evaluation of linear anionic polyacrylamide (LA-PAM) application to water delivery canals for seepage reduction. Desert Research Institute.

Tavakoli-Kivi, S., Bailey, R.T., Gates, T.K., 2018, A Coupled Reactive Transport and Equilibrium Chemistry Model for Assessment of Salinity in a Regional-Scale Agricultural Groundwater System, Under review by Journal of Water Resources Research

Zhang, W.L., Tian, Z.X., Zhang, N. and Li, X.Q., 1996, Nitrate pollution of groundwater in northern China. Agriculture, Ecosystems & Environment, 59(3), pp.223-231.

CHAPTER 5

CONCLUSIONS AND FUTURE WORK

The research presented herein summarizes efforts towards simulating salinity with a coupled reactive transport and equilibrium chemistry model over a regional scale in an irrigated agricultural system, resulting in the UZF-RT3D/SEC model. The efforts included developing an equilibrium chemistry module, coupling the module with a reactive transport model, calibrating and testing the model in the 500 km^2 agricultural region within the Lower Arkansas River Valley in southeastern Colorado, and assessing the effects of BMPs on soil salinity and associated crop yield, groundwater salinity, and salt mass loading to streams.

5.1. Conclusions from Modeling Sulfur Cycling and Sulfate Reactive Transport in an Agricultural Groundwater System

A groundwater reactive transport model for SO_4 fate and transport in an irrigated soil-aquifer-stream system was presented. The model, based on the UZF-RT3D modeling code, accounts for S cycling in the crop-soil zone (S organic matter composition, mineralization/immobilization, root uptake), oxidation-reduction reactions, including release of reduced S from marine shale material containing pyrite (FeS_2), and mass inputs/outputs associated with groundwater sources and sinks (irrigation, pumping, groundwater-surface water interactions). The model is applied at two scales (soil profile, regional aquifer system: 500 km^2) in the Lower Arkansas River Valley in southeastern Arkansas, a region with extremely high salinity, to demonstrate its capabilities. In both applications, the model under-predicted SO_4 concentration despite perturbations in key model parameters such as root uptake rate, chemical reduction of SO_4, and oxidation of SO_4

from shale. Hence, results point to the importance of salt mineral dissolution and precipitation in this particular soil-aquifer system.

As constructed, the S module for UZF-RT3D can be used to assess SO_4 fate and transport in agricultural areas that are not dominated by salt mineral dissolution and precipitation. However, for areas of extremely high salt ion concentration, such as in the LARV, these processes will need to be included to provide a modeling framework that can be used to investigate salinity remediation strategies.

5.2. Conclusions from a Coupled Reactive Transport and Equilibrium Chemistry Model for Assessment of Salinity in a Regional-Scale Agricultural Groundwater System

The UZF-RT3D variably-saturated multi-species reactive transport model was amended to include equilibrium chemical reactions for application in salt-affected agricultural groundwater systems. The developed Salinity Equilibrium Chemistry (SEC) module includes precipitation-dissolution, complexation, and cation exchange equilibrium reactions for the major cations and anions (calcium, magnesium, sodium, potassium, sulfate, chloride, bicarbonate, and carbonate). The module is imbedded into the UZF-RT3D modeling code to allow the fate and reactive transport of these ions to be simulated in both the unsaturated and saturated zones of an aquifer system. The resulting UZF-RT3D/SEC model also includes cycling of C, N, and S in the plant-soil system, with redox reactions and sorption included for dissolved oxygen, ammonium, nitrate, and sulfate.

The model is applied to a 500 km^2 irrigated groundwater system along the Lower Arkansas River alluvial aquifer system in southeastern Colorado, with model results tested against a large dataset of observed salt concentrations and estimates of groundwater salt ion mass loading to the river. Results indicate that including the SEC module results in simulated salt ion concentration values that approach the high observed concentrations in the study region. Of key importance is

the ability of the model to predict not only groundwater salt concentrations but also mass loadings to the river network, which affect downstream irrigated areas, and also to predict soil salinity, which can be used to determine impact on crop yield.

5.3. Conclusions from BMP assessment

The potential impacts of reduced irrigation and canal sealing on TDS mass loading from groundwater to nearby steam, TDS on the root zone, and the TDS on the groundwater in a regional scale (500 km^2) agricultural area which has been irrigated for more than a century in southeastern Colorado were simulated. The effectiveness of each BMP has been determined using a multi-decadal simulation of calibrated and tested model.

Overall, results demonstrated that implementing BMPs potentially have a significant impact on the either TDS mass loading or concentration in the root zone or groundwater. These results composes a first step in identifying remediation strategies for salinity. As a result, land managers could use the result of the BMP assessment as a guide to explore the effect of each practice on the specific field both temporally and spatially.

Each crop has a different salt tolerance. The effectiveness of each BMP could be assessed potentially by comparing the yield of cultivated crop. The crop productivity which is unique for each crop depends on the salinity in the root zone (Mass 1990). The TDS in the root zone can be converted to EC using a relationship factor (see Chapter 3) while the TDS in the root zone simulated under the implementation of each BMP. As a result, the goal of implementing each BMP would be either:

- Reducing the EC to be below the threshold of the specific crop which is cultivated in each region or

- Selecting the best crop for the simulated EC either by Baseline condition or each BMP to maximize the crop productivity under cultivated region.

5.4. Future work

Possible areas of future research fall into the five categories:

- **Incorporate the effect of salinity on crop ET**

The salt tolerance of each crop has been described based on the threshold of the soil water salinity at which crop yield begins to decline and on the rate of crop-yield reduction (Mass 1990). Salinity affects the plant growth through osmotic potential changes. Increased salinity causes reduction in osmotic potential thereby reducing plants' ability to acquire water. To be able to study the effect of the salinity on ET, a relationship between the salinity and ET needs to be implemented. A possible relationship for the response of ET to increased soil salinity would be the same as that between crop yield and soil salinity. In other words, a reduction in crop yield by 20% due to salinity is assumed to be attributed primarily to a reduction in ET by 20%.

- **Assess the implementation of other BMPs along with cost analysis**

To be able to assess the remediation practices, a different implementation level of other salinity BMPs such as land fallowing, enhanced riparian zones, and reduced fertilizer needs to be considered. Also, the BMP combination scenarios along with cost analysis would help decision maker to have a full understanding of each BMP within the entire region.

To simulate land fallowing BMPs, the total irrigated land will be decreased by a certain percentage from the Baseline scenario, meaning that the applied irrigation will be removed and potential ET rates will be adjusted. Adjusting the applied irrigation and ET rates would alter the water content in the unsaturated zone which is expected to change TDS and loading from the aquifer to the river. Also, as water table drops by fallowing cultivated lands, the upflux which

carries solutes from the saturated zone to the root zone decreases. To simulate reduced fertilizer application, the value of applied fertilizer (such as NH_4) will be decreased by a certain percentage for each cultivated field. To simulate enhanced riparian zones, the base reaction rates for denitrification, selenite reduction, and selenate reduction will be increased within the identified riparian areas. Reducing the applied fertilizer or enhancing the riparian zones will directly affect the NO_3 and dissolved oxygen concentrations which will potentially alter the SO_4 concentration in the unsaturated zone and the mass loading from the aquifer to the river.

- **Refine the model representation of conditions near the river and tributaries**

Determining a more accurate estimate of mass loading of TDS from the aquifer to streams needs to incorporate a more exact calculation of groundwater flux. The model needs some refinement to find the exact level of the water table and to weigh the contribution of loads from aquifer to the stream or the other way around. The model currently determines an average value of salt ion concentration for each grid cell. Using one value for the cell in which the water table resides, results in inaccuracies since a portion of the cell (above the water table) is unsaturated. Accounting for the level of the water table within each cell will allow a more accurate estimation of salinity concentration in the saturated zone, and hence a more accurate determination of the mass loading of salt from the aquifer to the river.

- **Include the full cycle of Carbon (C)**

The main source of HCO_3 in groundwater is the dissolution of $CaCO_3$, which is also a source of CO_3. The SEC module currently does not fully accommodate the C cycle in a closed system; instead, the simple dissolution formula for CaCO3 is used (see chapter 3). As a result, the model under-predicts C_{HCO_3}. By including the full C cycle and considering the partial CO_2 pressure, C_{HCO_3} would be calculated as a secondary component in $CaCO_3$ dissolution.

- **Include the effect of pH and temperature in the chemical SEC module**

The solubility product of each salt ion depends on temperature and pH. For instance, gypsum solubility could increase by approximately 13% as the temperature increases from zero to 40 ^{o}C (Merkel et al., 2005) and nearly a 12% increase as pH decreases from 8.5 to 2.5 (Shukla et al., 2008). Including the variability of pH and temperature in the SEC module would lead to better calibration of the model for the different canal command areas. Temperature within the LARV varies from 9-21.9 ^{o}C with average value of 15.3 ^{o}C and pH varies from 5.5-8.3 with average of 7.0.

5.5. Implication of Research for other Salt-Affected Regions

The aim of this dissertation was to introduce a tool which can reasonably simulate the fate and transport of salts in either regional-scale or small-scale stream-network systems. The results of this research have important implications for water management decision making. Although in this study the developed model was applied to the LARV in southeastern Colorado, this model could be applied to other regions dealing with salinity issues, regardless of size. One of the major strengths of the model is its linkage with MODFLOW which is used worldwide to develop groundwater flow models. Moreover, the procedure by which the SEC module was developed and imbedded into the UZF-RT3D modeling code allows users to amend the code to include any salt which potentially could be a major contributor to salinity in the region of interest. However, the availability of monitored data, such as soil and groundwater salinity, would be a first step in testing any model.

REFERENCES

Merkel, B.J., Planer-Friedrich, B. and Nordstrom, D.K., 2005, Groundwater geochemistry. A Practical Guide to Modeling of Natural and Contaminated Aquatic Systems, 2.

Shukla, J., Mohandas, V.P. and Kumar, A., 2008, Effect of pH on the Solubility of CaSO4· 2H2O in Aqueous NaCl solutions and Physicochemical Solution Properties at 35 C. Journal of Chemical & Engineering Data, 53(12), pp.2797-2800.

APPENDIX A

SUPPLEMENTARY DATA (CHAPTER 2)

Modeling Sulfur Cycling and Sulfate Reactive Transport in an Agricultural Groundwater System

Saman Tavakoli Kivi[1*] and Ryan T. Bailey[1]

[1] Department of Civil and Environmental Engineering, Colorado State University, 1372 Campus Delivery, Fort Collins, CO, 80523-1372, United States

** to whom correspondence should be addressed:*
Department of Civil and Environmental Engineering
Colorado State University
1372 Campus Delivery
Fort Collins, CO 80523
office: 970-491-5045
saman@engr.colostate.edu

Agricultural Water Management

Spatial distribution of material type for grid cells

In order to account for the autotrophic reduction of O_2 and NO_3 in the presence of shale and the resulting release of SO_4 into the groundwater, the spatial distribution of bedrock shale as well as shale near the ground surface needs to be delineated and mapped to the grid cells. During field sampling we recognized that a yellow clay material located in certain portions of the aquifer also contained residual S, and released SO_4 into the groundwater. Yellow clay hence is treated as a shale material in the model application.

To designate grid cells as shale, yellow clay, or alluvium, the spatial distribution of near-surface shale, along with known locations of yellow clay using borehole data, is mapped onto the model grid. Furthermore, the bottom layer of the grid comprises the bedrock and hence also is designated as shale. Using the 3-layer grid of Morway et al. (2013), the resulting material type for each grid cell for each of the three layers is shown in Figure S-1, with the shale material designated as Niobrara, Carlisle, or Graneros. Greenhorn Limestone also is present, and is treated as shale. The material type for each layer is then mapped to the seven-layer grid used by UZF-RT3D. The material type for each grid cell in the model domain is read into UZF-RT3D, and used to determine locations of autotrophic reduction of O_2 and NO_3. Autotrophic reduction proceeds within a given cell if any adjacent cell has a shale material type, with the possibility of multiple shale cells surrounding the cell.

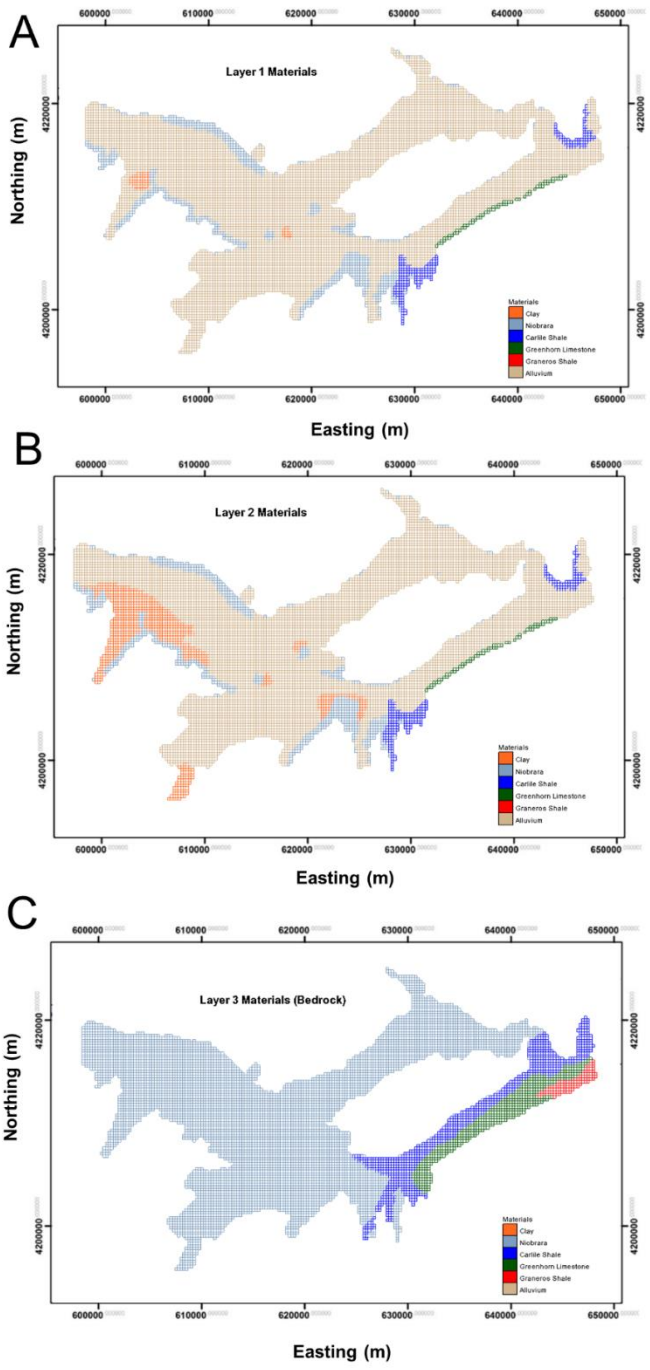

FIGURE S-1. MATERIAL TYPES (SHALE, YELLOW CLAY, OR ALLUVIUM) FOR THE THREE LAYERS IN THE GRID LAYERING IN MORWAY ET AL (2013). SHALE CONSISTS OF THE NIOBRARA, CARLISLE, AND GRANEROS FORMATIONS AS WELL AS GREENHORN LIMESTONE. THEY LAYER MATERIAL TYPES ARE MAPPED TO THE 7-LAYER GRID USING THE PROCESS SHOWN IN FIGURE S-2.

Timeline of annual agricultural practices

Figure S-2 shows the scheduling of cultivation practices (fertilizer loading, planting, irrigation application, harvesting, plowing) for a typical growing season in the LARV. Typically, 40% of the annual fertilizer load is applied one week before planting, with the remaining 60% applied six weeks after planting.

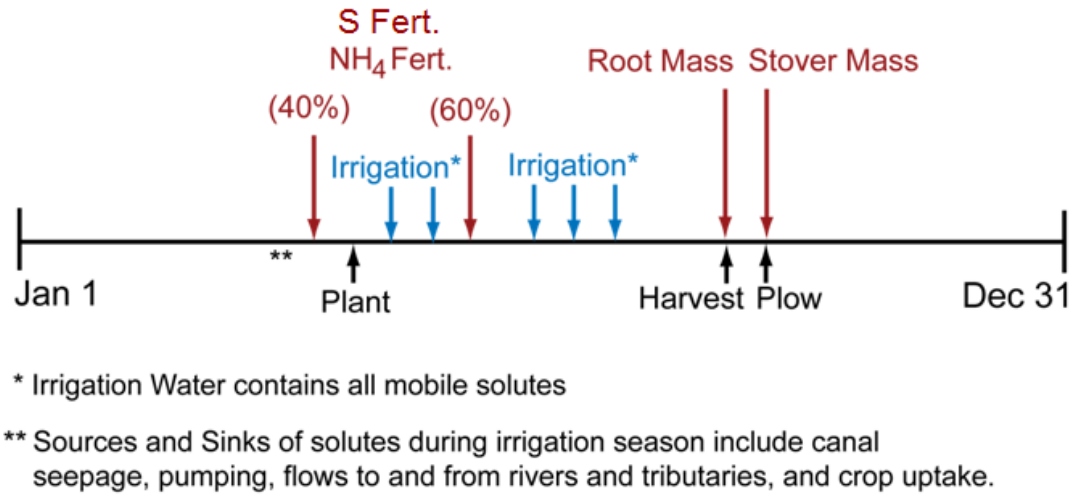

FIGURE S-2. SCHEDULING OF FERTILIZER LOADING, PLANTING, IRRIGATION WATER APPLICATION, HARVESTING, AND PLOWING DURING A TYPICAL GROWING SEASON IN THE LARV. ROOT MASS AND STOVER MASS ARE INCORPORATED INTO THE POOL OF SOIL ORGANIC MATTER DURING THE HARVEST AND PLOWING EVENTS, RESPECTIVELY.

Solute concentration in canals for 2006-2009

The mass of each species brought into or removed from the subsurface system via groundwater-surface water interaction is calculated for the cells designated as River cells in the MODFLOW-UZF simulation of Morway et al. (2013). For the case of groundwater discharge to surface water, the simulated species concentration in the grid cell is used in conjunction with the simulated volumetric flow rate to calculate the mass of each species removed from the aquifer and loaded to the surface water body. For the case of surface water seepage to the aquifer, the species concentration in the surface water is used with the simulated volumetric flow rate to calculate the mass of species entering the aquifer.

For the latter case, the concentration of each species in the surface water must be specified. As the model does not simulate chemical transport in surface water, field measurements are used to specify species concentration in the canals and in the Arkansas River. For this simulation, field measurements are available for the following dates: June 20 2006, May 24 2007, October 11 2007, May 20 2008, June 26 2008, August 14 2008, January 17 2009, May 14 2009, and July 22 2009.

For the canals, the species concentration at the canal diversion point on the Arkansas River is used, with the species concentration assumed to be constant along the length of the canal. The species concentrations for each canal for each of the 9 sampling events are presented in Table S-1. For the Arkansas River, species' concentrations are available for each of the 9 sampling events at 9 sampling points along the reach of the river within the model domain. For the Arkansas River tributaries (Patterson Hollow, Timpas Creek, Crooked Arroyo, Anderson, Horsecreek, and Adobe Creek), one measurement of species concentration is available for each of the 9 sampling events.

TABLE S-1. CONCENTRATION OF MOBILE SPECIES IN EACH CANAL FOR EACH SAMPLING EVENT OF 2006-2009. VALUES FOR C_{O_2}, C_{NH_4}, C_{NO_3}, C_{N_2}, C_{SO_4} AND ARE IN MG/L, WHEREAS VALUE FOR C_{SeO_4} ARE IN µG/L.

6/20/06	C_{O_2}	C_{NH_4}	C_{NO_3}	C_{N_2}	C_{SeO_4}	C_{SO_4}
RF Highline	7.43	0.00	1.20	0.00	2.63	53.51
Otero	7.43	0.00	1.20	0.00	3.28	58.73
Catlin	7.78	0.00	0.67	0.00	3.60	66.00
Rocky Ford	7.40	0.00	0.86	0.00	4.17	61.00
Fort Lyon	7.43	0.00	1.20	0.00	3.92	63.78
Holbrook	7.43	0.00	1.20	0.00	4.83	71.08
5/24/07						
RF Highline	9.57	0.00	1.33	0.00	4.50	78.85
Otero	9.57	0.00	1.33	0.00	4.99	96.56
Catlin	10.15	0.00	1.05	0.00	5.40	114.00
Rocky Ford	9.76	0.00	2.00	0.00	5.60	113.00
Fort Lyon	9.57	0.00	1.33	0.00	5.47	114.30
Holbrook	9.57	0.00	1.33	0.00	6.15	139.49
10/11/07						
RF Highline	9.67	0.00	1.32	0.00	8.92	139.49
Otero	9.67	0.00	1.32	0.00	8.92	224.50
Catlin	9.57	0.00	1.43	0.00	9.50	224.50
Rocky Ford	9.79	0.00	1.33	0.00	9.27	105.50
Fort Lyon	9.67	0.00	1.32	0.00	8.92	105.65
Holbrook	9.67	0.00	1.32	0.00	8.92	113.65
3/20/08						
RF Highline	9.44	0.00	1.88	0.00	6.23	70.47
Otero	9.44	0.00	1.88	0.00	8.32	116.49
Catlin	10.18	0.00	1.71	0.00	9.90	115.00
Rocky Ford	9.51	0.00	1.62	0.00	10.47	122.00
Fort Lyon	9.44	0.00	1.88	0.00	10.35	161.03
Holbrook	9.44	0.00	1.88	0.00	13.28	225.39
6/26/08						
RF Highline	7.71	0.00	0.60	0.00	2.57	31.02
Otero	7.71	0.00	0.60	0.00	3.09	43.52
Catlin	7.71	0.00	0.60	0.00	3.35	49.55
Rocky Ford	8.08	0.00	0.60	0.00	3.87	49.00
Fort Lyon	7.71	0.00	0.60	0.00	3.60	55.62
Holbrook	7.71	0.00	0.60	0.00	4.34	73.11
8/14/08						
RF Highline	9.32	0.00	2.00	0.00	6.00	113.17
Otero	9.32	0.00	2.00	0.00	8.74	148.68
Catlin	9.55	0.00	1.70	0.00	10.20	116.00
Rocky Ford	9.27	0.00	1.70	0.00	11.80	234.00
Fort Lyon	9.32	0.00	2.00	0.00	11.40	183.05
Holbrook	9.32	0.00	2.00	0.00	15.23	232.71
1/17/09						
RF Highline	13.22	0.00	2.87	0.00	14.71	9.80
Otero	13.22	0.00	2.87	0.00	14.71	111.47
Catlin	12.50	0.00	3.30	0.00	16.90	234.00
Rocky Ford	13.32	0.00	2.90	0.00	13.30	182.00
Fort Lyon	13.22	0.00	2.87	0.00	14.71	209.91
Holbrook	13.22	0.00	2.87	0.00	14.71	352.12
5/14/09						
RF Highline	8.58	0.00	1.09	0.00	6.72	37.55
Otero	8.58	0.00	1.09	0.00	7.14	62.51
Catlin	8.67	0.00	1.20	0.00	7.54	85.00
Rocky Ford	8.74	0.00	1.20	0.00	8.10	104.00

Fort Lyon	8.58	0.00	1.09	0.00	7.54	86.68
Holbrook	8.58	0.00	1.09	0.00	8.13	121.59
7/22/09						
RF Highline	8.52	0.00	0.90	0.00	6.10	51.64
Otero	8.52	0.00	0.90	0.00	6.10	83.54
Catlin	8.52	0.00	0.90	0.00	6.10	98.23
Rocky Ford	7.56	0.00	1.20	0.00	7.31	107.00
Fort Lyon	8.52	0.00	0.90	0.00	6.10	114.41
Holbrook	8.52	0.00	0.90	0.00	6.10	159.02

TABLE S-2. PARAMETERS FOR CHEMICAL REACTIONS INVOLVING ORGANIC MATTER DECOMPOSITION, DISSOLVED OXYGEN, NITROGEN SPECIES, AND SELENIUM SPECIES FOR THE MODEL APPLICATION TO THE UPSTREAM STUDY REGION IN THE LOWER ARKANSAS RIVER VALLEY, COLORADO.

Org. Matter Decomp.			Dissolved Oxygen			Nitrogen			Selenium		
Param.	Value	Unit	Param.	Value	Unit	Param.	Value	Unit	Param.	Value	Unit
λ_L	0.25	d^{-1}	$\lambda_{O_2}^{het}$	2.0	mg/L	$H_{C/N}$	12.0	-	$H_{C/Se}$	1.75×10^5	-
λ_H	0.003	d^{-1}	$\lambda_{O_2}^{auto}$	0.1	mg/L	$B_{C/N}$	8.0	-	$B_{C/Se}$	1.23×10^5	-
f_e	0.5	-	K_{O_2}	1.0	mg/L	I_{0_2}	1.0	mg/L	I_{NO_3}	0.50	mg/L
f_h	0.2	-				λ_{nit}	0.8	d^{-1}	$\lambda_{SeO_4}^{het}$	0.02	d^{-1}
K_{CO_2}	0.75	mg/L				λ_{vol}	0.1	d^{-1}	$\lambda_{SeO_3}^{het(Se_s)}$	0.02	d^{-1}
						$\lambda_{NO_3}^{het}$	0.1	d^{-1}	$\lambda_{SeO_3}^{het(SeMet)}$	0.02	d^{-1}
						$\lambda_{NO_3}^{auto}$	0.01	d^{-1}	λ_{SeMet}^{het}	0.02	d^{-1}
						K_{NO_3}	10.0	mg/L	ξ	3000	-
						K_{d,NH_4}	3.5	-	K_{d,SeO_3}	0.1	-

Air temperature and microbial activity

The first-order rate constant λ values represent the maximum rate of reaction for a given chemical reaction. These rates are tempered according to (i) concentration of species, (ii) concentration of other reactant species, (iii) the presence of e^- donors for reactions of chemical reduction, (iv) the presence of inhibiting, higher-redox species, and (v) soil temperature and soil water content. The measured daily average air temperature at the Rocky Ford climatic station at the Colorado State University (CSU) Arkansas Valley Research Center, used in the model to calculate soil temperature (Bailey et al., 2013), is shown in Figure S-3A. The percentage of maximum microbial activity as a function of percent soil saturation for mineralization, denitrification, and general chemical reactions is shown in Figure S-3B.

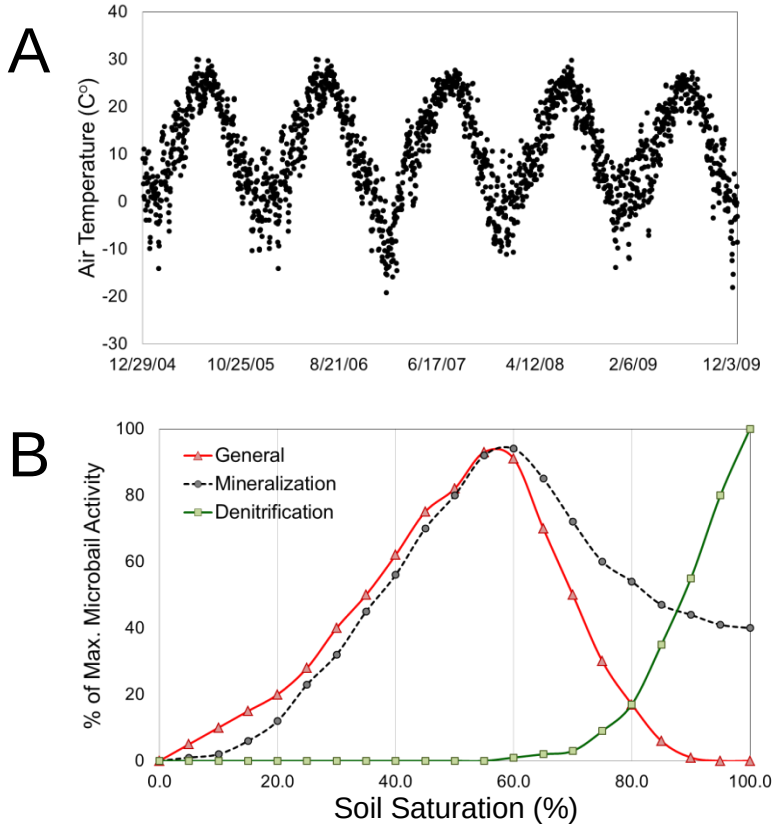

FIGURE S-3. SYSTEM VARIABLES INFLUENCING THE RATE OF REACTION OF MICROBIAL-MEDIATED CHEMICAL REACTIONS - (A) DAILY AVERAGE AIR TEMPERATURE AS MEASURED AT THE ROCKY FORD CLIMATIC STATION AT THE CSU ARKANSAS VALLEY RESEARCH CENTER, AND (B) PERCENT OF MAXIMUM MICROBIAL ACTIVITY AS A FUNCTION OF PERCENT SOIL SATURATION, DEMONSTRATING THE DEPENDENCE OF MICROBIAL-MEDIATED CHEMICAL REACTIONS ON THE PRESENCE/ABSENCE OF SOIL WATER.

References

Bailey, R.T., T.K. Gates, and Halvorson, A.D. (2013), Simulating variably-saturated reactive transport of selenium and nitrogen in agricultural groundwater systems. J. Contam. Hydro., 149, 27-45.

Morway, E. D., Gates, T. K., and Niswonger, R. G. (2013), Appraising options to enhance shallow groundwater table and flow conditions over regional scales in an irrigated alluvial aquifer system. J. Hydro., 495, 216-237.

APPENDIX B

Supplementary Data (Chapter 3)

A Coupled Reactive Transport and Equilibrium Chemistry Model for Assessment of Salinity in a Regional-Scale Agricultural Groundwater System

Saman Tavakoli-Kivi[1*], Ryan T. Bailey[1], Timothy K. Gates[1]

[1] Department of Civil and Environmental Engineering, Colorado State University, 1372 Campus Delivery, Fort Collins, CO, 80523-1372, United States

* *to whom correspondence should be addressed:*
Department of Civil and Environmental Engineering
Colorado State University
1372 Campus Delivery
Fort Collins, CO 80523
office: 970-491-5045
saman@colostate.edu

Environmental Modelling & Software

Solute concentration in canals for 2006-2009

The mass of each species brought into or removed from the subsurface system via groundwater-surface water interaction is calculated for the cells designated as River cells in the MODFLOW-UZF simulation of Morway et al. (2013). For the case of groundwater discharge to surface water, the simulated species concentration in the grid cell is used in conjunction with the simulated volumetric flow rate to calculate the mass of each species removed from the aquifer and loaded to the surface water body. For the case of surface water seepage to the aquifer, the species concentration in the surface water is used with the simulated volumetric flow rate to calculate the mass of species entering the aquifer.

For the latter case, the concentration of each species in the surface water must be specified. As the model does not simulate chemical transport in surface water, field measurements are used to specify species concentration in the canals and in the Arkansas River. For this simulation, field measurements are available for the following dates: June 20 2006, May 24 2007, October 11 2007, May 20 2008, June 26 2008, August 14 2008, January 17 2009, May 14 2009, and July 22 2009.

For the canals, the species concentration at the canal diversion point on the Arkansas River is used, with the species concentration assumed to be constant along the length of the canal. The species concentrations for each canal for each of the 9 sampling events are presented in Table S-1. For the Arkansas River, species' concentrations are available for each of the 9 sampling events at 9 sampling points along the reach of the river within the model domain. For the Arkansas River tributaries (Patterson Hollow, Timpas Creek, Crooked Arroyo, Anderson, Horsecreek, and Adobe Creek), one measurement of species concentration is available for each of the 9 sampling events.

TABLE S-1. CONCENTRATION OF MOBILE SPECIES IN EACH CANAL FOR EACH SAMPLING EVENT OF 2006-2009. VALUES FOR C_{O_2}, C_{NH_4}, C_{NO_3}, C_{N_2}, C_{SO_4}, C_{Ca}, C_{Mg} AND C_{Na} ARE IN MG/L.

6/20/06	C_{O_2}	C_{NH_4}	C_{NO_3}	C_{N_2}	C_{SO_4}	C_{Ca}	C_{Mg}	C_{Na}
RF Highline	7.43	0.00	1.20	0.00	53.51	35.67	10.52	21.79
Otero	7.43	0.00	1.20	0.00	58.73	45.1	13.75	28.53
Catlin	7.78	0.00	0.67	0.00	66.00	52.0	16.0	33.0
Rocky Ford	7.40	0.00	0.86	0.00	61.00	59.0	18.0	38.0
Fort Lyon	7.43	0.00	1.20	0.00	63.78	67.4	21.40	44.48
Holbrook	7.43	0.00	1.20	0.00	71.08	54.22	16.88	35.05
5/24/07								
RF Highline	9.57	0.00	1.33	0.00	78.85	58.82	18.88	50.07
Otero	9.57	0.00	1.33	0.00	96.56	66.69	20.82	53.72
Catlin	10.15	0.00	1.05	0.00	114.00	73.0	23.0	59.0
Rocky Ford	9.76	0.00	2.00	0.00	113.00	77.0	23.0	51.0
Fort Lyon	9.57	0.00	1.33	0.00	114.30	85.33	25.41	62.33
Holbrook	9.57	0.00	1.33	0.00	139.49	74.31	22.70	57.24
10/11/07								
RF Highline	9.67	0.00	1.32	0.00	139.49	70.91	27.19	39.04
Otero	9.67	0.00	1.32	0.00	224.50	84.48	31.53	52.33
Catlin	9.57	0.00	1.43	0.00	224.50	103.0	37.0	68.0
Rocky Ford	9.79	0.00	1.33	0.00	105.50	102.0	37.0	65.0
Fort Lyon	9.67	0.00	1.32	0.00	105.65	116.61	41.8	83.79
Holbrook	9.67	0.00	1.32	0.00	113.65	97.63	35.73	65.20
3/20/08								
RF Highline	9.44	0.00	1.88	0.00	70.47	13.24	4.17	9.98
Otero	9.44	0.00	1.88	0.00	116.49	51.58	21.48	57.66
Catlin	10.18	0.00	1.71	0.00	115.00	90.0	33.0	68.0
Rocky Ford	9.51	0.00	1.62	0.00	122.00	92.0	34.0	71.0
Fort Lyon	9.44	0.00	1.88	0.00	161.03	142.32	62.46	170.50
Holbrook	9.44	0.00	1.88	0.00	225.39	88.69	38.25	103.82
6/26/08								
RF Highline	7.71	0.00	0.60	0.00	31.02	15.78	5.07	31.17
Otero	7.71	0.00	0.60	0.00	43.52	30.78	9.99	31.17
Catlin	7.71	0.00	0.60	0.00	49.55	38.02	12.38	31.17
Rocky Ford	8.08	0.00	0.60	0.00	49.00	48.0	15.0	22.0
Fort Lyon	7.71	0.00	0.60	0.00	55.62	66.3	21.66	31.17
Holbrook	7.71	0.00	0.60	0.00	73.11	45.31	14.77	31.17
8/14/08								
RF Highline	9.32	0.00	2.00	0.00	113.17	42.51	7.98	4.89
Otero	9.32	0.00	2.00	0.00	148.68	54.18	14.01	23.29
Catlin	9.55	0.00	1.70	0.00	116.00	69.00	20.00	37.00
Rocky Ford	9.27	0.00	1.70	0.00	234.00	70.00	20.00	40.00
Fort Lyon	9.32	0.00	2.00	0.00	183.05	81.80	28.28	66.84
Holbrook	9.32	0.00	2.00	0.00	232.71	65.48	19.85	41.11
1/17/09								
RF Highline	13.22	0.00	2.87	0.00	9.80	220.29	27.84	52.81
Otero	13.22	0.00	2.87	0.00	111.47	220.29	45.00	86.04
Catlin	12.50	0.00	3.30	0.00	234.00	205.00	63.00	115.00
Rocky Ford	13.32	0.00	2.90	0.00	182.00	175.00	59.00	114.00
Fort Lyon	13.22	0.00	2.87	0.00	209.91	220.29	85.61	164.70
Holbrook	13.22	0.00	2.87	0.00	352.12	220.29	61.61	118.22
5/14/09								
RF Highline	8.58	0.00	1.09	0.00	37.55	61.88	16.09	27.94
Otero	8.58	0.00	1.09	0.00	62.51	72.19	20.96	38.92
Catlin	8.67	0.00	1.20	0.00	85.00	83.00	26.00	48.00
Rocky Ford	8.74	0.00	1.20	0.00	8.10	104.00	96.0	28.00	52.00

Fort Lyon	8.58	0.00	1.09	0.00	7.54	86.68	96.62	32.49	64.91
Holbrook	8.58	0.00	1.09	0.00	8.13	121.59	82.18	25.68	49.55
7/22/09									
RF Highline	8.52	0.00	0.90	0.00	6.10	51.64	61.88	16.09	27.94
Otero	8.52	0.00	0.90	0.00	6.10	83.54	61.05	16.33	79.17
Catlin	8.52	0.00	0.90	0.00	6.10	98.23	73.16	22.44	79.17
Rocky Ford	7.56	0.00	1.20	0.00	7.31	107.00	100.00	32.00	55.00
Fort Lyon	8.52	0.00	0.90	0.00	6.10	114.41	120.45	46.30	79.17
Holbrook	8.52	0.00	0.90	0.00	6.10	159.02	85.35	28.60	79.17

TABLE S-2. AGRICULTURAL MANAGEMENT AND CROP PARAMETER VALUES FOR THE MODEL APPLICATION TO THE STUDY REGION IN THE ARKANSAS RIVER VALLEY IN SOUTHEASTERN COLORADO.

Crop Type	Planting Day	Harvest Day	Plow Day	P_{St}	$d_{rt,max}$	F_S	S_{up}	$\alpha_{St,S}$	$\alpha_{Rt,S}$
Units	-	-	-	kg ha^{-1}	m	kg ha^{-1}	kg ha^{-1}	-	-
Alfalfa	30-Apr	30-Sep	20-Oct	561.6	1.83	20	24.5	0.0035	0.0023
Bean	20-May	30-Sep	20-Oct	561.6	0.91	20	20.0	0.0035	0.0023
Corn	1-May	25-Oct	14-Nov	5616	1.22	20	10.0	0.0035	0.0023
Melon	15-May	10-Aug	30-Aug	561.6	1.22	20	20.0	0.0035	0.0023
Onion	20-Mar	15-Sep	5-Oct	561.6	0.46	20	21.0	0.0035	0.0023
Pasture	30-Aug	30-Sep	20-Oct	0	0.91	20	10.0	0.0035	0.0023
Pumpkin	1-Jun	30-Sep	20-Oct	561.6	0.91	20	20.0	0.0035	0.0023
Sorghum	20-May	15-Oct	4-Nov	1684.8	0.91	20	11.5	0.0035	0.0023
Spring Grain	1-Apr	15-Jul	4-Aug	1684.8	0.91	20	11.5	0.0035	0.0023
Squash	20-May	25-Jul	14-Aug	561.6	0.91	20	20.0	0.0035	0.0023
Sunflower	1-Jun	10-Oct	30-Oct	561.6	0.91	20	20.0	0.0035	0.0023
Vegetable	25-Apr	30-Aug	19-Sep	561.6	0.91	20	20.0	0.0035	0.0023
Winter Wheat	30-Sep	5-Jul	25-Jul	1684.8	0.91	20	11.5	0.0035	0.0023

d_{pw} (depth of plowing) is 1.0 m for all crops except beans (0.8 m)
P_{Rt} (seasonal mass of root mass) is 500 kg ha^{-1} for all crop types

TABLE S-3. PARAMETERS FOR CHEMICAL REACTIONS INVOLVING ORGANIC MATTER DECOMPOSITION, DISSOLVED OXYGEN, AND NITROGEN SPECIES, FOR THE MODEL APPLICATION TO THE UPSTREAM STUDY REGION IN THE LOWER ARKANSAS RIVER VALLEY, COLORADO.

Org. Matter Decomp.			Dissolved Oxygen			Nitrogen		
Param.	Value	Unit	Param.	Value	Unit	Param.	Value	Unit
λ_L	0.25	d^{-1}	$\lambda_{O_2}^{het}$	2.0	mg/L	$H_{C/N}$	12.0	-
λ_H	0.003	d^{-1}	$\lambda_{O_2}^{auto}$	0.1	mg/L	$B_{C/N}$	8.0	-
f_e	0.5	-	K_{O_2}	1.0	mg/L	I_{O_2}	1.0	mg/L
f_h	0.2	-				λ_{nit}	0.8	d^{-1}
K_{CO_2}	0.75	mg/L				λ_{vol}	0.1	d^{-1}
						$\lambda_{NO_3}^{het}$	0.1	d^{-1}
						$\lambda_{NO_3}^{auto}$	0.01	d^{-1}
						K_{NO_3}	10.0	mg/L
						K_{d,NH_4}	3.5	-

Remaining Eight Complexation reactions:

$$K_3 = \frac{(Ca^{2+})(HCO_3^-)}{(CaHCO_3^+)} \quad (1)$$

$$K_4 = \frac{(Mg^{2+})(SO_4^{2-})}{(MgSO_4^0)} \quad (2)$$

$$K_5 = \frac{(Ca^{2+})(CO_3^{2-})}{(MgCO_3^0)} \quad (3)$$

$$K_6 = \frac{(Mg^{2+})(HCO_3^-)}{(MgHCO_3^+)} \quad (4)$$

$$K_7 = \frac{(Na^{+})(SO_4^{2-})}{(NaSO_4^-)} \quad (5)$$

$$K_8 = \frac{(Na^{2+})(CO_3^{2-})}{(NaCO_3^-)} \quad (6)$$

$$K_9 = \frac{(Na^+)(HCO_3^-)}{(NaHCO_3^0)} \quad (7)$$

$$K_{10} = \frac{(K^+)(SO_4^{2-})}{(KSO_4^-)} \quad (8)$$

Exchangeable amount for Mg, Na, and K:

$$X_{\frac{1}{2}Mg} = CEC \div [\frac{(Ca)^{\frac{1}{2}}}{(Mg)^{\frac{1}{2}} * K_1} + 1 + \frac{(Na)}{(Mg)^{\frac{1}{2}} * K_4} + \frac{(K)}{(Mg)^{\frac{1}{2}} * K_5}] \quad (9)$$

$$X_{Na} = CEC \div [\frac{(Ca)^{\frac{1}{2}} K_2}{(Na)} + \frac{K_5 (Mg)^{\frac{1}{2}}}{(Na)} + 1 + \frac{K_6 (K)}{(Na)}] \quad (10)$$

$$X_K = CEC \div [\frac{(Ca)^{\frac{1}{2}} K_3}{(K)} + \frac{K_4 * (Mg)^{\frac{1}{2}}}{(K)} + \frac{(Na)}{(K) * K_6} + 1] \quad (11)$$

Solid Species reactions:

$$MgCO_3(s) \leftrightarrow Mg^{2+} + CO_3^{2-} \quad (12)$$

$$MgSO_4(s) \leftrightarrow Mg^{2+} + SO_4^{2-} \quad (13)$$

$$NaCl(s) \leftrightarrow Na^+ + Cl^- \quad (14)$$

The solubility products for solid species:

$$K_{sp_3} = \frac{(Mg^{2+})(CO_3^{2-})}{(MgCO_3)} \quad (15)$$

$$K_{sp_4} = \frac{(Mg^{2+})(SO_4^{2-})}{(MgSO_4)} \quad (16)$$

$$K_{sp_5} = \frac{(Na^+)(Cl^-)}{(NaCl)} \quad (17)$$

References

Bailey, R.T., T.K. Gates, and Halvorson, A.D. (2013), Simulating variably-saturated reactive transport of selenium and nitrogen in agricultural groundwater systems. J. Contam. Hydro., 149, 27-45.

Morway, E. D., Gates, T. K., and Niswonger, R. G. (2013), Appraising options to enhance shallow groundwater table and flow conditions over regional scales in an irrigated alluvial aquifer system. J. Hydro., 495, 216-237.

GLOSSARY OF TERMS

General Terms		Agricultural parameters and inputs	
Litter pool	L	Solute conc. in irrigation water	$C_{x,canal}$
Humus pool	H	Maximum rooting depth	$d_{rt,max}$
Manure pool	M	Plowing Depth	d_{pw}
Mineralization	min	Sulfur seasonal crop uptake	S_{up}
Immobilization	imm	Inorganic fertilizer loading rate	F
Organic matter decomposition	dec	Solid-phase source rate	P
Autotrophic chemical reduction	$auto$	Fraction of solid-phase mass source	α
Heterotrophic chemical reduction	het	**Organic Matter Decomposition**	
Root mass	Rt	Synthesis efficiency	f_e
After-harvest Stover mass	St	Humification factor	f_h
Soil parameters and variables		Humus mass ratio	H
soil porosity	ϕ	Microbial mass ratio	B
water content	θ	**Oxidation-reduction reactions**	
solid content	ε	First-order kinetic rate constant	λ
Soil bulk densitry	ρ_b	Monod half-saturation constant	K
solute concentration	C	Chemical reduction ihibition term	I
Partitioning coefficient	K_d	S:Se shale mass ratio	ξ
Environmental reduction factor	E		
Soil Temp. Factor Change	Q_{10}		
Base soil temperature	T_B		